

**TRƯỜNG ĐẠI HỌC QUY NHƠN**  
**QUY NHON UNIVERSITY**

**TẠP CHÍ KHOA HỌC**  
**JOURNAL OF SCIENCE**

**CHUYÊN SAN KHOA HỌC TỰ NHIÊN VÀ KỸ THUẬT**  
**ISSUE: NATURAL SCIENCES AND ENGINEERING**

**14 (5)**  

---

**2020**

**BÌNH ĐỊNH, 10/2020**



## MỤC LỤC

1. Một áp dụng của Định lý tuyến tính hóa đối với bài toán hội tụ Tauber trong không gian có trọng của các hàm chỉnh hình Gâteaux  
**Dương Thanh Vỹ** ..... 5
2. Thác triển chỉnh hình của các hàm chỉnh hình yếu trong không gian có trọng của các hàm chỉnh hình  
**Nguyễn Văn Đại** ..... 17
3. Một số bất đẳng thức cho đa thức ma trận  
**Phạm Quang Hưng, Phạm Nữ Ngọc Diệp** ..... 27
4. Thuật toán khai phá đồ thị con thường xuyên theo mô hình MapReduce  
**Trần Thiên Thành, Trần Thị Liên, Nguyễn Thị Kim Phụng** ..... 35
5. Một kỹ thuật phát hiện u gan dựa trên mô hình chất liệu  
**Lê Thị Kim Nga, Đoàn Thị Xương** ..... 43
6. Một kỹ thuật xác định điểm bao phục vụ đánh giá sự thay đổi của vùng bất thường trên ảnh y tế  
**Lê Thị Kim Nga, Đoàn Thị Xương, Đoàn Thị Thu Cúc** ..... 51
7. Ứng dụng công nghệ xử lý ảnh trong phân loại cà chua sau thu hoạch  
**Nguyễn Trường Duy, Trần Đình Huy Đức, Bùi Văn Vũ, Đỗ Văn Cần** ..... 59
8. Hệ thống giám sát và cảnh báo lũ lụt thời gian thực ứng dụng công nghệ LoRa cho lưu vực sông Côn - Hà Thanh, tỉnh Bình Định  
**Trần Văn Trung, Nguyễn Đức Thiện, Lê Song Toàn, Ngô Văn Tâm, Hồ Văn Phi** ..... 69
9. Ảnh hưởng của độ mặn đến sinh trưởng và sống sót của cá rô đầu vuông (*Anabas testudineus*) ở giai đoạn cá hương đến cá giống  
**Phùng Thị Hồng Diên, Võ Văn Chí** ..... 79

10. Đặc điểm sinh học dinh dưỡng của cá Thát lát (*Notopterus notopterus*) phân bố tại đầm Trà Ổ, tỉnh Bình Định  
**Đặng Thị Thạch Trúc, Võ Văn Chí** ..... 89
11. Ảnh hưởng của pH đến quá trình hấp phụ - xúc tác quang của  $WS_2$   
**Nguyễn Thị Thanh Bích, Nguyễn Đức Nhân, Huỳnh Hữu Điền, Nguyễn Tống Yến Như, Phạm Thị Yến Nhi, Nguyễn Văn Phúc, Trương Duy Hương, Võ Viễn** ..... 95

# Một áp dụng của Định lý tuyến tính hóa đối với bài toán hội tụ Tauber trong không gian có trọng của các hàm chỉnh hình Gâteaux

Dương Thanh Vỹ

*Khoa Toán và Thống kê, Trường Đại học Quy Nhơn, Việt Nam*

*Ngày nhận bài: 18/09/2020; Ngày đăng bài: 18/10/2020*

## TÓM TẮT

Mục đích của bài báo là nghiên cứu Định lý tuyến tính hóa để giải quyết một bài toán về hội tụ Tauber trên không gian Banach có trọng các hàm chỉnh hình Gâteaux giữa các không gian lồi địa phương.

**Từ khóa:** *Tuyến tính hóa, không gian lồi địa phương, các bất biến tôpô tuyến tính, các hàm chỉnh hình, các hàm đa điều hòa dưới.*

\* Tác giả liên hệ chính.

Email: duongthanhvy@qnu.edu.vn

# An application of Linearization Theorem to the problem on Tauberian convergence in weighted space of Gâteaux holomorphic functions

Duong Thanh Vy

*Faculty of Mathematics and Statistics, Quy Nhon University, Vietnam*

*Received: 18/09/2020; Accepted: 18/10/2020*

## ABSTRACT

The aim of this paper is to study a linearization theorem for weighted spaces of Gâteaux holomorphic functions between locally convex spaces and its applications to the problem on Tauberian convergence.

**Keywords:** *Linearization, locally convex spaces, topological linear invariants, holomorphic functions, plurisubharmonic functions.*

## 1. INTRODUCTION

It is known that linearization technique is very important because it can help us in simplifying calculations. Indeed, if  $E$  and  $F$  are Banach spaces and  $U$  is an open subset of  $E$ , then the linearization results help in identifying a given class of holomorphic functions defined on  $U$ ,  $F$ -valued with the space of continuous linear mappings from a certain Banach space  $G$  to  $F$ , i.e., a holomorphic mapping is being identified with a linear operator through linearization results. The first linearization result for such spaces was obtained by Mazet in 1984. The problem has received much attention in the past few years. However, most of the results are directed to spaces of functions between Banach spaces. Six years after the announcement of Mazet, Mujica obtained a linearization theorem for the space  $H^\infty(D, F)$  of Banach-valued bounded holomorphic mappings defined on an open subset of a Banach space.

Weighted spaces of holomorphic functions defined on an open subset of a finite or infinite dimensional Banach space have been studied widely in

the literature by several mathematicians. Whereas the results in the finite dimensional case, we attribute to the contributions of Bierstedt, Bonet, Galbis, Summers, Meise, Rubel, Shields, etc., the infinite dimensional case was introduced by Garcia, Maestre, and Rueda, and further investigated by Beltran, Jordá, Rueda, Gupta, Baweja, etc.

In this paper, we are concerned with proving a linearization theorem for weighted Gâteaux holomorphic functions between locally convex spaces and applying to solve some related problems in weighted spaces of holomorphic functions.

Let  $E, F$  be locally convex spaces and  $v$  be a weight on a domain  $D$  in  $E$ . Denote  $H_v(D, F)$  (resp.  $H_{G,v}(D, F)$ ) the space of all  $F$ -valued (resp. Gâteaux) holomorphic functions on  $D$  such that  $(v.f)(D)$  is bounded in  $F$  equipped with the topology induced by the family  $\{\|\cdot\|_{v,p}\}_{p \in cs(F)}$  of semi-norms where

$$\|f\|_{v,p} := \sup_{x \in D} v(x)p(f(x)) \quad \forall p \in cs(F).$$

Let  $A_v(D)$  (resp.  $A_{G,v}(D)$ ) be a subspace of  $H_v(D)$  (resp.  $H_{G,v}(D)$ ) such that the closed unit ball

---

\*Corresponding author  
Email: duongthanvvy@qnu.edu.vn

is compact for the compact open topology  $\tau_0$ . Denote

$$A_v(D, F) := \{f : D \rightarrow F : u \circ f \in A_v(D) \forall u \in F'\}.$$

We wish to investigate the linearization theorem in the weighted spaces of  $F$ -valued functions in a weak sense

$$A_{G,v}(D, F) := \{f : D \rightarrow F : u \circ f \in A_{G,v}(D) \forall u \in F'\}.$$

We will use these result as one of main tools to study the problem of Tauberian convergences which is to look for additional properties to ensure that every sequence/net of  $F$ -valued functions defined and converging on a subset of  $D$  is convergent entirely on  $D$ . The classical theorem of Vitali is an important example on the Tauberian convergence for holomorphic functions. For a sequense  $\{f_m\}_{m \geq 1}$  of scalar-valued holomorphic functions which is uniformly bounded on compact subsets of a domain  $D$  in  $\mathbb{C}^n$  the theorem says that if it is pointwise convergent to a function  $f$  on a subset  $X$  of  $D$  then it converges uniformly on compact subsets of  $D$  whenever  $X$  is not contained in any complex hypersurface.

In 2000, Arendt and Nikolski proved Vitali's theorem for nets of Banach-valued, one-complex variable holomorphic functions in the case where the small subset has an accumulation point (see <sup>1</sup> [Theorem 3.1]). They gave an easy direct proof based on the theorem on very weakly holomorphic and the uniqueness theorem. After that, more general, in 2013 Quang, Lam and Dai <sup>2</sup> have introduced theorems of Vitali-type for sequences, which are locally bounded as well as are bounded on bounded subsets, of Fréchet-valued holomorphic functions on a domain in a Fréchet space (see <sup>2</sup> [Theorems 6.1, 6.2, 6.3 and Corollaries]). The tools of linear topological invariants, introduced and investigated by Vogt (see <sup>3,4,5</sup>), were used in their proofs.

Very recently, Dieu, Manh, Bang and Hung <sup>6</sup> are concerned with finding analogues theorem of Vitali in which the uniform boundedness of the sequence under consideration is omitted. A possible approach is to impose stronger mode of convergence and/or the size of the small subset. The versions of Vitali theorem for bounded holomorphic functions and rational functions that are rapidly pointwise convergent on a non-pluripolar subset of a domain in  $\mathbb{C}^n$

have been considered in their work. Here the speed of approximation is measured in terms of the growth of the sup-norms of functions. Motivated by the problem of finding local conditions for single-valuedness of holomorphic continuation, Gonchar <sup>7</sup> proved that a sequence of rational functions  $\{r_m\}_{m \geq 1}$  in  $\mathbb{C}^n$  ( $\deg r_m \leq m$ ) that converges rapidly in measure on an open set  $X$  to a holomorphic function  $f$  defined on a bounded domain  $D$  ( $X \subset D$ ) must converge rapidly in measure to  $f$  on the whole domain  $D$ . Much later, by using techniques of pluripotential theory, in <sup>8</sup> [Theorem 2.1] Bloom was able to prove an analogous result in which rapidly convergence in measure is replaced by rapidly convergence in capacity and the small subset  $X$  is only required to be compact and non-pluripolar.

Most recently, the problem on rapidly Tauberian convergence for sequences of polynomials have been studied by Quang, Vy, Hung and Bang <sup>9</sup> based on their researchs on Zorn spaces. They establish some results on the holomorphic extension of a Fréchet-valued continuous function  $f$  to an entire function from some non-polar balanced convex compact subset  $B$  of a Fréchet space whenever  $f$  is approximated fast enough on  $B$  by a sequence of polynomials.

In this paper, we use the linearization technique of weighted holomorphic functions to investigate the Tauberian convergence of sequences/nets in  $H_v(E, F)$  and  $A_v(D, F)$  as well as the holomorphic extension of weak-type holomorphic functions from a small subset of  $D$  in the weighted space  $A_v(D, F)$ , where  $E, F$  are Fréchet spaces.

The organization of the article is as follows.

We set up review in Section 2 some notations and terminologies of functional analysis, of holomorphic functions on locally convex spaces and of weighted spaces of holomorphic functions pertaining to our work. Some linear topological invariants of Fréchet spaces introduced and investigated by Vogt and some results on pluripolar/non-pluripolar sets are also recalled in this section.

In Section 3, we modify the method of Mujica in <sup>10</sup> to obtain Theorems 3.2 which permit to identify  $A_{G,v}(D, F)$  with  $F$ -valued continuous linear mappings from a dense subspace  $P_{A_v(D)}^0$  of the predual space  $P_{A_v(D)}$ . Recent works of Carando and Zalduendo <sup>11</sup>, and of Mujica <sup>12</sup> are devoted to get lin-

earization results for (unweighted) spaces of holomorphic functions between locally convex spaces; and of Beltrán <sup>13</sup> for weighted (LB)-spaces of entire functions on Banach spaces.

Based on the results from the previous work, in Section 4 we will investigate the problem on Tauberian convergences for sequences/nets in weighted spaces  $H_{G,v}(E, F)$  and  $A_{G,v}(D, F)$ .

The first part of the section, we present some notations and state (without proofs) theorems on Zorn's property for the space  $(E_B, \tau_E)$ , where  $E_B$  the linear hull of some compact, absolutely convex subset  $B$  of a Fréchet space  $E$  and the topology  $\tau_E$  on  $E_B$  is induced by the topology of  $E$ . The proofs of these results are analogous to the those encountered in the recent work of Quang and his colleagues <sup>9</sup>. We devoted to the study of the Tauberian convergence of sequences of Fréchet-valued Gâteaux holomorphic functions on a dense subset of a domain in a Fréchet space and holomorphic extension of the limit function in weighted space. Combining the results on (BB)-Zorn spaces with the linearization theorems, we give the conditions under which every bounded sequence  $\{f_m\}_{m \in \mathbb{N}}$  of holomorphic functions in  $H_{G,v}((E_K, \tau_E), F)$  is convergent to a function  $f \in H_{G,v}((E_K, \tau_E), F)$  uniformly on the compact subsets of  $(E_K, \tau_E)$  whenever  $\{f_m\}_{m \in \mathbb{N}}$  converges at every point of  $K$  where  $\tau_E$  is the topology of  $E_K$  induced by the topology of  $E$ . Moreover, the function  $f$  admits a holomorphic extension in  $H_v(E, F)$  if it is continuous at a simple point in  $K$  (Theorems 4.3, 4.4).

## 2. PRELIMINARIES

### 2.1. General notations

Standard notations of the theory of locally convex spaces as presented in the book of Schaefer <sup>14</sup> will be used in the paper. A locally convex space is always a complex vector space with a locally convex Hausdorff topology.

We always assume that the locally convex structure of a Fréchet space  $E$  is generated by an increasing system  $\{\|\cdot\|_k\}_{k \in \mathbb{N}}$  of semi-norms. Then we denote by  $E_k$  the completion of the canonically normed space  $E/\ker \|\cdot\|_k$ , by  $\omega_k : E \rightarrow E_k$  the canonical map

and by  $U_k$  the set  $\{x \in E : \|x\|_k < 1\}$ . Sometimes it is convenient to assume that  $\{U_k\}_{k \in \mathbb{N}}$  is a neighbourhood basis of zero (shortly  $\mathcal{U}(E)$ ).

If  $B$  is an absolutely convex subset of  $E$  we define a norm  $\|\cdot\|_B^*$  on  $E'$ , the strongly dual space of  $E$  with values in  $[0, +\infty]$  by

$$\|u\|_B^* = \sup\{|u(x)|, x \in B\}.$$

Obviously  $\|\cdot\|_B^*$  is the gauge functional of  $B^\circ$ . Instead of  $\|\cdot\|_{U_k}^*$  we write  $\|\cdot\|_k^*$ . By  $E_B$  we denote the linear hull of  $B$  which becomes a normed space in a canonical way if  $B$  is bounded.

### 2.2. Some linear topological invariants

We say that a Fréchet space  $E$  has the property  $(\tilde{\Omega})$ , and write  $E \in (\tilde{\Omega})$ , if

$$\forall p \exists q \ d > 0 \ \forall k \exists C > 0 \quad \text{such that}$$

$$\|\cdot\|_q^{*1+d} \leq C \|\cdot\|_k^* \|\cdot\|_p^{*d}.$$

For  $B \in \mathcal{B}(E)$ , the family of closed, bounded, absolutely convex sets in  $E$ , we say that  $E$  has the property  $(\tilde{\Omega}_B)$ , and write  $E \in (\tilde{\Omega}_B)$ , if

$$\forall p \exists q, d, C > 0 \quad \text{such that}$$

$$\|\cdot\|_q^{*1+d} \leq C \|\cdot\|_B^* \|\cdot\|_p^{*d}.$$

The above properties have been introduced and investigated by Vogt <sup>3,4,5</sup>.

Note that in <sup>15</sup> Dineen, Meise and Vogt proved that  $E \in (\tilde{\Omega})$  if and only if there exists  $B \in \mathcal{K}(E)$  such that  $E \in (\tilde{\Omega}_B)$  where  $\mathcal{K}(E)$  is the family of compact, absolutely convex subsets of  $E$ .

### 2.3. Weighted spaces of holomorphic functions

Let  $E$  and  $F$  be locally convex spaces and  $D$  be a domain in  $E$ . A function  $f : D \rightarrow F$  is called *Gâteaux holomorphic* if for every  $a \in D, b \in E$  and  $\varphi \in F'$ , the  $\mathbb{C}$ -valued function of one complex variable

$$\lambda \mapsto (\varphi \circ f)(a + \lambda b)$$

is holomorphic on a neighborhood of  $0 \in \mathbb{C}$ .

The function  $f$  is said to be *holomorphic* if it is Gâteaux holomorphic and continuous.



By  $H(D, F)$  (resp.  $H_G(D, F)$ ) we denote the vector space of all holomorphic (resp. Gâteaux holomorphic) functions on  $D$  with values in  $F$ . The space  $H(D, F)$  equipped with the compact-open topology  $\tau_0$ . We use  $H_b(E, F)$  to denote the space of holomorphic functions from  $E$  into  $F$  which are bounded on every bounded set in  $E$ , and  $H_{ub}(E, F)$  to indicate the set of holomorphic functions which are bounded on  $rU$  for some neighbourhood  $U$  of  $0 \in E$  and for all  $r > 0$ . Note that  $H_{ub}(E, F) \subseteq H_b(E, F)$ .

Instead of  $H(D, \mathbb{C})$ ,  $H_G(D, \mathbb{C})$ ,  $H_b(E, \mathbb{C})$ ,  $H_{ub}(E, \mathbb{C})$  we write  $H(D)$ ,  $H_G(D)$ ,  $H_b(E)$ ,  $H_{ub}(E)$  respectively.

For details concerning holomorphic functions on locally convex spaces, we refer to the book of Dineen.<sup>16</sup>

For a domain  $D$  in  $E$ , a *weight*  $v : D \rightarrow (0, \infty)$  is a continuous function which is strictly positive. Denote  $H_v(D, F)$

$$:= \{f \in H(D, F) : (v \cdot f)(D) \text{ is bounded on } D\};$$

$$H_v(D) := H_v(D, \mathbb{C})$$

$$= \{f \in H(D) : \|f\|_v := \sup_{x \in D} v(x)|f(x)| < \infty\};$$

$$H_{G,v}(D, F)$$

$$:= \{f \in H_G(D, F) : (v \cdot f)(D) \text{ is bounded on } D\};$$

$$H_{G,v}(D) = H_{G,v}(D, \mathbb{C})$$

$$= \{f \in H_G(D) : \|f\|_v := \sup_{x \in D} v(x)|f(x)| < \infty\}.$$

The space  $H_v(D, F)$  equipped with the topology generated by the family  $\{\|\cdot\|_{v,p}\}_{p \in cs(F)}$  of seminorms. Then  $H_v(D, F)$  is complete whenever  $F$  is complete, in particular, it is Banach if  $F$  is Banach. It is easy to check that

$$H_v(D, F) = \varprojlim_{p \in cs(F)} H_v(D, F_p)$$

where  $F_p$  is the completion of the canonically normed space  $F/\ker p$ .

## 2.4. Pluripolar sets

Let  $D$  be an open subset of a topological vector space  $E$ . An upper-semicontinuous function  $\varphi : D \rightarrow$

$[-\infty, +\infty)$  is called *plurisubharmonic*, and write  $\varphi \in PSH(D)$ , if for every  $a \in D$  and  $b \in E$  the function

$$\lambda \mapsto \varphi(a + \lambda b)$$

is subharmonic as a function of one complex variable on a neighborhood of  $0 \in \mathbb{C}$ . For example, if  $f \in H(D, F)$ , where  $D$  is an open subset of a locally convex space and  $F$  is a vector space with a seminorm  $\|\cdot\|$  then the function  $z \mapsto \log \|f(z)\|$  is plurisubharmonic on  $D$ .

**Definition 2.1.** A subset  $B \subset D$  is said to be *pluripolar* in  $D$  if there exists a  $\varphi \in PSH(D)$  such that  $\varphi \not\equiv -\infty$  on any connected component of  $D$  and  $\varphi|_B = -\infty$ .

It is clear that the union of a finite number of pluripolar sets is pluripolar. We should say that pluripolar sets in infinite dimension space can be complicated. For example, there exist Fréchet spaces in which *every* bounded sets is pluripolar.

In the case where  $\dim E < \infty$ , a fundamental result of Josefson (see <sup>17</sup>, [Theorem 4.7.4]) says that the function  $\varphi$  above can be chosen to be *globally* defined on  $E$ . That means a subset  $X$  of  $\mathbb{C}^p$  is pluripolar if and only if there exists  $\varphi \in PSH(\mathbb{C}^p)$ ,  $\varphi \neq -\infty$  such that

$$X \subset \{z \in \mathbb{C}^p : \varphi(z) = -\infty\}.$$

Polarity of subsets in infinite dimensional spaces has been dealt with in detail in many places, and the reader is referred to <sup>15,18,19</sup> for further details.

## 3. LINEARIZATION OF WEIGHTED SPACES OF GÂTEAUX HOLOMORPHIC FUNCTIONS

Let  $A_v(D)$  be a subspace of  $H_v(D)$  such that the closed unit ball  $B_{A_v(D)}$  is compact for the topology  $\tau_0$ . Note that this condition implies that  $A_v(D)$  is norm-closed and hence Banach because  $H_v(D)$  is Banach. First, we present two illustrative examples for this assumption in the next section.

In <sup>21</sup> [Theorem 7] Jordá showed that if, for  $m \in \mathbb{N}$ , the space  $\mathcal{P}^m(E)$  of continuous  $m$ -homogeneous polynomials on a Fréchet  $E$ , endowed with its norm topology, is contained  $H_v(D)$  then the closed unit ball of  $\mathcal{P}^m(E)$  is compact for the topology  $\tau_0$ .

Now, we present another illustrative example. For each  $f \in H(D)$  we consider the Taylor series representation at zero

$$f(z) = \sum_{k=0}^{\infty} (P_k f)(z), \quad z \in D,$$

where  $P_k f$  is a  $k$ -homogeneous polynomial,  $k = 0, 1, \dots$ . The series converges to  $f$  uniformly on each compact subset of  $D$ .

Now given a sequence  $\alpha := \{\alpha_n\}_{n \geq 0} \subset \mathbb{C} \setminus \{0\}$ . For each  $k \geq 1$ , let us denote  $|\alpha|_k = \sum_{m=0}^k |\alpha_m|$ . For each  $n \geq 0$ , consider the linear operator  $C_n : H_v(D) \rightarrow H_v(D)$  given by

$$(C_n f)(z) = \frac{1}{|\alpha|_n} \sum_{k=0}^n \left( \alpha_k \sum_{j=0}^k (P_j f)(z) \right), \quad z \in D. \tag{1}$$

Put

$$C_{n,v}(D) = C_n(H_v(D)), C_v(D) = \bigcup_{n \geq 0} C_{n,v}(D)$$

and

$$A_v(D) := \overline{C_v(D)}^{\tau_v}. \tag{2}$$

In <sup>20</sup> [Proposition 4] Quang showed that if, for  $D$  is a balanced, bounded open set in a Fréchet-Montel space  $E$  having the  $(BB)_{\infty}$ -property,  $v$  is a weight on  $D$  which is radial and vanishes at infinity outside compact sets of  $D$ , and  $A_v(D)$  is defined by (2). Then, the closed unit ball of  $(A_v(D), \tau_v)$  is  $\tau_0$ -compact.

In <sup>22</sup> [Theorem 2.2.1] Vy have given linearization theorem for weighted holomorphic functions between locally convex spaces as follows.

**Proposition 3.1.** *Let  $v$  be a weight on a domain  $D$  in a metrizable locally convex space  $E$  and  $A_v(D)$  be a subspace of  $H_v(D)$  such that the closed unit ball is  $\tau_0$ -compact. Then there exist a Banach space  $P_{A_v(D)}$  and a mapping  $\delta_D \in H(D, P_{A_v(D)})$  with the following universal property: For each complete locally convex space  $F$ , a function  $f \in A_v(D, F)$  if and only if there is a unique mapping  $T_f \in L(P_{A_v(D)}, F)$  such that  $T_f \circ \delta_D = f$ . This property characterize  $P_{A_v(D)}$  uniquely up to an isometric isomorphism.*

Moreover, the mapping

$$\Phi : f \in A_v(D, F) \mapsto T_f \in (L(P_{A_v(D)}, F), \tau_{\ell})$$

$$:= \varprojlim_{p \in cs(F)} (L(P_{A_v(D)}, F_p))$$

is a topological isomorphism.

By the Ng Theorem <sup>23</sup> [Theorem 1] the evaluation mapping

$$J : (A_v(D), \|\cdot\|_v) \rightarrow (P_{A_v(D)})'$$

given by

$$(Jf)(u) = u(f) \quad \forall u \in P_{A_v(D)},$$

is a topological isomorphism. Hence, the space  $P_{A_v(D)}$  is called the predual of  $A_v(D)$ .

Now we consider the above result for weighted Gâteaux holomorphic functions.

Let  $D$  be an open subset of metrizable locally convex space  $E$ . Denote  $\mathcal{F}(E)$  the family of all finite dimensional subspaces of  $E$ . By Proposition 3.1, for each  $Y \in \mathcal{F}(E)$  there exists a unique map  $p_Y \in L(P_{A_v(D \cap Y)}, P_{A_v(D)})$  such that the following diagram is commutative

$$\begin{array}{ccc} D \cap Y & \xrightarrow{id} & D \\ \downarrow \delta_{D \cap Y} & & \downarrow \delta_D \\ P_{A_v(D \cap Y)} & \xrightarrow{p_Y} & P_{A_v(D)} \end{array} \tag{3}$$

where  $id$  is the identity mapping and  $P_{A_v(D \cap Y)}$  denotes the predual of  $A_v(D \cap Y)$ .

If  $Y, Z \in \mathcal{F}(E)$  such that  $Y \subset Z$ , then by Proposition 3.1 again, there exists a unique map  $p_{ZY} \in L(P_{A_v(D \cap Y)}, P_{A_v(D \cap Z)})$  such that the following diagram is commutative

$$\begin{array}{ccc} D \cap Y & \xrightarrow{id} & D \cap Z \\ \downarrow \delta_{D \cap Y} & & \downarrow \delta_{D \cap Z} \\ P_{A_v(D \cap Y)} & \xrightarrow{p_{ZY}} & P_{A_v(D \cap Z)} \end{array}$$

It follows that  $p_Z \circ p_{ZY} = p_Y$  whenever  $Y \subset Z$ . Denote

$$P_{A_v(D)}^0 := \bigcup_{Y \in \mathcal{F}(E)} p_Y(P_{A_v(D \cap Y)})$$

and equip  $P_{A_v(D)}^0$  with the topology induced by  $P_{A_v(D)}$ .

Let  $A_{G,v}(D)$  be a subspace of  $H_{G,v}(D)$  such that the closed unit ball is compact for the topology  $\tau_0$ . For each complete locally convex space  $F$ , we put

$$A_{G,v}(D, F) := \{f : D \rightarrow F : u \circ f \in A_{G,v}(D) \forall u \in F'\}.$$

**Theorem 3.2.** *Under the assumptions of Proposition 3.1,*

- (a)  $P_{A_v(D)}^0$  is a dense subspace of  $P_{A_v(D)}$ ;
- (b)  $\delta_D \in H(D, P_{A_v(D)}^0)$ ;
- (c) For each complete locally convex space  $F$ , the function  $f \in A_{G,v}(D, F)$  if and only if there exists a unique linear mapping  $T_f : P_{A_v(D)}^0 \rightarrow F$  such that  $T_f \circ \delta_D = f$ . Moreover,  $T_f$  is continuous if and only if  $f$  is continuous.

*Proof.* (a) By <sup>22</sup> [Theorem 3.1] we have  $\delta_D : D \rightarrow P_{A_v(D)}$  be the evaluation mapping given by

$$\delta_D(x) = \delta_x$$

with  $\delta_x$  is the evaluation, that means  $\delta_x(g) := g(x)$  for all  $g \in A_v(D)$ ; then, we have

$$\text{span}\{\delta_x : x \in D\} \text{ is a dense subspace of } P_{A_v(D)}. \tag{4}$$

By the commutative diagram (3),  $\delta_x \in P_{A_v(D)}^0$  for every  $x \in D$ . Thus, by (4),  $P_{A_v(D)}^0$  is dense in  $P_{A_v(D)}$ .

(b) It is known that  $\delta_D \in H(D, P_{A_v(D)})$  (see Proposition 3.1) and  $\delta_D(x) \in P_{A_v(D)}^0$  for all  $x \in D$ . For each  $z \in D$  we write

$$\delta_D(z) = \sum_{n=0}^{\infty} P_n \delta_D(z).$$

Thus, in order to prove  $\delta_D \in H(D, P_{A_v(D)}^0)$  it suffices to check that

$$P_n \delta_D(a) \in \mathcal{P}^n(E, P_{A_v(D)}^0)$$

for every  $a \in D$  and  $n \in \mathbb{N}$ , where  $\mathcal{P}^n(E, P_{A_v(D)}^0)$  denotes the vector space of all continuous  $n$ -homogeneous polynomials from  $E$  into  $P_{A_v(D)}^0$ .

Fix  $a \in D, n \in \mathbb{N}$  and  $t \in E$ . Let  $r > 0$  such that  $a + \eta t \in D$  for all  $\eta \in \overline{D}_r = \{\lambda \in \mathbb{C} : |\lambda| \leq r\}$  and let  $Y \in \mathcal{F}(E)$  which is generated by  $a$  and  $t$ . Then, it follows from the commutative diagram (3) that

$$\begin{aligned} P_n \delta_D(a)(t) &= \frac{1}{2\pi i} \int_{|\eta|=r} \frac{\delta_D(a + \eta t)}{\eta^{n+1}} d\eta \\ &= \frac{1}{2\pi i} \int_{|\eta|=r} \frac{p_Y \circ \delta_{D \cap Y}(a + \eta t)}{\eta^{n+1}} d\eta \\ &= p_Y(P_n \delta_{D \cap Y})(a)(t), \end{aligned}$$

and hence  $P_n \delta_D(a)(t) \in p_Y(P_{A_v(D \cap Y)}) \subset P_{A_v(D)}^0$ .

(c) First, given a function  $f : D \rightarrow F$ . Assume that there exists a unique linear mapping  $T_f : P_{A_v(D)}^0 \rightarrow F$  such that  $T_f \circ \delta_D = f$ . Then, the commutative diagram (3) implies that  $T_{Y,f} \circ \delta_{D \cap Y} = f|_{D \cap Y}$  for every  $Y \in \mathcal{F}(E)$ , where  $T_{Y,f} := T_f|_{p_Y(P_{A_v(D \cap Y)})} \in L(P_{A_v(D \cap Y)}, F)$ . By Theorem 3.1,  $f|_{D \cap Y} \in A_v(D \cap Y, F)$ . Hence  $f \in A_{G,v}(D, F)$ .

Conversely, for each  $f \in A_{G,v}(D, F)$  and  $Y \in \mathcal{F}(E)$ , the function  $f_Y := f|_{D \cap Y} \in A_v(D \cap Y)$ . By Theorem 3.1, there is a unique map  $T_Y \in L(P_{A_v(D \cap Y)}, F)$  such that  $T_Y \circ \delta_{D \cap Y} = f_Y$ . If  $Y, Z \in \mathcal{F}(E)$  with  $Y \subset Z$ , the following diagram is commutative

$$\begin{array}{ccccc} D \cap Y & \xrightarrow{id} & D \cap Z & \xrightarrow{id} & D \\ \downarrow \delta_{D \cap Y} & & \downarrow \delta_{D \cap Z} & & \downarrow f \\ P_{A_v(D \cap Y)} & \xrightarrow{p_{ZY}} & P_{A_v(D \cap Z)} & \xrightarrow{T_Z} & F \end{array}$$

This implies that  $T_Z \circ p_{ZY} = T_Y$  whenever  $Y \subset Z$ . Thus, there is a linear map  $T : P_{A_v(D)}^0 \rightarrow F$  such that  $T \circ p_Y = T_Y$  for each  $Y \in \mathcal{F}(X)$ . Since  $T_Y \circ \delta_{D \cap Y} = f_Y$  we obtain  $T \circ \delta_D = f$ .

If we can find  $S : P_{A_v(D)}^0 \rightarrow F$  such that  $T \circ \delta_D = f$  then  $S \circ p_Y = T_Y = T \circ p_Y$  for every  $Y \in \mathcal{F}(E)$ . This yields  $S = T$ .

Finally, since  $f = T \circ \delta_D$ , it is obvious that  $f$  is continuous if  $T$  is continuous. The converse inclusion follows from Theorem 3.1.

Now, note that a family  $\mathcal{F} \subset A_v(D, F)$  is bounded if and only if it is amply bounded, that means the family  $\{\omega_p \circ f : f \in \mathcal{F}\}$  is bounded in  $A_v(D, F_p)$  for all  $p \in cs(F)$ , where  $\omega_p : F \rightarrow F_p$  is the canonical map.

**Proposition 3.3.** *Under the assumptions of Proposition 3.1, a family  $\{f_j\}_{j \in I} \subset A_v(D, F)$  is bounded if and only if the corresponding family  $T_{f_j} \subset L(P_{A_v(D)}, F)$  is equicontinuous.*

*Proof.* Let  $\{T_{f_j}\}_{j \in I}$  be the corresponding family of  $\{f_j\}_{j \in I}$ , that is  $f_j(x) = T_{f_j}(\delta_x)$  for each  $x \in D$  (see Proposition 3.1). Let  $D_v^* := \{v(x)\delta_x : x \in D\} \subset P_{A_v(D)}$ .

Assume that  $\{T_{f_j}\}_{j \in I} \subset L(P_{A_v(D)}, F)$  is equicontinuous. Then for each  $p \in cs(F)$  there exists  $C_p > 0$  such that

$$T_{\omega_p \circ f_j}(D_v^*) = \{v(x)(\omega_p \circ f_j)(x) : x \in D\}$$

$$\subset C_p B_{F_p} \quad \forall j \in I$$

where  $B_{F_p}$  is the unit ball of  $F_p$ .

We now note that

$$\overline{\text{acx}}(D_v^*) = (D_v^*)^{\circ\circ} = B_{A_v(D)}^\circ = B_{P_{A_v(D)}} \quad (5)$$

where  $\overline{\text{acx}}(D_v^*)$  denotes the closed balanced convex hull of  $D_v^* := \{v(x)\delta_x : x \in D\}$  in  $P_{A_v(D)}$ . Thus, we have

$$\begin{aligned} T_{\omega_p \circ f_j}(B_{P_{A_v(D)}}) &= T_{\omega_p \circ f_j}(\overline{\text{acx}}(D_v^*)) \\ &\subset \overline{\text{acx}}(T_{\omega_p \circ f_j}(D_v^*)) \\ &\subset C_p \overline{B}_{F_p} \quad \forall j \in I. \end{aligned}$$

This implies that the family  $\{\omega_p \circ f_j\}_{j \in I}$  is bounded for all  $p \in cs(F)$ , hence the family  $\{f_j\}_{j \in I}$  is bounded.

Conversely, take a 0-neighbourhood  $V$  in  $F$ . We can assume that  $V := \varepsilon \bigcap_{i=1}^m \omega_{p_i}^{-1}(B_{F_{p_i}})$ . By the hypothesis, for each  $p_i$ ,  $1 \leq i \leq m$ , there exists  $C_{p_i} > 0$  such that

$$\{v(x)(\omega_{p_i} \circ f_j)(x) : x \in D\} \subset \varepsilon C_{p_i}(B_{F_{p_i}}) \quad \forall j \in I$$

and hence

$$\{v(x)f_j(x) : x \in D\} \subset V \quad \forall j \in I.$$

Then we have

$$\begin{aligned} T_{f_j}(D_v^*) &= \{v(x)T_{f_j}(\delta_x) : x \in D\} \\ &= \{v(x)f_j(x) : x \in D\} \subset V \quad \forall j \in I. \end{aligned}$$

Consequently,

$$T_{f_j}(B_{P_{A_v(D)}}) = T_{f_j}(\overline{\text{acx}}(D_v^*)) \subset \overline{V} \quad \forall j \in I,$$

and the proposition is proved.

The following is a consequence of Theorem 3.2 and Proposition 3.3.

**Corollary 3.4.** *Under the assumptions of Theorem 3.1, a family  $\{f_j\}_{j \in I} \subset A_{G,v}(D, F)$  is bounded if and only if the corresponding family  $T_{f_j} \subset L(P_{A_v(D)}^0, F)$  is equicontinuous.*

#### 4. TAUBERIAN CONVERGENCES IN WEIGHTED SPACES OF GÂTEAUX HOLOMORPHIC FUNCTIONS

We will apply the results of the previous section to investigate the problem on Tauberian convergences for

sequences/nets as well as the extension of limit functions in weighted spaces  $H_v(E, F)$  and  $A_v(D, F)$ .

First, we present some notions which will be needed in subsequent sections.

A subset  $M \subseteq D$  is said to be a *set of uniqueness* for  $A_v(D)$  if each  $f \in A_v(D)$  such that  $f|_M = 0$  then  $f \equiv 0$ .

A subset  $M \subset D$  is said to be *sampling* for  $A_v(D)$  if there exists a constant  $C \geq 1$  such that for every  $f \in A_v(D)$  we have

$$\sup_{z \in D} v(z)|f(z)| \leq C \sup_{z \in M} v(z)|f(z)|. \quad (6)$$

*Remark 1.* For  $M \subset D$ , denote  $M_v^* := \{v(x)\delta_x : x \in M\} \subset B_{P_{A_v(D)}}$  where  $B_{P_{A_v(D)}}$  denotes the unit ball of  $P_{A_v(D)}$ .

1. Since the closed unit ball  $B_{A_v(D)}$  of the space  $A_v(D)$  is  $\tau_0$ -compact, by the Hahn-Banach theorem, it is easy to check that the following are equivalent:

(i)  $M$  is a set of uniqueness for  $A_v(D)$ ;

(ii)  $M_v^*$  is separating in  $A_v(D)$ ;

(iii)  $\langle M_v^* \rangle := \text{span}M_v^*$  is  $\sigma(P_{A_v(D)}, A_v(D))$ -dense.

2. For the norm given by  $\|f\|_{M,v} := \sup_{z \in M} v(z)|f(z)|$  on  $A_v(D)$ , it is obvious that the following are equivalent:

(i)  $M$  is sampling for  $A_v(D)$ ;

(ii)  $\|\cdot\|_v \simeq \|\cdot\|_{M,v}$  on  $A_v(D)$ .

3. Obviously, if  $M$  is sampling for  $A_v(D)$  then  $M_v^*$  is separating in  $A_v(D)$ , hence,  $M$  is a set of uniqueness for  $A_v(D)$ .

Now, we state Theorems of Zorn type which will be needed in subsequent sections.

**Definition 4.1.** A locally convex space  $E$  is said to be *(BB)-Zorn space* (or, to have *(BB)-Zorn Property*) if for every open subset  $D$  of  $E$ , every  $f \in H_G(D)$  which is bounded on bounded sets in  $D$  and continuous at a single point of  $D$  is holomorphic on  $D$ .

In <sup>9</sup>, Quang and his colleagues have investigated the Zorn property of the linear hull of some convex balanced compact subset  $B$  of a Fréchet space. In the same way as in <sup>9</sup> we get the following.

**Theorem 4.1.** *Let  $E$  be a nuclear Fréchet space with the topology  $\tau_E$  and  $E \in (\tilde{\Omega})$ . Then there exists  $K \in \mathcal{K}(E)$  such that  $(E_K, \tau_E)$  is a (BB)-Zorn space. Moreover, for every domain  $D$  in  $E$  we have*

$$H_b(D(K), \tau_E) = H_b(D)$$

where  $D(K) := D \cap E_K$ .

In particular,  $H(E_K, \tau_E) = H(E) = H_{ub}(E)$ .

**Theorem 4.2.** *Let  $E$  be a Fréchet-Schwartz space with an absolute Schauder basis and the topology  $\tau_E$  and  $E \in (\tilde{\Omega})$ . Then there exists a non-pluripolar set  $K \in \mathcal{K}(E)$  such that  $(E_K, \tau_E)$  is a (BB)-Zorn space. Moreover, for every domain  $D$  in  $E$  we have*

$$H_b(D(K), \tau_E) = H_b(D)$$

where  $D(K) := D \cap E_K$ .

In particular,  $H_b(E_K, \tau_E) = H(E) = H_b(E)$ .

Note that, under the assumptions of  $E$  the set  $K$  is non-pluripolar (see <sup>15</sup> [Theorem 9]).

The first results of this section are concerned with the weighted Tauberian convergence of sequences of Gâteaux holomorphic functions in a space  $(E_K, \tau_E)$ , where  $E_K$  the linear hull of some  $K \in \mathcal{K}(E)$  where the topology  $\tau_E$  on  $E_K$  is induced by the topology of a Fréchet space  $E$ .

**Theorem 4.3.** *Let  $E, F$  be Fréchet spaces and  $v$  be a weight on  $E$ . Assume that  $E$  is nuclear with the topology  $\tau_E$  and  $E \in (\tilde{\Omega})$ . Then there exists a non-pluripolar set  $K \in \mathcal{K}(E)$  satisfying the following: if  $\{f_m\}_{m \in \mathbb{N}}$  is a bounded sequence in  $H_{G,v}((E_K, \tau_E), F)$  such that  $\{f_m\}_{m \in \mathbb{N}}$  is convergent at each  $x \in K$  to a function  $f$  which is continuous at some  $x_0 \in K$  then  $f$  has an extension  $\tilde{f} \in H_v(E, F)$  and  $\{f_m\}_{m \in \mathbb{N}}$  is convergent to  $\tilde{f}$  uniformly on the compact subsets of  $(E_K, \tau_E)$ .*

*Proof.* By Theorem 4.1 there exists a non-pluripolar  $K \in \mathcal{K}(E)$  such that  $(E_K, \tau_E)$  is a (BB)-Zorn space.

First, without loss of generality we may assume that  $\mathcal{F}((E_K, \tau_E)) = \{Q_1, \dots, Q_n, \dots\}$  where

$\dim Q_n = n$  and  $Q_n \subset Q_{n+1} \subset (E_K, \tau_E)$  for all  $n \in \mathbb{N}$ . Then

$$(E_K, \tau_E) = \bigcup_{n \in \mathbb{N}} Q_n.$$

Since  $\dim Q_n = n < \infty$ , by Montel's theorem, the closed unit ball  $B_{n,v}$  of  $H_v(Q_n)$  is  $\tau_0$ -compact. As in Theorem 3.2 we denote

$$P_{H_v(E_K, \tau_E)}^0 := \bigcup_{n \in \mathbb{N}} p_{Q_n}(P_{H_v(Q_n)})$$

and equip  $P_{H_v(E_K, \tau_E)}^0$  with the topology induced by the predual  $P_{H_v(E_K, \tau_E)}$  of  $H_v(E_K, \tau_E)$ .

Let  $\{f_m\}_{m \in \mathbb{N}}$  be a sequence as in the theorem. From Theorem 3.2 there exists a sequence  $\{T_{f_m}\}_{m \in \mathbb{N}} \subset L(P_{H_v(E_K, \tau_E)}^0, F)$  such that  $T_{f_m} \circ \delta_{E_K} = f_m$  for all  $m \in \mathbb{N}$ .

Then, since  $\{f_m\}_{m \in \mathbb{N}}$  is bounded, it follows from Corollary 3.4 that  $\{T_{f_m}\}_{m \in \mathbb{N}}$  is equicontinuous.

Then the topology of pointwise convergence on  $P_{H_v(E_K, \tau_E)}$  coincides with the topology of pointwise convergence on  $(E_K, \tau_E)_v^*$  by <sup>24</sup> [39.4(1)]. Thus  $\{T_j\}_{j \in I}$  is pointwise convergent to  $T \in L(P_{H_v(E_K, \tau_E)}^0, F)$ . The convergence is uniform on the compact subsets of  $P_{H_v(E_K, \tau_E)}^0$ , by <sup>24</sup> [39.4(2)].

By Proposition 3.1 there exists  $f^* \in H_{G,v}((E_K, \tau_E), F)$  such that  $f^*(x) = T(\delta_x)$  for all  $x \in E_K$ . It is obvious that  $\{f_j\}_{j \in J}$  is convergent to  $f^*$ . On the other hand, the function  $\delta_{E_K} : x \mapsto \delta_x$  is holomorphic (see Proposition 3.1) and then continuous. Thus, if  $L \subset E_B$  is compact then  $\{\delta_x : x \in L\}$  is compact in  $P_{H_v(E_K, \tau_E)}$ . It follows that  $\{f_j\}_{j \in J}$  is convergent to  $f^*$  uniformly on the compact subsets of  $(E_K, \tau_E)$ . It is obvious that  $f^* = f$  on  $K$ .

On the other hand, since  $K$  is not pluripolar, by <sup>15</sup> [Theorem 2]  $E \in (\tilde{\Omega}_K)$ . It implies that  $E_K$  is dense in  $E$ .

Then, because  $f$  is continuous at some  $x_0 \in K$ , by Theorem 4.1,  $u \circ f^* \in H_v(E_K, \tau_E)$  for all  $u \in F'$ . Consequently, it follows from Theorem 4.1 that  $u \circ f^* \in H(E_K, \tau_E)$  admits an extension  $f_u^* \in H_v(E)$  for all  $u \in F'$ .

Now, because  $E \in (\tilde{\Omega}_K)$ , by <sup>25</sup> [Lemma 2.2],  $K$  is a set of uniqueness for  $H(E)$ , hence, it is also of uniqueness for  $H_v(E)$ .

From Remark 1,  $\langle K_v^* \rangle := \text{span}K_v^*$  is  $\sigma(P_{H_v(E)}, H_v(E))$ -dense, and hence it is norm-dense.

Put  $\widehat{T} : \langle K_v^* \rangle \rightarrow F, \widehat{T}(\delta_x) := f^*(x)$ .

Since  $F'$  is separating,  $\widehat{T}$  is well defined.

Let  $x = \sum_{k=1}^n \alpha_k v(x_k) \delta_{x_k} \in B_{\langle K_v^* \rangle}$ , the unit ball of  $\langle K_v^* \rangle$ . For each  $u \in F'$  we have the estimate

$$\begin{aligned} |\langle \widehat{T}x, u \rangle| &= \left| \left\langle \sum_{k=1}^n \alpha_k v(x_k) f^*(x_k), u \circ f^* \right\rangle \right| \\ &= \left| \left\langle \sum_{k=1}^n \alpha_k v(x_k) \delta_{x_k}, u \circ f \right\rangle \right| \\ &\leq \|u \circ f^*\|_v. \end{aligned}$$

This means that  $\widehat{T}(B_{\langle K_v^* \rangle})$  is  $\sigma(F, F')$ -bounded and then it is bounded. Thus,  $\widehat{T}$  is a bounded linear mapping.

Since  $\langle K_v^* \rangle$  is norm-dense in  $P_{H_v(E)}$  we can extend  $\widehat{T}$  to  $\widetilde{T} : P_{H_v(E)} \rightarrow F$ .

Finally, by applying Proposition 3.1 there exists unique  $\widetilde{f} \in H_v(E, F)$  such that  $\widetilde{T} \circ \delta_E = \widetilde{f}$ . Obviously,  $\widetilde{f} = f^*$  on  $E_K$ .

From Theorem 4.2, as Theorem 4.3, we have

**Theorem 4.4.** *Let  $E, F$  be Fréchet spaces and  $v$  be a weight on  $E$ . Assume that  $E$  is Schwartz with an absolute Schauder basis and the topology  $\tau_E$  and  $E \in (\widetilde{\Omega})$ . Then there exists a non-pluripolar set  $K \in \mathcal{K}(E)$  satisfying the following: if  $\{f_m\}_{m \in \mathbb{N}}$  is a bounded sequence in  $H_{G,v}((E_K, \tau_E), F)$  such that  $\{f_m\}_{m \in \mathbb{N}}$  is convergent at each  $x \in K$  to a function  $f$  which is continuous at some  $x_0 \in K$  then  $f$  has an extension  $\widetilde{f} \in H_v(E, F)$  and  $\{f_m\}_{m \in \mathbb{N}}$  is convergent to a function  $\widetilde{f}$  uniformly on the compact subsets of  $(E_K, \tau_E)$ .*

#### ACKNOWLEDGMENTS

This study is conducted within the framework of science and technology projects at institutional level of Quy Nhon University under the project code T2020.655.03.

#### REFERENCES

1. W. Arendt and N. Nikolski. Vector-valued holomorphic functions revisited, *Math. Z.*, **2000**, 234, 777-805.

2. T. T. Quang, L. V. Lam and N. V. Dai. On  $\sigma(\cdot, W)$ -holomorphic functions and theorems of Vitali-type, *Complex Anal. Oper. Theory*, **2013**, 7(1), 237-259.
3. D. Vogt. Charakterisierung der Unterräume von  $s$ , *Math. Z.*, **1977**, 155, 109-117.
4. D. Vogt. Subspaces and quotient spaces of  $s$ , in *Functional Analysis: Surveys and Recent Results III* (ed. K. D. Bierstedt, B. Fuchssteiner), North-Holland. *Math. Studies*, **1977**, 27, 167-187.
5. D. Vogt. Eine Charakterisierung der Potenzreihenräume von endlichem typ und ihre Folgerungen, *Manuscripta Math.*, **1982**, 37, 269-301.
6. N. Q. Dieu, P. V. Manh, P. H. Bang and L. T. Hung. Vitali's theorem without uniform boundedness, *Publ. Mat.*, **2016**, 60, 311-334.
7. A. A. Gonchar. A local condition for the single-valuedness of analytic functions of several variables, (*Russian*), *Mat. Sb. (N.S.)*, **1974**, 93(135), 296-313.
8. T. Bloom. On the convergence in capacity of rational approximants, *Constr. Approx.*, **2001**, 17(1), 91-102.
9. T. T. Quang, D. T. Vy, L. T. Hung and P. H. Bang. The Zorn property for holomorphic functions, *Ann. Polon. Math.*, **2017**, 120(2), 115-133.
10. J. Mujica. A completeness criterion for inductive limits of Banach spaces, In: *Functional Analysis, Holomorphy and Approximation Theory II*, North-Holland *Math. Studies*, North-Holland Amsterdam, **1984**, 86, 319-329.
11. D. Carando and I. Zalduendo. Linearization of functions, *Math. Ann.*, **2004**, 328(4), 683-700.
12. J. Mujica. Linearization of bounded holomorphic mappings on Banach spaces, *Trans. Amer. Math. Soc.*, **1991**, 324(2), 867-887.
13. M. J. Beltrán. Linearization of weighted (LB)-spaces of entire functions on Banach spaces, *Revis. Real Acad. Ciencias Exactas, Físicas y Naturales A*, **2012**, 106(2), 275-286.

14. H. Schaefer. *Topological vector spaces*, Springer Verlag, 1971.
15. S. Dineen, R. Meise and D. Vogt. Characterization of nuclear Fréchet spaces in which every bounded set is polar, *Bull. Soc. Math. France.*, **1984**, *112*, 41-68.
16. S. Dineen. *Complex Analysis on Infinite Dimensional Spaces*, Springer, New York, 1999.
17. M. Klimek. *Pluripotential Theory*, Oxford Press, 1991.
18. S. Dineen, R. Meise, D. Vogt. Polar Subsets of Locally Convex Spaces, in: *Aspects of Mathematics and its Applications*, Ed. J. A. Barroso, Elsevier Science Publisher, B.V., **1986**, *34*, 295-319.
19. S. Dineen and Ph. Noverraz. Gaussian measures and polar sets in locally convex spaces, *Arkiv. Mat.*, **1979**, *17*, 217-223.
20. T. T. Quang. On some classes of weighted spaces of weakly holomorphic functions, *Acta Mathematica Vietnamica*, (accepted), DOI: 10.1007/s40306-020-00394-y.
21. E. Jordá. Weighted Vector-Valued Holomorphic Functions on Banach Spaces, *Abstract and Applied Analysis Volume 2013*, **2013**, 9 pages.
22. Dương Thanh Vỹ. *Hội tụ kiểu Tauber cho hàm và ánh xạ chỉnh hình*, luận án tiến sĩ, Trường Đại học Quy Nhơn, 2019.
23. K. F. Ng. On a theorem of Dixmier, *Math. Scand.*, **1971**, *29*, 279-280.
24. G. Köthe. *Topological Vector Spaces II*, Springer, Berlin, Germany, 1979.
25. N. D. Lan.  $LB^\infty$ - structure of space of germs of holomorphic functions, *Publ. Mat.*, **2000**, *44*, 177-192.





# Thác triển chỉnh hình của các hàm chỉnh hình yếu trong không gian có trọng của các hàm chỉnh hình

Nguyễn Văn Đại

*Khoa Toán và Thống kê, Trường Đại học Quy Nhơn, Việt Nam*

*Ngày nhận bài: 17/09/2020; Ngày đăng bài: 17/10/2020*

## TÓM TẮT

Cho  $v$  là một trọng trên một miền  $D$  trong không gian lồi địa phương khả metric  $E$  và  $F$  là không gian lồi địa phương đầy đủ. Ký hiệu  $H_v(D, F)$  là không gian có trọng của các hàm chỉnh hình trên  $D$  nhận giá trị trong  $F$  và  $A_v(D)$  là không gian con của  $H_v(D, \mathbb{C})$  sao cho hình cầu đơn vị đóng của nó là compact theo tôpô compact mở. Trong bài báo này, áp dụng một định lý về tuyến tính hóa trong không gian có trọng các hàm chỉnh hình, chúng tôi đưa ra các điều kiện đối với các tập  $M \subset D$  và  $W \subset F'$  để mỗi hàm  $f : M \rightarrow F$  được thác triển chỉnh hình đến  $D$  nếu  $u \circ f$  có một thác triển chỉnh hình đến  $D$  với mỗi  $u \in W$ .

**Từ khóa:** *Tuyến tính hóa, không gian lồi địa phương, bất biến tôpô tuyến tính, chỉnh hình vô hạn chiều, hàm chỉnh hình.*

\*Tác giả liên hệ chính.

Email: nguyenvandai@qnu.edu.vn

# Holomorphic extensions of weakly holomorphic functions in weighted spaces of holomorphic functions

Nguyen Van Dai

*Faculty of Mathematics and Statistics, Quy Nhon University, Vietnam*

*Received: 17/09/2020; Accepted: 17/10/2020*

## ABSTRACT

Let  $v$  be a weight on a domain  $D$  in a metrizable locally convex space  $E$  and  $F$  be a complete locally convex space. Denote  $H_v(D, F)$  the weighted space of  $F$ -valued holomorphic functions on  $D$ , and  $A_v(D)$  is a subspace of  $H_v(D, \mathbb{C})$  with the closed unit ball which is compact for the open-compact topology. Using a linearization theorem of weighted spaces of holomorphic functions in this paper, we set up characterizations for  $M \subset D$  and  $W \subset F'$  such that every function  $f : M \rightarrow F$  can be holomorphically extended to the whole domain  $D$  in the case  $u \circ f$  admits a holomorphic extension to  $D$  for every  $u \in W$ .

**Keywords:** *Linearization, locally convex spaces, topological linear invariants, infinite-dimensional holomorphy, holomorphic functions*

## 1. INTRODUCTION

Let  $E, F$  be locally convex spaces and  $D$  a domain (open, connected set) in  $E$ . Holomorphic functions on  $D$  with values in  $F$  are useful in analytic functional calculus and in the theory of 1-parameter semigroups. As far as we know, in functional analysis, essentially two approaches to analyticity of vector-valued functions are through the notions of a (very) weakly holomorphic and a (strongly) holomorphic function, and the first way is easier to check in practical examples. Here, a function  $f : D \rightarrow F$  is (very) weakly holomorphic if  $u \circ f$  is holomorphic for each  $u \in F'$ . It is known that holomorphic functions are always (very) weakly holomorphic. It seems that the first answer of the question

“what conditions decide the holomorphy of a (very) weakly holomorphic function” belongs to Dunford,<sup>1</sup> who proved that the class of Banach-valued (very) weakly holomorphic functions defining on a domain in  $\mathbb{C}$  satisfies the requirement. Grothendieck<sup>2</sup> extended the result for the case the underlying spaces are quasicomplete. The assertion, in fact, is true in the case where  $E, F$  are Hausdorff locally convex spaces and  $E$  is metrizable (see<sup>3</sup> [Théorème 1.2.10]). Then, it is natural to ask (addressed by Grosse-Erdmann,<sup>4,5</sup> Arendt and Nikolski<sup>6</sup>) whether or not (proper/smallest) subsets  $W$  of the dual  $F'$  of the underlying spaces  $F$  such that a function  $f$  is holomorphic whenever  $f$  is (not very) weak holomorphic, i.e.  $u \circ f$  is holomorphic for all  $u \in W$ . In other

---

\*Corresponding author.  
Email: Nguyenvandai@qnu.edu.vn

words, we have to determine the minimal assumptions under which a weakly holomorphic function is (strongly) holomorphic as well. Arendt and Nikolski considered this problem when  $D \subset \mathbb{C}$  and  $F$  is a complex Banach space. Let  $W \subset F'$  be a subset and  $\sigma(F, W)$  be the weak topology on  $F$  induced by  $W$ . A result in <sup>6</sup> claimed that a  $\sigma(F, W)$ -holomorphic function  $f : D \rightarrow F$  is holomorphic if and only if  $W$  determines boundedness, in the sense that each  $\sigma(F, W)$ -bounded set in  $F$  is bounded. If  $f : D \rightarrow F$  is additionally assumed to be locally bounded then  $f$  is holomorphic when  $W$  is just a separating subspace of  $F'$ . A generalization of this result to the case where  $F$  is a locally complete locally convex space was obtained by Grosse-Erdmann. <sup>5</sup> Under additional assumptions that  $E$  and  $F$  satisfy some linear topological invariants, in <sup>7</sup>, Hai extended the results of Arendt and Nikolski in <sup>6</sup> for the case where  $f$  defines on an open set  $D$  either in a Schwartz-Fréchet space  $E \in (\Omega)$  with values in a Schwartz-Fréchet space  $F \in (LB_\infty)$  or in  $\mathbb{C}$  with values in a Fréchet space  $F \in (LB_\infty)$  <sup>7</sup> [Theorems 4.1, 4.2]. Note that, in the case of  $E = \mathbb{C}$  the hypothesis “Schwartz” for  $F$  is superfluous. Recently, Quang, Lam and Dai <sup>8</sup> have considered the above problem in the cases where Fréchet spaces  $E, F$  have stronger conditions,  $E \in (\Omega)$  and  $F \in (LB_\infty)$  or  $F \in (DN)$ ; but the locally boundedness of  $f$  is dropped to a weaker property, the boundedness on bounded sets in  $D$ .

This question is closely related to the problem of holomorphic extension. One of the extension results given by Bogdanowicz <sup>9</sup> through weak extension says that a function  $f$  defined on a domain  $D_1$  in  $\mathbb{C}$  with values in a sequentially complete,

complex locally convex Hausdorff space  $F$  such that  $u \circ f$  can be holomorphically extended to a domain  $D_2 \supset D_1$  for each  $u \in F'$ , must admit a holomorphic extension to  $D_2$ .

More recently, Grosse - Erdmann, <sup>5</sup> Arendt and Nikolski, <sup>6</sup> Bonet, Frerick and Jordá, <sup>10</sup> Frerick and Jordá, <sup>11</sup> Frerick, Jordá and Wengenroth <sup>12</sup> have given results in this way but with requiring extensions of  $u \circ f$  only for a proper subset  $W \subset F'$  and the conditions on  $D_1$  are smoother. Also, Laitila and Tylli <sup>13</sup> have recently discussed the difference between strong and weak definitions for important spaces of vector-valued functions. Most recently, this problem is also investigated for more general cases, for instance, on Fréchet spaces with the linear topological invariants by Quang, Lam and Dai, <sup>8</sup> Quang and Dai; <sup>14,15</sup> and for weakly meromorphic functions by Quang and Lam <sup>16,17</sup>.

The aim of this paper is to investigate the holomorphic extension of holomorphic functions in a subspaces of the weighted space  $H_v(D, F)$  of *weakly-type holomorphic functions* of a between locally convex spaces given by

$$A_v(D, F) :=$$

$$\{f : D \rightarrow F : u \circ f \in A_v(D) \forall u \in F'\}.$$

The rest of the paper is organized as follows. Section 2 presents some preliminaries. The main results will be introduced in Section 3. We give the conditions for subsets  $W \subset F'$  under which every  $F$ -valued function  $f$  can be extended (unique) to a function  $\tilde{f} \in A_v(D, F)$  from a (thin) subset of uniqueness (Theorems 3.2, 3.3) and from a (fat) sampling subset (Theorem 3.4)  $M$  of  $D$  whenever  $u \circ f$  admits a unique extension  $f_u \in A_v(D)$  for

all  $u \in W$ .

The main tool for our proofs will be the linearization theorems in  $A_v(D, F)$  that has been proven by T. T. Quang et al. in <sup>18</sup>.

Our notation for locally convex spaces and functional analysis is standard and we refer to the book of Jarchow.<sup>19</sup> A locally convex space is always a complex vector space with a locally convex Hausdorff topology.

For more background and details about the theory of infinite dimensional holomorphy we refer to <sup>20</sup> and the reference given therein.

## 2. PRELIMINARIES

### 2.1. General notations

We always assume that the locally convex structure of a Fréchet space  $E$  is generated by an increasing system  $\{\|\cdot\|_k\}_{k \in \mathbb{N}}$  of seminorms. Then we denote by  $E_k$  the completion of the canonically normed space  $E/\ker \|\cdot\|_k$ , by  $\omega_k : E \rightarrow E_k$  the canonical map and by  $U_k$  the set  $\{x \in E : \|x\|_k < 1\}$ . Sometimes it is convenient to assume that  $\{U_k\}_{k \in \mathbb{N}}$  is a neighbourhood basis of zero (shortly  $\mathcal{U}(E)$ ).

If  $B$  is an absolutely convex subset of  $E$  we define a norm  $\|\cdot\|_B^*$  on  $E'$ , the strongly dual space of  $E$  with values in  $[0, +\infty]$  by

$$\|u\|_B^* = \sup\{|u(x)|, x \in B\}.$$

Obviously  $\|\cdot\|_B^*$  is the gauge functional of  $B^\circ$ . Instead of  $\|\cdot\|_{U_k}^*$  we write  $\|\cdot\|_k^*$ . By  $E_B$  we denote the linear hull of  $B$  which becomes a normed space in a canonical way if  $B$  is bounded. The space  $E$  is called *locally complete* if for every absolutely convex, closed and bounded  $B$  of  $E$  the space  $E_B$  is Banach.

**Definition 2.1.** Let  $F$  be a locally convex space. A subset  $W$  of  $F'$  is called

- *separating* if  $u(x) = 0$  for each  $u \in W$  implies  $x = 0$ . Clearly this is equivalent to the span of  $W$  being weak\*-dense (or dense in the co-topology);
- *determining boundedness* if every subset  $B \subset F$  is bounded whenever  $u(B)$  is bounded in  $\mathbb{C}$  for all  $u \in W$ . This holds if and only if every  $\sigma(F, \text{span}W)$ -bounded set is  $F$ -bounded. Obviously, the linear span of such sets is  $\sigma(F', F)$ -dense;

Clearly, if  $W \subset F'$  determines boundedness in  $F'$  then  $W$  is separating.

### 2.2. Weighted spaces of holomorphic functions

Let  $E$  and  $F$  be locally convex spaces and  $D$  be a domain in  $E$ . By  $H(D, F)$  we denote the vector space of all holomorphic. Instead of  $H(D, \mathbb{C})$ , we write  $H(D)$ .

For a domain  $D$  in  $E$ , a *weight*  $v : D \rightarrow (0, \infty)$  is a continuous function which is strictly positive. The space

$$\begin{aligned} H_v(D, F) &:= \\ &\{f \in H(D, F) : (v \cdot f)(D) \text{ is bounded on } D\} \\ &= \{f \in H(D, F) : \\ &\quad \|f\|_{v,p} := \sup_{x \in D} v(x)p(f(x)) < \infty \\ &\quad \forall p \in cs(F)\} \end{aligned}$$

equipped with the topology generated by the family  $\{\|\cdot\|_{v,p}\}_{p \in cs(F)}$  of semi-norms. Then  $H_v(D, F)$  is complete whenever  $F$  is complete, in particular, it is Banach if  $F$  is Banach. It is easy to check that

$$H_v(D, F) = \varprojlim_{p \in cs(F)} H_v(D, F_p)$$

where  $F_p$  is the completion of the canonically normed space  $F/\ker p$ .

We also write

$$\begin{aligned} H_v(D) &:= H_v(D, \mathbb{C}) = \\ &= \{f \in H(D) : \\ &\quad \|f\|_v := \sup_{x \in D} v(x)|f(x)| < \infty\}. \end{aligned}$$

**Remark 2.1.** In the case  $E$  is metrizable we have

$$H(D, F) = H(D, F)_w$$

$$:= \{f : D \rightarrow F : u \circ f \in H(D) \forall u \in F'\}$$

(see <sup>3</sup> [Theorem 1.2.10], also (<sup>20</sup> [Example 3.8(g)]).

Let  $A_v(D)$  be a subspace of  $H_v(D)$  such that the closed unit ball  $B_{A_v(D)}$  is compact for the topology  $\tau_0$ . Note that this condition implies that  $A_v(D)$  is norm-closed and hence Banach because  $H_v(D)$  is Banach.

In <sup>21</sup> [Theorem 7] Jordá showed that if, for  $m \in \mathbb{N}$ , the space  $\mathcal{P}^{(m)}E$  of continuous  $m$ -homogeneous polynomials on a Fréchet  $E$ , endowed with its norm topology, is contained  $H_v(D)$  then the closed unit ball of  $\mathcal{P}^{(m)}E$  is compact for the topology  $\tau_0$ .

Another illustrative example of  $A_v(D, F)$  has been built by Quang in <sup>22</sup>. We briefly sketch this example as follows.

Let  $D$  be a balanced, bounded open set in a Fréchet space  $E$ . Let  $v$  be a weight on  $D$  satisfying the following conditions:

- (i)  $v$  is radial in the sense that

$$v(\lambda z) = v(z)$$

$$\forall z \in D, \forall \lambda \in \partial\Delta := \{\lambda \in \mathbb{C} : |\lambda| = 1\},$$

- (ii)  $v$  vanishes at infinity outside compact sets of  $D$  in the sense, if for every  $\varepsilon > 0$  there exists a compact subset  $K$  of  $D$  such that  $|v(z)| < \varepsilon$  for all  $z \in D \setminus K$ .

For each  $f \in H(D)$  we consider the Taylor series representation at zero

$$f(z) = \sum_{k=0}^{\infty} (P_k f)(z), \quad z \in D,$$

where  $P_n f$  is a  $k$ -homogeneous polynomial,  $k = 0, 1, \dots$ . The series converges to  $f$  uniformly on each compact subset of  $D$ .

Now for each  $n \geq 0$  we consider the linear operator

$$C_n : H_v(D) \rightarrow H_v(D)$$

given by Cesàro means  $C_n f$  of the partial sums of the Taylor series of  $f$  :

$$(C_n f)(z) = \frac{1}{n+1} \sum_{j=0}^n \sum_{k=0}^j (P_k f)(z), \quad z \in D.$$

Put

$$C_{n,v}(D) = C_n(H_v(D)),$$

$$C_v(D) = \bigcup_{n \geq 0} C_{n,v}(D),$$

$$A_v(D) = \overline{C_v(D)}^{\tau_v}.$$

Then we have the following

**Proposition 2.1** (<sup>22</sup> Proposition 4).

Let  $D$  be a balanced, bounded open set in a Fréchet-Montel space  $E$  having the  $(BB)_{\infty}$ -property and  $v$  be a weight on  $D$  which vanishes at infinity outside compact sets of  $D$ . Then, the closed unit ball of  $(A_v(D), \|\cdot\|_v)$  is  $\tau_0$ -compact.

Here, we recall that a locally convex space  $E$  has the  $(BB)_n$ -property if each bounded subset of  $\widehat{\otimes}_{n,s,\pi} E$  is contained in  $\overline{\text{acx}}(\otimes_{n,s} B)$  for some bounded subset  $B$  of  $E$ , where

$$\otimes_{n,s} B := \{x \otimes \dots \otimes x : x \in B\}$$

and  $\otimes_{n,s,\pi} E$  denotes the space  $\otimes_{n,s} E$  endowed with the projective topology  $\tau_\pi$  and  $\widehat{\otimes_{n,s,\pi} E}$  is its completion.

If  $E$  has  $(BB)_n$  for all  $n$  we say that  $E$  has  $(BB)_\infty$ -property.

### 3. THE PROBLEM OF WEIGHTED HOLOMORPHIC EXTENSIONS

In this section we present the main results of the paper. First, we recall the linearization theorem which has been proven in [18].

Let us denote by  $P_{A_v(D)}$  the closed subspace of all linear functionals  $u \in (A_v(D), \|\cdot\|_v)'$  such that  $u|_{B_{A_v(D)}}$  is  $\tau_0$ -continuous.

By the Ng Theorem [23] [Theorem 1] the evaluation mapping

$$J : (A_v(D), \|\cdot\|_v) \rightarrow (P_{A_v(D)})'$$

given by

$$(Jf)(u) = u(f) \quad \forall u \in P_{A_v(D)},$$

is a topological isomorphism. This is why the space  $P_{A_v(D)}$  is called the predual of  $A_v(D)$ .

**Theorem 3.1.** *Let  $v$  be a weight on a domain  $D$  in a metrizable locally convex space  $E$  and  $A_v(D)$  be a subspace of  $H_v(D)$  such that the closed unit ball is  $\tau_0$ -compact. Then there exists a mapping  $\delta_D \in H(D, P_{A_v(D)})$  with the following universal property: For each complete locally convex space  $F$ , a function  $f \in A_v(D, F)$  if and only if there is a unique mapping  $T_f \in L(P_{A_v(D)}, F)$  such that  $T_f \circ \delta_D = f$ . This property characterizes  $P_{A_v(D)}$  uniquely up to an isometric isomorphism.*

Moreover, the mapping

$$\Phi : f \in A_v(D, F) \mapsto T_f \in (L(P_{A_v(D)}, F), \tau_c)$$

$$:= \varprojlim_{p \in cs(F)} (L(P_{A_v(D)}, F_p))$$

is a topological isomorphism.

Note that,  $\delta_D : D \rightarrow P_{A_v(D)}$  is the evaluation mapping given by

$$\delta_D(x) = \delta_x$$

with  $\delta_x(g) := g(x)$  for all  $g \in A_v(D)$ .

First we present some notions which will be needed in subsequent sections.

A subset  $M \subseteq D$  is said to be a *set of uniqueness for  $A_v(D)$*  if each  $f \in A_v(D)$  such that  $f|_M = 0$  then  $f \equiv 0$ .

A subset  $M \subset D$  is said to be *sampling for  $A_v(D)$*  if there exists a constant  $C \geq 1$  such that for every  $f \in A_v(D)$  we have

$$\sup_{z \in D} v(z)|f(z)| \leq C \sup_{z \in M} v(z)|f(z)|. \quad (3.1)$$

**Remark 3.1.** For  $M \subset D$ , denote

$$M_v^* := \{v(x)\delta_x : x \in M\} \subset B_{P_{A_v(D)}}$$

where  $B_{P_{A_v(D)}}$  denotes the unit ball of  $P_{A_v(D)}$ .

1. Since the closed unit ball  $B_{A_v(D)}$  of the space  $A_v(D)$  is  $\tau_0$ -compact, by the Hahn-Banach theorem, it is easy to check that the following are equivalent:

- (i)  $M$  is a set of uniqueness for  $A_v(D)$ ;
- (ii)  $M_v^*$  is separating in  $A_v(D)$ ;
- (iii)  $\langle M_v^* \rangle := \text{span} M_v^*$  is  $\sigma(P_{A_v(D)}, A_v(D))$ -dense.

2. For the norm given by

$$\|f\|_{M,v} := \sup_{z \in M} v(z)|f(z)|$$

on  $A_v(D)$ , it is obvious that the following are equivalent:

- (i)  $M$  is a sampling for  $A_v(D)$ ;

(ii)  $\| \cdot \|_v \simeq \| \cdot \|_{M,v}$  on  $A_v(D)$ .

3. Obviously, if  $M$  is sampling for  $A_v(D)$  then  $M_v^*$  is separating in  $A_v(D)$ , hence,  $M$  is a set of uniqueness for  $A_v(D)$ .

Given a Fréchet space  $E$ , an increasing sequence  $\{B_n\}_n$  of bounded subsets of  $E'$  is said to *fix the topology* if the polars  $\{B_n^\circ\}_n$  taken in  $E$  form a fundamental system of 0-neighbourhoods of  $E$ . Let us recall the following result.

**Lemma 3.1** (<sup>11</sup>, Proposition 7). *Let  $\{B_n\}_n$  be an increasing sequence of bounded subsets of  $F'$ . The following assertions are equivalent:*

- (i)  $\{B_n\}_n$  fixes the topology of  $F$ ;
- (ii)  $F'((B_n)_{n \in \mathbb{N}})$  determines boundedness in  $F$ ;
- (iii)  $\text{span} \bigcup_n \overline{B_n}^{\sigma(F',F)}$  determines boundedness in  $F$ .

**Theorem 3.2.** *Let  $v$  be a weight on a domain  $D$  in a metrizable locally convex space and  $A_v(D)$  a subspace of  $H_v(D)$  such that the closed unit ball  $B_{A_v(D)}$  is  $\tau_0$ -compact. Let  $M \subset D$  be a set of uniqueness for  $A_v(D)$ . Let  $F$  be a complete locally convex space and  $W \subset F'$  be a subspace which determines boundedness in  $F$ . If  $f : M \rightarrow F$  is a function such that  $u \circ f$  has an extension  $f_u \in A_v(D)$  for each  $u \in W$  then  $f$  admits a unique extension  $\tilde{f} \in A_v(D, F)$ .*

*Chứng minh.* By Remark 3.1,  $\langle M_v^* \rangle$  is  $\sigma(P_{A_v(D)}, A_v(D))$ -dense, and hence it is norm-dense.

Now we take a function  $f : M \rightarrow F$  satisfying the assumptions of Theorem.

Put  $T : \langle M_v^* \rangle \rightarrow F$ ,  $T(\delta_x) := f(x)$ . Since  $W$  is separating,  $T$  is well defined.

Let  $x = \sum_{k=1}^n \alpha_k v(x_k) \delta_{x_k} \in B_{\langle M_v^* \rangle}$ , the unit ball of  $\langle M_v^* \rangle$ . For each  $u \in W$  we have the estimate

$$\begin{aligned} |\langle Tx, u \rangle| &= \left| \left\langle \sum_{k=1}^n \alpha_k v(x_k) f(x_k), u \circ f \right\rangle \right| \\ &= \left| \left\langle \sum_{k=1}^n \alpha_k v(x_k) \delta_{x_k}, u \circ f \right\rangle \right| \\ &\leq \|u \circ f\|_v. \end{aligned}$$

This means that  $T(B_{\langle M_v^* \rangle})$  is  $\sigma(F, W)$ -bounded and then it is bounded. Thus,  $T$  is a bounded linear mapping. Since  $\langle M_v^* \rangle$  is norm-dense in  $P_{A_v(D)}$  we can extend  $T$  to  $\tilde{T} : P_{A_v(D)} \rightarrow F$ . Now, the proof is complete by applying Theorem 3.1.  $\square$

In the case where  $D$  is a domain in a Banach space, by Montel's theorem, the closed unit ball  $B_{H_v(D)}$  of the space  $H_v(D)$  is  $\tau_0$ -compact. Therefore, from Theorem 3.1 and Remark 2.1 we get the following:

**Corollary 3.1.** *Let  $D$  be a domain in a Banach space and  $v$  be a weight on  $D$  and  $M \subset D$  be a set of uniqueness for  $H_v(D)$ . Let  $F$  be a complete locally convex space and  $W \subset F'$  be a subspace which determines boundedness in  $F$ . If  $f : M \rightarrow F$  is a function such that  $u \circ f$  has an extension  $f_u \in H_v(D)$  for each  $u \in W$  then  $f$  admits a unique extension  $\tilde{f} \in H_v(D, F)$ .*

**Theorem 3.3.** *Let  $v$  be a weight on a domain  $D$  in a metrizable locally convex space and  $A_v(D)$  a subspace of  $H_v(D)$  such that the closed unit ball  $B_{A_v(D)}$  is  $\tau_0$ -compact. Let  $M \subset D$  be a set of uniqueness for  $A_v(D)$ . Let  $F$  be a Fréchet space and  $W = \cup_n B_n \subset F'$  where  $\{B_n\}_n$  fixes the topology of  $F$ . If  $f : M \rightarrow F$  is a function such that  $u \circ f$  has an extension*

$f_u \in A_v(D)$  for each  $u \in W$  and  $\{f_u\}_{u \in B_n}$  is bounded in  $A_v(D)$  for all  $n$  then  $f$  admits a unique extension  $\tilde{f} \in A_v(D, F)$ .

*Chứng minh.* By Lemma 3.1,

$$\tilde{W} := \text{span} \bigcup_n \overline{B_n}^{\sigma(F', F)}$$

determines boundedness in  $F$ . For each  $u \in \tilde{W}$  we write  $u$  in the form

$$u = \sum_{i=1}^{n_0} \alpha_i u_i$$

with  $u_i \in \overline{B_i}^{\sigma(F', F)}$ ,  $i = 1, \dots, n_0$ . Because  $\{B_n\}_n$  is increasing we have  $u \in (\sum_{i=1}^{n_0} \alpha_i) \overline{B_{n_0}}^{\sigma(F', F)}$ . Without loss of generality we can assume that  $\sum_{i=1}^{n_0} \alpha_i = 1$ . Then there exists  $\{u_k^0\}_k \subset B_{n_0}$  such that  $u_k^0 \rightarrow u$  in the topology  $\sigma(F', F)$ . It follows from the hypothesis that  $\{f_{u_k^0}\}_k$  is a bounded sequence in  $A_v(D)$  and  $\{f_{u_k^0}(x)\}$  converges to  $u(f(x))$  for each  $x \in M$ . Therefore, by <sup>18</sup>[Theorem 4.3], there exists  $f_u \in A_v(D)$  such that  $\{f_{u_k^0}(x)\}$  converges  $f_u(x)$  for each  $x \in D$ . Then, since  $u \in \tilde{W}$  is arbitrary, the conclusion is a consequence of Theorem 3.2.  $\square$

**Theorem 3.4.** *Let  $v$  be a weight on a domain  $D$  in a metrizable locally convex space and  $A_v(D)$  a subspace of  $H_v(D)$  such that the closed unit ball  $B_{A_v(D)}$  is  $\tau_0$ -compact. Let  $M$  be a sampling set for  $A_v(D)$  and  $W$  a  $\sigma(F', F)$ -dense subspace of the dual  $F'$  of a locally complete locally convex space  $F$ . If  $f : M \rightarrow F$  is a function such that*

$$\sup_{x \in M} v(x)p(f(x)) < \infty \quad \text{for all } p \in cs(F) \tag{3.2}$$

and  $u \circ f$  has an extension  $f_u \in A_v(D)$  for each  $u \in W$  then  $f$  admits a unique extension  $\tilde{f} \in A_v(D, F)$ .

*Chứng minh.* Consider the Banach space

$$\ell_1(M) := \left\{ \alpha := (\alpha_x)_{x \in M} : M \rightarrow \mathbb{C} : \|\alpha\| := \sum_{x \in M} |\alpha_x| < \infty \right\}$$

where  $\alpha_x = \alpha(x)$  and the sum is defined by

$$\sum_{x \in M} |\alpha_x| := \sup \left\{ \sum_{x \in \gamma} |\alpha_x| : \gamma \text{ a finite subset of } M \right\}.$$

Put

$$\ell_1(M_v^*) := \left\{ g \in P_{A_v(D)} : \exists (\alpha_x)_{x \in M} \in \ell_1(M) : g = \sum_{x \in M} \alpha_x v(x) \delta_x \right\}$$

where

$$\sum_{x \in M} \alpha_x v(x) \delta_x := \lim_{\gamma \in \mathcal{F}_M} \sum_{x \in \gamma} \alpha_x v(x) \delta_x$$

with  $\mathcal{F}_M$  be the directed set of all finite sets of  $M$  ordered under inclusion. It is easy to check that the space  $\ell_1(M_v^*)$  is Banach with the following norm

$$\|g\|_M := \inf \left\{ \sum_{x \in M} |\alpha_x| v(x) \|\delta_x\| : (\alpha_x)_{x \in M} \in \widehat{g}_{\ell_1} \right\}$$

where

$$\widehat{g}_{\ell_1} = \left\{ (\beta_x)_{x \in M} \in \ell_1(M) : g = \sum_{x \in M} \beta_x v(x) \delta_x = \sum_{x \in M} \alpha_x v(x) \delta_x \right\}.$$

We denote  $P_{A_{M,v}(D)}$  the predual of  $(A_v(D), \|\cdot\|_{M,v})$  and  $B_{P_{M,v}(D)}$  is its unit ball. Define

$$S : \ell_1(M) \rightarrow P_{A_{M,v}(D)}$$

by

$$S((\alpha_x)_{x \in M}) := \sum_{x \in M} \alpha_x v(x) \delta_x.$$



It is easy to see that  $S$  is bounded linear, moreover

$$B_{P_{M,v}(D)} \subset \overline{\text{acx}}(M_v^*) \subseteq \overline{S(B_{\ell_1(M)})}.$$

Since  $\|\cdot\|_v \simeq \|\cdot\|_{M,v}$  (see Remark 3.1)  $S : \ell_1(M) \rightarrow P_{A_v(D)}$  is bounded. Then, by the Schauder lemma <sup>24</sup> [Lemma 3.9],  $S$  is open and then surjective. This implies that the injection of  $\ell_1(M_v^*)$  is an onto isomorphism. Therefore, for each  $g \in P_{A_v(D)}$  there exists  $\alpha := (\alpha_x)_{x \in M} \in \ell_1(M)$  such that

$$g = \sum_{x \in M} \alpha_x v(x) \delta_x.$$

Take  $f$  as in the hypothesis. We define  $T : P_{A_v(D)} \rightarrow F$  with  $T(g) := \sum_{x \in M} \alpha_x v(x) f(x)$ . Since (3.2) the series is convergent. Moreover, if  $\sum_{x \in M} \alpha_x v(x) \delta_x = 0$  then for all  $u \in W$  we have

$$\begin{aligned} u\left(\sum_{x \in M} \alpha_x v(x) f(x)\right) &= \left\langle \sum_{x \in M} \alpha_x v(x) \delta_x, f_u \right\rangle \\ &= 0, \end{aligned}$$

and then, because  $W$  is separating,  $T$  is well defined. From (3.2) and  $\|\cdot\|_v \simeq \|\cdot\|_{M,v}$ , it implies that  $T(B_{P_{A_v(D)}})$  is bounded. Finally, the proof is complete by applying Theorem 3.1.  $\square$

## ACKNOWLEDGMENTS

This study is conducted within the framework of science and technology projects at institutional level of Quy Nhon University under the project code T2020.654.02.

## REFERENCES

1. N. Dunford. Uniformity in linear spaces, *Trans. Amer. Math. Soc.*, **1938**, 44(2), 305-356.

2. A. Grothendieck. Sur certains espaces de fonctions holomorphes. I, *Journal für die Reine und Angewandte Mathematik*, **1953**, 192, 35-64.
3. Ph. Noverraz. Pseudo-convexite, Convexite Polynomiale et Domaines d'Holomorphie en Dimension Infinie, *North-Holland Math. Stud.*, **1973**, 3.
4. K. G. Grosse-Erdmann. *The Borel-Okada theorem revisited*, Habilitationsschrift Fernuniversität Hagen, Hagen, 1992.
5. K. G. Grosse-Erdmann. A weak criterion for vector-valued holomorphy, *Math. Proc. Cambridge Philos. Soc.*, **2004**, 136, 399-411.
6. W. Arendt and N. Nikolski. Vector-valued holomorphic functions revisited, *Math. Z.*, **2000**, 234, 777-805.
7. L. M. Hai. The property  $(LB_\infty)$  and Frechet-valued holomorphic functions on compact sets, *Vietnam J. Math.*, **2002**, 31(3), 281-294.
8. T. T. Quang, L. V. Lam and N. V. Dai. On  $\sigma(\cdot, W)$ -holomorphic functions and theorems of Vitali-type, *Complex Anal. Oper. Theory*, **2013**, 7(1), 237-259.
9. W. M. Bogdanowicz. Analytic continuation of holomorphic functions with values in a locally convex space, *Proc. Amer. Math. Soc.*, **1969**, 22, 660-666.
10. J. Bonet, L. Frerick and E. Jordá. Extension of vector valued holomorphic and harmonic functions, *Studia Math.*, **2007**, 183, 225-248.

11. L. Frerick and E. Jordá. Extension of vector-valued functions, *Bull. Belg. Math. Soc. Simon Stevin*, **2007**, *14*(3), 499-507.
12. L. Frerick, E. Jordá and J. Wengenroth. Extension of vector-valued functions, *Math. Nachr.*, **2009**, *282*, 690-696.
13. J. Laitila and H.-O. Tylli. Composition operators on vector-valued harmonic functions and Cauchy transforms, *Indiana Univ. Math. J.*, **2006**, *55*(2), 719-746.
14. T. T. Quang and N. V. Dai. On the holomorphic extension of vector valued functions, *Complex Anal. Oper. Theory*, **2015**, *9*(3), 567-591.
15. T. T. Quang and N. V. Dai. On Hartogs extension theorems for separately  $(\cdot, W)$ -holomorphic functions, *International J. Math.*, **2014**, *25*(12), 15 pages.
16. T. T. Quang and L. V. Lam. Levi extension theorems for meromorphic functions of weak type in infinite dimension, *Complex Anal. Oper. Theory*, **2016**, *10*, 1619-1654.
17. T. T. Quang and L. V. Lam. Cross theorems for separately  $(\cdot, W)$ -meromorphic functions, *Taiwan. J. Math.*, **2016**, *20*(5), 1009-1039.
18. T. T. Quang, N. V. Dai, L. V. Lam and D. T. Vy. Linearization of Weakly Holomorphic Functions in Weighted Spaces and Its Applications, (*sub. to Results in Math.*).
19. H. Jarchow. *Locally Convex Spaces*, Teubner Stuttgart, 1981.
20. S. Dineen. *Complex Analysis on Infinite Dimensional Spaces*, Springer, New York, 1999.
21. E. Jordá. Weighted Vector-Valued Holomorphic Functions on Banach Spaces, *Abstract and Applied Analysis*, **2013**, 501592, 1-9.
22. T. T. Quang. On Some Classes of Weighted Spaces of Weakly Holomorphic Functions, (*to appear in Acta. Math. Vietnam.*)
23. K. F. Ng. On a theorem of Dixmier, *Math. Scand.*, **1971**, *29*, 279-280.
24. R. Meise and D. Vogt. *Introduction to Functional Analysis*, The Clarendon Press Oxford University Press, New York, NY, USA, 1997.

## Một số bất đẳng thức cho đa thức ma trận

Phạm Quang Hưng\*, Phạm Nữ Ngọc Diệp

Sinh viên lớp Sư phạm Toán K40, khoa Sư phạm, Trường Đại học Quy Nhơn, Việt Nam

Ngày nhận bài: 20/05/2020; Ngày đăng bài: 27/06/2020

### TÓM TẮT

Đa thức ma trận (đôi khi được gọi là  $\lambda$ -ma trận) là đa thức một biến phức với hệ số là các ma trận. Đa thức ma trận đóng một vai trò quan trọng trong khoa học và kỹ thuật. Mục đích chính của bài báo này là nghiên cứu một số bất đẳng thức có liên quan đến giá trị riêng và chuẩn của đa thức ma trận.

**Từ khóa:** Đa thức ma trận, bất đẳng thức, giá trị riêng, chuẩn.

\* Tác giả liên hệ chính.

Email: phamquanghung720@gmail.com

## Some inequalities for matrix polynomials

Pham Quang Hung\*, Pham Nu Ngoc Diep

*Student of Mathematics Pedagogy class - Course 40, Faculty of Education, Quy Nhon University, Vietnam*

*Received: 20/05/2020; Accepted: 27/06/2020*

### ABSTRACT

A matrix polynomial (sometimes known as a  $\lambda$ -matrix) is a polynomial of a complex variable with matrix coefficients. Matrix polynomials play a crucial role in science and engineering. The main aim of this paper is to study some inequalities which are related to eigenvalues and norms of matrix polynomials.

**Key words:** *Matrix polynomial, inequalities, eigenvalue, norm.*

### 1. INTRODUCTION

Let  $\mathbb{C}^{n \times n}$  denote the set of scalar matrices of size  $n \times n$  whose entries are complex numbers. For a *matrix polynomial* we mean the matrix-valued function of a complex variable of the form

$$P(z) = A_d z^d + \dots + A_1 z + A_0,$$

where  $A_i \in \mathbb{C}^{n \times n}$  for all  $i = 0, \dots, d$ . If  $A_d \neq 0$ ,  $P(z)$  is called a matrix polynomial of *degree*  $d$ . When  $A_d = I$ , the identity matrix in  $\mathbb{C}^{n \times n}$ , the matrix polynomial  $P(z)$  is called a *monic*.

A number  $\lambda \in \mathbb{C}$  is called an *eigenvalue* of the matrix polynomial  $P(z)$ , if there exists a nonzero vector  $x \in \mathbb{C}^n$  such that  $P(\lambda)x = 0$ . Then the vector  $x$  is called, as usual, an *eigenvector* of  $P(z)$  associated to the eigenvalue  $\lambda$ . Note that each eigenvalue of  $P(z)$  is a root of the *characteristic polynomial*  $\det(P(z))$ .

The *polynomial eigenvalue problem (PEP)* is to find an eigenvalue  $\lambda$  and a non-zero vector  $x \in \mathbb{C}^n$  such that  $P(\lambda)x = 0$ . For  $m = 1$ , (PEP) is actually the *generalized eigenvalue problem (GEP)*

$$Ax = \lambda Bx,$$

and, in addition, if  $B = I$ , we have the standard eigenvalue problem

$$Ax = \lambda x.$$

For  $m = 2$  we have the *quadratic eigenvalue problem (QEP)*.

The theory of matrix polynomials was primarily devoted by two works, both of which are strongly motivated by the theory of *vibrating systems*: one by Frazer, Duncan, and Collar in 1938 [FDC], and the other by P. Lancaster in 1966.<sup>1</sup>

(QEPs), and more generally (PEPs), play an important role in applications to science and engineering. We refer to the book of I. Gohberg, P. Lancaster and L. Rodman<sup>2</sup> for a theory of matrix polynomials and their applications.

Matrix analysis is a research field of basic interest and has applications in scientific computing, control and systems theory, operations research, mathematical physics, statistics, economics and engineering disciplines. Sometimes it is also needed in other areas of pure mathematics.

A lot of theorems in matrix analysis appear in the form of inequalities. Given any complex-valued function defined on matrices, there are inequalities for it. We may say that matrix inequalities reflect the quantitative aspect of matrix analysis.

In this paper, we propose some inequalities which are related to eigenvalues and norms of matrix polynomials.

The paper is organized as follows. In the

\*Corresponding author.

Email: phamquanghung720@gmail.com

next section we recall some preliminaries. In Section 3 we establish some inequalities related to norms of matrix polynomials. Finally, in the last section we propose some inequalities for eigenvalues of matrix polynomials.

**2. PRELIMINARIES**

Throughout this paper, by a positive integer  $p$  we mean  $p \geq 1$  or  $p = \infty$ .

For a matrix  $A = (a_{ij}) \in \mathbb{C}^{m \times n}$ , a positive integer  $p$  and a vector  $p$ -norm  $|\cdot|_p$  on  $\mathbb{C}^n$ , the matrix  $p$ -norm of  $A$  is defined by

$$|A|_p := \begin{cases} \left( \sum_{i,j=1}^n |a_{ij}|^p \right)^{\frac{1}{p}}, & (1 \leq p < \infty), \\ \max_{i,j=1,\dots,n} |a_{ij}|, & (p = \infty). \end{cases}$$

The operator  $p$ -norm of  $A$  is defined by  $\|A\|_p := \max\{|Ax|_p : |x|_p = 1\}$ .

For any matrix  $A \in \mathbb{C}^{n \times n}$ , the number

$$\rho(A) := \max\{|\lambda|, \lambda \in \sigma(A)\}$$

is called the spectral radius of  $A$ , where  $\sigma(A)$  denotes the spectrum of  $A$ , i.e. the set of all eigenvalues of  $A$ .

The spectral radius can be compared to the operator  $p$ -norm, as follows.

**Lemma 2.1.**<sup>3</sup>. For any  $A \in \mathbb{C}^{n \times n}$ ,  $\rho(A) \leq \|A\|_p$ .

For a  $(d + 1)$  - tuple  $\mathbf{A} = (A_0, \dots, A_d)$  of matrices  $A_i \in \mathbb{C}^{n \times n}$ , the matrix polynomial

$$P_{\mathbf{A}}(z) = A_d z^d + \dots + A_1 z + A_0$$

is called the matrix polynomial associated to  $\mathbf{A}$ . The spectrum of the matrix polynomial  $P_{\mathbf{A}}(z)$  is defined by

$$\sigma(\mathbf{A}) := \sigma(P_{\mathbf{A}}(z)) = \{\lambda \in \mathbb{C} | \det(P_{\mathbf{A}}(z)) = 0\},$$

which is the set of all its eigenvalues.

For a monic matrix polynomial  $P_{\mathbf{A}}(z) = I \cdot z^d + A_{d-1} z^{d-1} + \dots + A_1 z + A_0$ , with  $A_i \in \mathbb{C}^{n \times n}$ , the  $(dn \times dn)$ -matrix

$$C_{\mathbf{A}} := \begin{bmatrix} 0 & I & 0 & \dots & 0 \\ 0 & 0 & I & \dots & 0 \\ \vdots & \vdots & \vdots & \ddots & \vdots \\ 0 & 0 & 0 & \dots & I \\ -A_0 & -A_1 & -A_2 & \dots & -A_{d-1} \end{bmatrix}$$

is called the companion matrix of the matrix polynomial  $P_{\mathbf{A}}(z)$  or of the tuple  $(A_0, \dots, A_{d-1}, I)$ .

Note that the spectrum  $\sigma(A)$  of  $P_{\mathbf{A}}(z)$  coincides to the spectrum  $\sigma(C_{\mathbf{A}})$  of  $C_{\mathbf{A}}$ <sup>2</sup>

For two  $(d+1)$ -tuples  $\mathbf{A} = (A_0, \dots, A_{d-1}, I)$  and  $\bar{\mathbf{A}} = (\bar{A}_0, \dots, \bar{A}_{d-1}, I)$ , the relation between the operator norms of their difference and those of their companion matrices is given in the following lemma.

**Lemma 2.2.**<sup>4</sup>. Let  $\mathbf{A} = (A_0, \dots, A_{d-1}, I)$  and  $\bar{\mathbf{A}} = (\bar{A}_0, \dots, \bar{A}_{d-1}, I)$  be  $(d + 1)$ -tuples. Then for any integer  $p > 0$ , we have

$$\|C_{\mathbf{A}} - C_{\bar{\mathbf{A}}}\|_p = \|\mathbf{A} - \bar{\mathbf{A}}\|_p.$$

**Theorem 2.1.**<sup>5</sup>. Let  $Z \in \mathbb{C}^{n \times n}$  be a positive definite matrix with extremal eigenvalues  $a, b$ . Then for all vectors  $h \in \mathbb{C}^n$ ,

$$|h|_p \cdot |Zh|_p \leq \frac{(\frac{a}{b})^{\frac{1}{2}} + (\frac{b}{a})^{\frac{1}{2}}}{2} \langle h, Zh \rangle,$$

where  $|\cdot|_p$  denotes the matrix  $p$ -norm.

For a vector  $x \in \mathbb{C}^n$ . Note that  $x^*$  is the conjugate transpose of  $x$ .

Concerning inequalities of eigenvalues of scalar matrices, we have the following results obtained by Hassan (2014).

**Theorem 2.2.**<sup>6</sup>. Let  $A \in \mathbb{C}^{n \times n}$  be a positive definite matrix and  $x$  and  $y \in \mathbb{C}^n$  such that  $|x| = |y| = 1$  and  $x^*y = 0$ . Assume that the eigenvalues of  $A$ , in increasing order, are  $\lambda_1 \leq \lambda_2 \leq \dots \leq \lambda_n$ . Then we have the following Wielandt inequalities.

- (1)  $|x^*Ay| \leq \frac{\lambda_n - \lambda_1}{\lambda_n + \lambda_1} \sqrt{(x^*Ax)(y^*Ay)}$ ;
- (2)  $|x^*Ax - y^*Ay| \leq \frac{\lambda_n - \lambda_1}{\lambda_n + \lambda_1} ((x^*Ax + y^*Ay)^2 - 4(x^*Ay)^2)^{\frac{1}{2}}$ ;
- (3)  $|x^*Ay|^2 \leq \max \left\{ \left( \frac{\lambda_i - \lambda_j}{\lambda_i^r + \lambda_j^r} \right)^2 \right\}_{\substack{i,j=1 \\ i \neq j}}^n (x^*A^r x) \cdot (y^*A^r y)$ .

**Theorem 2.3.**<sup>6</sup>. Let  $A \in \mathbb{C}^{n \times n}$  be a positive definite matrix and  $x$  and  $y \in \mathbb{C}^n$  such that  $|x| = |y| = 1$  and  $x^*y = 0$ . Assume that the eigenvalues of  $A$ , in increasing order, are  $\lambda_1 \leq \lambda_2 \leq \dots \leq \lambda_n$ . Then

$$|x^*Ay| \leq \frac{1}{2} \frac{\lambda_n - \lambda_1}{\lambda_n + \lambda_1} (x^*Ax + y^*Ay).$$

**Theorem 2.4.**<sup>6</sup>. Assume that  $A$  is a positive definite matrix of size  $n$ , and let the eigenvalues of  $A$ , in increasing order, be  $\lambda_1 \leq \lambda_2 \leq \dots \leq \lambda_n$ . Then

$$|x^*Ax - y^*Ay| \leq \frac{\lambda_n - \lambda_1}{\lambda_n + \lambda_1} (x^*Ax + y^*Ay).$$

### 3. SOME INEQUALITIES FOR NORMS OF MATRIX POLYNOMIALS

In this section, we will propose some inequalities for norms of matrix polynomials.

For an  $(d+1)$ -tuple  $\mathbf{A} = (A_0, \dots, A_{d-1}, A_d)$  of matrices  $A_i \in \mathbb{C}^{n \times n}$ .  $\|\mathbf{A}\|_p := \max\{|Ax|_p : |x|_p = 1\}$  with  $\mathbf{A}$  is a matrix of dimension  $(d+1)n \times n$ .

Firstly, we establish some properties of norms of tuples of matrices.

**Proposition 3.1.** Let  $\mathbf{A} = (A_0, \dots, A_{d-1}, A_d)$  and  $\mathbf{B} = (B_0, \dots, B_{d-1}, B_d)$ , where  $A_i, B_j \in \mathbb{C}^{n \times n}$ . Then for any positive integer  $p$ , the followings hold true.

- (1) There is a constant  $c \geq 0$  such that  $|Av|_p \leq c|v|_p$  for any vector  $v \in \mathbb{C}^n$ .
- (2)  $\|\mathbf{A}\|_p \geq 0$ , with equality if and only if  $\mathbf{A} = \mathbf{0}$ .
- (3)  $\|\mathbf{A} + \mathbf{B}\|_p \leq \|\mathbf{A}\|_p + \|\mathbf{B}\|_p$ .
- (4)  $\|c\mathbf{A}\|_p = |c| \cdot \|\mathbf{A}\|_p$ , for  $c \in \mathbb{R}$ .
- (5)  $\|\mathbf{A}^T \mathbf{B}\|_p \leq \|\mathbf{A}^T\|_p \|\mathbf{B}\|_p$ .
- (6)  $\|\mathbf{A}\|_p = \|\mathbf{A}^T\|_p$ .
- (7)  $\|\mathbf{A}^T \mathbf{A}\|_p = \|\mathbf{A} \mathbf{A}^T\|_p = \|\mathbf{A}\|_p^2$ .
- (8)  $|(\mathbf{A}v, w)| \leq \|\mathbf{A}\|_p \cdot |v|_p \cdot |w|_p$ , for any  $v \in \mathbb{C}^n$  and  $w \in \mathbb{C}^{(d+1)n \times n}$ .
- (9)  $\|\mathbf{A}\|_1 \leq n^2 \|\mathbf{A}\|_p$ .

*Proof.* Note that for a matrix  $A = (a_{ij}) \in \mathbb{C}^{m \times n}$ ,  $p \in \mathbb{Z}^+$

$\|A\|_p = \inf\{c \geq 0 : |Ax|_p \leq c|x|_p, x \in \mathbb{C}^n\}$ .  
 (1) For any vector  $v \in \mathbb{C}^n$ , we have

$$\mathbf{A}v = \begin{bmatrix} A_0v \\ A_1v \\ \vdots \\ A_dv \end{bmatrix}.$$

For  $1 \leq p < \infty$ , we have

$$|\mathbf{A}v|_p^p = \sum_{i=0}^d |A_i v|_p^p.$$

For each  $i = 0, \dots, d$ , there exists  $c_i > 0$  such that  $|A_i v|_p \leq c_i |v|_p$ , for all  $i = 0, \dots, d$ .

Taking  $c' = \max_{i=0, \dots, d} \{c_i\}$ , we get  $|\mathbf{A}v|_p \leq c|v|_p$ , where  $c = c'(d+1)^{1/p}$ .

For  $p = \infty$ , we have

$$|\mathbf{A}v|_\infty = \max_{i=0, \dots, d} |A_i v|_\infty.$$

For each  $i = 0, \dots, d$ , there exists  $c_i > 0$  such that  $|A_i v|_\infty \leq c_i |v|_\infty$ , for all  $i = 0, \dots, d$ .

Taking  $c = \max_{i=0, \dots, d} \{c_i\}$ , we have  $|\mathbf{A}v|_\infty \leq c|v|_\infty$ .

(2) It is obvious that  $\|\mathbf{A}\|_p \geq 0$ .

$\|\mathbf{A}\|_p = 0$  if and only if

$$|\mathbf{A}x|_p = 0 \Leftrightarrow \left\| \begin{bmatrix} A_0x \\ \vdots \\ A_dx \end{bmatrix} \right\|_p = 0$$

$$\Leftrightarrow |A_i x|_p = 0, \forall i = 0, \dots, d.$$

$$\Leftrightarrow \|A_i\|_p = 0, \forall i = 0, \dots, d.$$

$$\Leftrightarrow A_i = 0, \forall i = 0, \dots, d.$$

Thus  $\mathbf{A} = \mathbf{0}$ .

(3) We have

$$\|\mathbf{A} + \mathbf{B}\|_p = \max\{|(\mathbf{A} + \mathbf{B})x|_p : |x|_p = 1\}.$$

For any  $x \in \mathbb{C}^n$  such that  $|x|_p = 1$ , we have

$$|(\mathbf{A} + \mathbf{B})x|_p = |\mathbf{A}x + \mathbf{B}x|_p \leq |\mathbf{A}x|_p + |\mathbf{B}x|_p.$$

Taking maximum over all  $x \in \mathbb{C}^n$  such that

$|x|_p = 1$ , we obtain  $\|\mathbf{A} + \mathbf{B}\|_p \leq \|\mathbf{A}\|_p + \|\mathbf{B}\|_p$ .

(4) We have  $\|c\mathbf{A}\|_p = \max\{|c\mathbf{A}x|_p : |x|_p = 1\}$

$$= \max\{|c| \cdot |\mathbf{A}x|_p : |x|_p = 1\}$$

$$= |c| \cdot \max\{|\mathbf{A}x|_p : |x|_p = 1\}$$

$$= |c| \cdot \|\mathbf{A}\|_p.$$

(5) For any  $x \in \mathbb{C}^n$  such that  $|x|_p = 1$ , we have

$$|(\mathbf{A}^T \mathbf{B})x|_p = |\mathbf{A}^T(\mathbf{B}x)|_p$$

$$\leq \|A^T\| \|Bx\|_p \leq \|A^T\| \|B\| \|x\|_p.$$

Thus  $\|A^T B\| \leq \|A^T\| \|B\|$ .

(6) For any vector  $x \in \mathbb{C}^n$ , we have

$$\begin{aligned} |Ax|_p^2 &= |(Ax, Ax)| = |(x, A^T Ax)| \\ &\leq |x|_p \cdot |A^T Ax|_p \text{ (Cauchy-Schwarz inequality)} \\ &\leq \|A^T A\|_p \cdot |x|_p^2 \\ \Rightarrow |Ax|_p^2 &\leq \|A^T A\|_p \cdot |x|_p^2 \\ \Rightarrow |Ax|_p &\leq \sqrt{\|A^T A\|_p} \cdot |x|_p \\ \Rightarrow \|A\|_p &\leq \sqrt{\|A^T A\|_p} \\ \Rightarrow \|A\|_p^2 &\leq \|A^T A\|_p \leq \|A^T\|_p \|A\|_p. \end{aligned} \tag{3}$$

When  $A \neq 0$ , we receive  $\|A\|_p \leq \|A^T\|_p$  and  $\|A^T\|_p \leq \|(A^T)^T\|_p$ . So  $\|A\|_p = \|A^T\|_p$ .

(7) From (5) and (6), we have  $\|A\|_p^2 \leq \|A^T A\|_p \leq \|A^T\|_p \|A\|_p = \|A\|_p^2$

Thus  $\|A\|_p^2 = \|A^T A\|_p$ .

(8) For any  $v \in \mathbb{C}^n, w \in \mathbb{C}^{(d+1)n \times n}$ , apply the Cauchy-Schwarz inequality, we obtain

$$|(Av, w)| \leq |Av|_p \cdot |w|_p \leq \|A\|_p \cdot |v|_p \cdot |w|_p.$$

(9) From (8), let  $v = e_i \in \mathbb{C}^n, w = e_j \in \mathbb{C}^{(d+1)n}$ , we have

$$|a_{ij}| = |(Ae_i, e_j)| \leq \|A\|_p$$

with  $i = 1, \dots, n$  and  $j = 1, \dots, (d+1)n$ .

Hence,  $\sum_{i,j=1}^n |a_{ij}| \leq n^2 \|A\|_p$  and  $\|A_0\| \leq n^2 \|A\|$ .

Similarly  $\|A_i\| \leq n^2 \|A\|_p, \forall i = 0, \dots, d$ .

Therefore,  $\max_{i=0, \dots, d} \|A_i\| \leq n^2 \|A\|_p$ .

Thus  $\|A\|_1 \leq n^2 \|A\|_p$ .

In order to prepare for main results of this section, we need the following lemmas.

**Lemma 3.1.** Let  $P_{\bar{A}}(\lambda) = I \cdot \lambda^d$  be a monic matrix polynomial whose corresponding companion matrix is  $C_{\bar{A}}$ . Then for any integer  $p > 0$ , we have

$$\|C_{\bar{A}}\|_p \leq 1.$$

*Proof.* We have

$$C_{\bar{A}} = \begin{bmatrix} 0 & I & 0 & \dots & 0 \\ 0 & 0 & I & \dots & 0 \\ \vdots & \vdots & \vdots & & \vdots \\ 0 & 0 & 0 & \dots & I \\ 0 & 0 & 0 & \dots & 0 \end{bmatrix}.$$

For any  $x = (x_1, x_2, \dots, x_{dn})^T \in \mathbb{C}^{dn}$  such that

$|x|_p = 1$ , we have

$$C_{\bar{A}} x = \begin{bmatrix} 0 & I & 0 & \dots & 0 \\ 0 & 0 & I & \dots & 0 \\ \vdots & \vdots & \vdots & & \vdots \\ 0 & 0 & 0 & \dots & I \\ 0 & 0 & 0 & \dots & 0 \end{bmatrix} \begin{bmatrix} x_1 \\ \cdot \\ \cdot \\ \cdot \\ x_{dn} \end{bmatrix} = \begin{bmatrix} x_{n+1} \\ \cdot \\ x_{dn} \\ 0 \\ \cdot \\ 0 \end{bmatrix}$$

and

$$\left\| \begin{bmatrix} x_{n+1} \\ \cdot \\ x_{dn} \\ 0 \\ \cdot \\ 0 \end{bmatrix} \right\|_p = \begin{cases} (\sum_{i=n+1}^{dn} |x_i|^p)^{\frac{1}{p}}, & p \geq 1 \\ \max_{i=n+1, \dots, dn} |x_i|, & p = \infty. \end{cases}$$

Moreover,

$$\left( \sum_{i=n+1}^{dn} |x_i|^p \right)^{\frac{1}{p}} \leq \left( \sum_{i=1}^{dn} |x_i|^p \right)^{\frac{1}{p}} = |x|_p = 1$$

and

$$\max_{i=n+1, \dots, dn} |x_i| \leq 1.$$

Thus

$$\left\| \begin{bmatrix} x_{n+1} \\ \cdot \\ x_{dn} \\ 0 \\ \cdot \\ 0 \end{bmatrix} \right\|_p \leq 1, \text{ for any } p \geq 1.$$

It follows that  $|C_{\bar{A}} x|_p \leq 1$  for any  $p \geq 1$ . Since  $\|C_{\bar{A}}\|_p = \max\{|C_{\bar{A}} x|_p : |x|_p = 1\}$ , we have  $\|C_{\bar{A}}\|_p \leq 1$ .

The proof is complete.

**Lemma 3.2.** Let  $A = (A_0, \dots, A_{d-1}, I)$  and  $\bar{A} = (0, \dots, 0, I)$  be  $(d+1)$ -tuples. Then for any integer  $p > 0$ , we have

$$\|A - \bar{A}\|_p \leq \|A\|_p.$$

*Proof.* We have

$$\|A - \bar{A}\|_p = \max\{|(A - \bar{A})x|_p : |x|_p = 1\}.$$

Note that the  $(d+1)$ -tuple  $(A - \bar{A}) = (A_0, A_1, \dots, A_{d-1}, 0)$  is a matrix of dimension

$(d + 1)n \times n$ :

$$\mathbf{A} - \bar{\mathbf{A}} = \begin{bmatrix} A_0 \\ A_1 \\ \vdots \\ A_{d-1} \\ 0 \end{bmatrix}.$$

Then, with  $x = (x_1, \dots, x_n)^T \in \mathbb{C}^n$ , we have

$$(\mathbf{A} - \bar{\mathbf{A}})x = \begin{bmatrix} A_0 \\ A_1 \\ \vdots \\ A_{d-1} \\ 0 \end{bmatrix} x = \begin{bmatrix} A_0 x \\ A_1 x \\ \vdots \\ A_{d-1} x \\ 0 \end{bmatrix} = \begin{bmatrix} t_1 \\ \vdots \\ t_n \\ \vdots \\ t_{dn} \\ 0 \\ \vdots \\ 0 \end{bmatrix},$$

with  $\begin{bmatrix} t_{in+1} \\ \vdots \\ t_{(i+1)n} \end{bmatrix} = A_i x, \forall i = 0, \dots, d - 1$ .

Thus

$$\begin{aligned} |(\mathbf{A} - \bar{\mathbf{A}})x|_p &= \left( \sum_{i=1}^{dn} |t_i|^p \right)^{1/p} \\ &\leq \left( \sum_{i=1}^{dn} |t_i|^p + \sum_{j=1}^n |x_j|^p \right)^{1/p} \quad (1). \end{aligned}$$

We also have

$$\mathbf{A}x = \begin{bmatrix} A_0 x \\ A_1 x \\ \vdots \\ A_{d-1} x \\ Ix \end{bmatrix} = \begin{bmatrix} t_1 \\ \vdots \\ t_n \\ \vdots \\ t_{dn} \\ x_1 \\ \vdots \\ x_n \end{bmatrix},$$

and  $|Ax|_p = \left( \sum_{i=1}^{dn} |t_i|^p + \sum_{j=1}^n |x_j|^p \right)^{1/p} \quad (2)$ .

It follows from (1) and (2) that

$$|(\mathbf{A} - \bar{\mathbf{A}})x|_p \leq |Ax|_p.$$

Then  $\max\{|(\mathbf{A} - \bar{\mathbf{A}})x|_p : |x|_p = 1\} \leq \max\{|Ax|_p : |x|_p = 1\}$ .

Thus  $\|\mathbf{A} - \bar{\mathbf{A}}\|_p \leq \|\mathbf{A}\|_p$ .

The proof is complete.

The first main result in this section is presented as follows, which is a version for matrix polynomials of Lemma 2.1.

**Theorem 3.1.** Let  $P_{\mathbf{A}}(\lambda) = I.\lambda^d + A_{d-1}\lambda^{d-1} + \dots + A_1\lambda + A_0$  be a monic matrix polynomial whose corresponding  $(d + 1)$ - tuple is  $\mathbf{A} = (A_0, \dots, A_{d-1}, I)$ . Then for any integer  $p > 0$ , we have

$$\rho(\mathbf{A}) \leq \|\mathbf{A}\|_p + 1.$$

*Proof.* It follows from Lemma 2.1 that

$$\rho(C_{\mathbf{A}}) \leq \|C_{\mathbf{A}}\|_p.$$

From the sub-additivity of the operator  $p$ -norm, we have

$$\|C_{\mathbf{A}}\|_p \leq \|C_{\mathbf{A}} - C_{\bar{\mathbf{A}}}\|_p + \|C_{\bar{\mathbf{A}}}\|_p,$$

where  $C_{\bar{\mathbf{A}}}$  is the companion matrix of the matrix polynomial  $P_{\bar{\mathbf{A}}}(\lambda) = I.\lambda^d$ .

It follows from Lemma 3.1 and Lemma 3.2 that

$$\|C_{\mathbf{A}} - C_{\bar{\mathbf{A}}}\|_p \leq \|\mathbf{A}\|_p \quad \text{and} \quad \|C_{\bar{\mathbf{A}}}\|_p \leq 1.$$

Since  $\rho(\mathbf{A}) = \rho(C_{\mathbf{A}})$ , we have

$$\rho(\mathbf{A}) \leq \|\mathbf{A}\|_p + 1.$$

The proof is complete.

For a matrix  $A \in \mathbb{C}^{n \times n}$ . If  $A$  is positive definite matrix then we write  $A > 0$ .

Now we establish a version for matrix polynomials of Theorem 2.1.

**Theorem 3.2.** Let  $P_{\mathbf{A}}(\lambda) = \sum_{i=0}^d A_i \lambda^i$  be a matrix polynomial with  $A_i > 0$ . Let  $a_i, b_i$  be extremal eigenvalues of  $A_i$ , for all  $i=0, \dots, d$ . Then for any vector  $h \in \mathbb{C}^n$ , we have

$$|h|_p \cdot |P_{\mathbf{A}}(\lambda).h|_p \leq H \langle h, P_{\mathbf{A}}(|\lambda|)h \rangle,$$

where  $H = \max \left\{ \frac{a_i + b_i}{2\sqrt{a_i b_i}} \right\}_{i=0}^d$ .

*Proof.* We have

$$\begin{aligned} |h|_p \cdot |P_{\mathbf{A}}(\lambda).h|_p &= |h|_p \cdot \left| \sum_{i=0}^d A_i \lambda^i . h \right|_p, \\ &\leq |h|_p \cdot \sum_{i=0}^d |A_i \lambda^i . h|_p, \\ &\leq |h|_p \cdot \sum_{i=0}^d (|A_i . h|_p) (|\lambda^i|), \\ &= \sum_{i=0}^d (|h|_p \cdot |A_i . h|_p) \cdot (|\lambda^i|). \end{aligned}$$

It follows from Theorem 2.1 that

$$|h|_p \cdot |A_i . h|_p \leq \frac{\left(\frac{a_i}{b_i}\right)^{\frac{1}{2}} + \left(\frac{b_i}{a_i}\right)^{\frac{1}{2}}}{2} \cdot \langle h, A_i h \rangle.$$

Thus



$$\begin{aligned}
 & |h|_p |P_A(\lambda) \cdot h|_p \\
 & \leq \sum_{i=0}^d \left( \frac{\left(\frac{a_i}{b_i}\right)^{\frac{1}{2}} + \left(\frac{b_i}{a_i}\right)^{\frac{1}{2}}}{2} \right) \langle h, A_i h \rangle \cdot |\lambda|^i \\
 & \leq H \cdot \sum_{i=0}^d \langle h, A_i h \rangle \cdot |\lambda|^i \\
 & = H \cdot \sum_{i=0}^d \langle h, A_i h \rangle \\
 & = H \cdot \left\langle h, \sum_{i=0}^d A_i |\lambda|^i \cdot h \right\rangle \\
 & = H \cdot \langle h, P_A(|\lambda|) h \rangle.
 \end{aligned}$$

The proof is complete.

#### 4. SOME INEQUALITIES FOR EIGENVALUES OF MATRIX POLYNOMIALS

In this section we establish some inequalities for eigenvalues of matrix polynomials.

Firstly, we propose a version of Theorem 2.2 for matrix polynomials.

**Theorem 4.1.** Let  $P_A(\lambda) = \sum_{i=0}^d A_i \lambda^i$  be a

matrix polynomial whose coefficient matrices  $A_i \in \mathbb{C}^{n \times n}$  are positive definite. Let  $x, y \in \mathbb{C}^n$  be such that  $|x| = |y| = 1$  and  $x^* y = 0$ . Assume  $\sigma(A_i) = \{\lambda_1^i, \dots, \lambda_{n_i}^i\}$  is the spectrum of the matrix  $A_i$  and  $\lambda_1^i \leq \lambda_2^i \leq \dots \leq \lambda_{n_i}^i$ , for all  $i = 0, \dots, d$ . Then the followings hold true.

$$(1) |x^* P_A(\lambda) y| \leq K ((x^* P_A(|\lambda|) x)(y^* P_A(|\lambda|) y))^{\frac{1}{2}}.$$

$$\begin{aligned}
 (2) |x^* P_A(\lambda) x - y^* P_A(\lambda) y| \\
 \leq K ((d+1)(x^* P_A(|\lambda|) x + y^* P_A(|\lambda|) y)^2 \\
 - 4(x^* P_A(|\lambda|) y)^2)^{\frac{1}{2}}.
 \end{aligned}$$

Here  $K = \max_{i=0}^d \left\{ \frac{\lambda_{n_i}^i - \lambda_1^i}{\lambda_{n_i}^i + \lambda_1^i} \right\}$ .

*Proof.* (1) We have

$$|x^* P_A(\lambda) y| = \left| \sum_{i=0}^d x^* A_i \lambda^i y \right| \leq \sum_{i=0}^d |x^* A_i y| \cdot |\lambda|^i.$$

It follows from Theorem 2.2 (1) that

$$\begin{aligned}
 \sum_{i=0}^d |x^* A_i y| |\lambda|^i & \leq \sum_{i=0}^d \left( \frac{\lambda_{n_i}^i - \lambda_1^i}{\lambda_{n_i}^i + \lambda_1^i} \right) \cdot (x^* A_i x)^{\frac{1}{2}} \cdot (y^* A_i y)^{\frac{1}{2}} \cdot |\lambda|^i \\
 & \leq K \cdot \sum_{i=0}^d (x^* A_i |\lambda|^i x)^{\frac{1}{2}} \cdot (y^* A_i |\lambda|^i y)^{\frac{1}{2}} \\
 & \leq K \cdot \left( \sum_{i=0}^d x^* A_i |\lambda|^i x \right)^{\frac{1}{2}} \cdot \left( \sum_{i=0}^d y^* A_i |\lambda|^i y \right)^{\frac{1}{2}}
 \end{aligned}$$

$$\begin{aligned}
 & = K \cdot (x^* (\sum_{i=0}^d A_i |\lambda|^i) x)^{\frac{1}{2}} \cdot (y^* (\sum_{i=0}^d A_i |\lambda|^i) y)^{\frac{1}{2}} \\
 & = K \cdot \sqrt{(x^* P_A(|\lambda|) x)(y^* P_A(|\lambda|) y)}.
 \end{aligned}$$

The proof is complete.

(2) Similarly to the arguments given in (1).

**Theorem 4.2.** Let  $P_A(\lambda) = \sum_{i=0}^d A_i \lambda^i$  be a

matrix polynomial whose coefficient matrices  $A_i \in \mathbb{C}^{n \times n}$  are positive definite for all  $i = 0, \dots, d$  and  $A_i A_j > 0$  for all  $i, j = 0, \dots, d$ . Let  $x, y \in \mathbb{C}^n$  such that  $|x| = |y| = 1$  and  $x^* y = 0$ . Assume  $\sigma(A_i) = \{\lambda_1^i, \dots, \lambda_{n_i}^i\}$  is the spectrum of the matrix  $A_i$  and  $\lambda_1^i \leq \lambda_2^i \leq \dots \leq \lambda_{n_i}^i$ , for all  $i = 0, \dots, d$ . Then, we have

$$\begin{aligned}
 & |x^* P_A(\lambda) y|^2 \leq \\
 & \begin{cases} M \cdot (x^* P_A^2(|\lambda|) x)(y^* P_A^2(|\lambda|) y) & , |\lambda| \geq 1 \\ M \cdot (x^* P_A^2(|\lambda+2|) x)(y^* P_A^2(|\lambda+2|) y) & , |\lambda| < 1, \end{cases}
 \end{aligned}$$

where  $M = (d+1) \cdot \max_{m \neq k} \left\{ \max_{m, k=1}^n \left\{ \left( \frac{\lambda_m^i - \lambda_k^i}{(\lambda_m^i)^2 + (\lambda_k^i)^2} \right)^2 \right\} \right\}_{i=0}^d$ .

*Proof.* We have

$$\begin{aligned}
 |x^* P_A(\lambda) y|^2 & = \left( \sum_{i=0}^d x^* A_i \lambda^i y \right)^2 \\
 & \leq (d+1) \sum_{i=0}^d (x^* A_i y)^2 (\lambda^i)^2.
 \end{aligned}$$

It follows from Theorem 2(3) that

$$\begin{aligned}
 (d+1) \sum_{i=0}^d (x^* A_i y)^2 (\lambda^i)^2 & \leq (d+1) \cdot \\
 \sum_{i=0}^d \max_{m \neq k} \left\{ \left( \frac{\lambda_m^i - \lambda_k^i}{(\lambda_m^i)^2 + (\lambda_k^i)^2} \right)^2 \right\}_{m, k=1}^{n_i} (x^* A_i^2 x)(y^* A_i^2 y) (\lambda^i)^2 \\
 & \leq M \cdot \sum_{i=0}^d (x^* A_i^2 x)(y^* A_i^2 y) (|\lambda^i|)^2.
 \end{aligned}$$

When  $|\lambda| \geq 1$ :

$$|x^* P_A(\lambda) y|^2 \leq M \cdot \sum_{i=0}^d (x^* A_i^2 x)(y^* A_i^2 y) (|\lambda^i|)^4$$

$$\begin{aligned}
 & = M \cdot \sum_{i=0}^d (x^* A_i^2 |\lambda|^i x)(y^* A_i^2 |\lambda|^i y) \\
 & \leq M \cdot \sqrt{\left( \sum_{i=0}^d (x^* A_i^2 |\lambda|^i x)^2 \right) \cdot \left( \sum_{i=0}^d (y^* A_i^2 |\lambda|^i y)^2 \right)}.
 \end{aligned}$$

Since  $A_i^2 > 0, \forall i = 0, \dots, d$ , thus,

$$\begin{aligned}
 |x^* P_A(\lambda) y|^2 & \leq M \cdot \sqrt{\left( \sum_{i=0}^d x^* A_i^2 |\lambda|^i x \right)^2 \cdot \left( \sum_{i=0}^d y^* A_i^2 |\lambda|^i y \right)^2} \\
 & = M \cdot \left[ x^* \left( \sum_{i=0}^d A_i^2 |\lambda|^i \right) x \right] \cdot \left[ y^* \left( \sum_{i=0}^d A_i^2 |\lambda|^i \right) y \right].
 \end{aligned}$$

Since  $A_i A_j > 0, \forall i = 0, \dots, d, i \neq j$  hence

$$|x^* P_A(\lambda) y|^2 \leq M \cdot \left[ x^* \left( \sum_{i=0}^d A_i |\lambda^i| \right)^2 x \right] \cdot \left[ y^* \left( \sum_{i=0}^d A_i |\lambda^i| \right)^2 y \right]$$

$$= M \cdot (x^* P_A^2(|\lambda|) x) (y^* P_A^2(|\lambda|) y).$$

When  $|\lambda| < 1$ :

It is easy to see that  $|\lambda|^2 \leq (|\lambda + 2|^i)^4$ . Hence

$$|x^* P_A(\lambda) y|^2 \leq M \cdot \sum_{i=0}^d (x^* A_i^2 x) (y^* A_i^2 y) \cdot (|\lambda + 2|^i)^4$$

$$= M \cdot \sum_{i=0}^d (x^* A_i^2 (|\lambda + 2|^i)^2 x) \cdot (y^* A_i^2 (|\lambda + 2|^i)^2 y).$$

Similarly, we receive

$$|x^* P_A(\lambda) y|^2 \leq M \cdot (x^* P_A^2(|\lambda + 2|) x) (y^* P_A^2(|\lambda + 2|) y).$$

The proof is complete.

**Theorem 4.3.** Let  $P_A(\lambda) = \sum_{i=0}^d A_i \lambda^i$  be a

matrix polynomial whose coefficient matrices  $A_i \in \mathbb{C}^{n \times n}$  are positive definite for all  $i = 0, \dots, d$ . Let  $x, y \in \mathbb{C}^n$  such that  $|x| = |y| = 1$  and  $x^* y = 0$ . Assume  $\sigma(A_i) = \{\lambda_1^i, \dots, \lambda_{n_i}^i\}$  is spectrum of matrix  $A_i$  and  $\lambda_1^i \leq \lambda_2^i \leq \dots \leq \lambda_{n_i}^i$ , for all  $i = 0, \dots, d$ . Then we have

$$|x^* P_A(\lambda) y| \leq \frac{1}{2} K \cdot \left( x^* P_A(|\lambda|) x + y^* P_A(|\lambda|) y \right),$$

where  $K = \max \left\{ \frac{\lambda_{n_i}^i - \lambda_1^i}{\lambda_{n_i}^i + \lambda_1^i} \right\}_{i=0}^d$ .

*Proof.* We have

$$|x^* P_A(\lambda) y| = \left| \sum_{i=0}^d x^* A_i \lambda^i y \right| \leq \sum_{i=0}^d |x^* A_i y| \cdot |\lambda|^i$$

$$\leq \sum_{i=0}^d \frac{1}{2} \left( \frac{\lambda_{n_i}^i - \lambda_1^i}{\lambda_{n_i}^i + \lambda_1^i} \right) (x^* A_i x + y^* A_i y) \cdot |\lambda|^i$$

$$\leq \frac{1}{2} K \cdot \sum_{i=0}^d (x^* A_i |\lambda|^i x + y^* A_i |\lambda|^i y)$$

$$\leq \frac{1}{2} K \cdot \left( \sum_{i=0}^d x^* A_i |\lambda|^i x + \sum_{i=0}^d y^* A_i |\lambda|^i y \right)$$

$$= \frac{1}{2} K \cdot \left( x^* P_A(|\lambda|) x + y^* P_A(|\lambda|) y \right).$$

The proof is complete.

**Theorem 4.4.** Let  $P_A(\lambda) = \sum_{i=0}^d A_i \lambda^i$  be a

matrix polynomial whose coefficient matrices  $A_i \in \mathbb{C}^{n \times n}$  are positive definite for all  $i = 0, \dots, d$ . Assume  $\sigma(A_i) = \{\lambda_1^i, \dots, \lambda_{n_i}^i\}$  is spectrum of matrix  $A_i$  and  $\lambda_1^i \leq \lambda_2^i \leq \dots \leq \lambda_{n_i}^i$ , for all  $i = 0, \dots, d$ . Then we have

$$|x^* P_A(\lambda) x - y^* P_A(\lambda) y| \leq K \cdot \left( x^* P_A(|\lambda|) x + y^* P_A(|\lambda|) y \right),$$

with  $K = \max \left\{ \frac{\lambda_{n_i}^i - \lambda_1^i}{\lambda_{n_i}^i + \lambda_1^i} \right\}_{i=0}^d$ .

## REFERENCES

1. P. Lancaster. *Lambda-matrices and vibrating systems*, Pergamon, Oxford, 1966.
2. I. Gohberg, P. Lancaster and L. Rodman. *Matrix Polynomials*, Academic Press, New York, 1982.
3. R.A. Horn and C.R. Johnson. *Matrix Analysis*, Cambridge University Press, 1999.
4. C.-T. Le, On Wielandt-Mirsky's conjecture for matrix polynomials, *Bull. Korean Math. Soc.* **2019**, 56 (5), 1273-1283.
5. E.-Y. Lee, A matrix reverse Cauchy – Schwarz inequality, *Linear Alg. Appl.* **2009**, 430 (2-3), 805-810.
6. M. A. Hasan, Generalized Wielandt and Cauchy-Schwarz Inequalities, in *Proc. Amer. Contr. Conf., Boston*, **2014**, 2142–2147.

# Thuật toán khai phá đồ thị con thường xuyên theo mô hình MapReduce

Trần Thiên Thành\*, Trần Thị Liên, Nguyễn Thị Kim Phượng

*Khoa Công nghệ thông tin, Trường Đại học Quy Nhơn, Việt Nam*

*Ngày nhận bài: 05/05/2020; Ngày nhận đăng: 03/07/2020*

## TÓM TẮT

Trong bài báo này chúng tôi trình bày về thuật toán gSpanMR, một thuật toán khai phá đồ thị con thường xuyên theo mô hình lập trình MapReduce. Thuật toán gSpanMR (gSpan MapReduce) được phát triển dựa trên kết quả mã hóa đồ thị bằng DFS code của thuật toán gSpan và thuật toán khai phá đồ thị con thường xuyên trên mô hình MapReduce FSM-H. Thuật toán được cài đặt và thực nghiệm trên cụm máy tính sử dụng nền tảng Hadoop cho thấy tốc độ có cải tiến so với thuật toán FSM-H.

**Từ khóa:** *Khai phá đồ thị con thường xuyên, MapReduce, DFS Code.*

---

\*Tác giả liên hệ chính.

Email: [tranthienthanh@qnu.edu.vn](mailto:tranthienthanh@qnu.edu.vn)

# A frequent subgraph mining algorithm on the MapReduce model

Tran Thien Thanh\*, Tran Thi Lien, Nguyen Thi Kim Phuong

*Faculty of Information Technology, Quy Nhon University, Vietnam*

*Received: 05/05/2020; Accepted: 03/07/2020*

## ABSTRACT

In this paper, we present the gSpanMR algorithm, a frequent subgraph mining on the MapReduce programming model. The gSpanMR algorithm (gSpan MapReduce) was developed based on the results of encoding graphs using the DFS code in gSpan algorithm and FSM-H algorithm on the MapReduce model. gSpanMR algorithm has been installed and tested on computer clusters using Hadoop platform, which shows better execution time than FSM-H algorithm.

**Keywords:** *Frequent subgraph mining, MapReduce, DFS Code.*

## 1. INTRODUCTION

Frequent subgraph mining has been an emerging data mining problem with many scientific and commercial applications. There exist many algorithms for solving the in-memory version of frequent subgraph mining task, most notable among them are AGM,<sup>1</sup> FSG,<sup>2</sup> gSpan,<sup>3</sup> Gaston,<sup>4</sup> and DMTL.<sup>5</sup> These methods assume that the dataset is small and the mining task finishes in a reasonable amount of time using an in-memory method. To consider the large data scenario, a few traditional database based graph mining algorithms, such as, DB-Subdue,<sup>6</sup> and DB-FSG<sup>7</sup> and OOFSG<sup>8</sup> are also proposed. The kernel of frequent subgraph mining is subgraph isomorphism test. Lots of well-known pair-wise isomorphism testing algorithms were developed. However, the frequent subgraph mining problem was not explored well. One approach used by many researchers to solve problems with large data and complexity is to

use parallel computational models on computer clusters. We use the results of DFS code proposed in gSpan algorithm<sup>3</sup> combined with the idea of implementing FSM-H algorithm<sup>9</sup> on Hadoop to build the gSpanMR algorithm to frequent subgraphs mining on the MapReduce programming model.

The paper is organized as follows: Section 1 introduces research issues; Section 2 presents some concepts of frequent subgraph mining and two algorithms gSpan, FSM-H; Section 3 presents the details of the gSpanMR algorithm; Section 4 presents the experimental time comparison of FSM-H and gSpanMR algorithms; The final section are conclusions and some further developments of the paper.

## 2. FREQUENT SUBGRAPH MINING

**Definition 1** (*Labeled graph*)<sup>3</sup> A labeled graph can be represented by a 4-type,  $G = (V, E, L, I)$ , where:

\*Corresponding author.

Email: tranthienthanh@qnu.edu.vn

- $V$  is a set of vetices,
- $E \subseteq V \times V$  is a set of edges,
- $L$  is a set of labels,
- $l: V \cup E \rightarrow L$  is a function assigning labels to the vetices and the edges.

**Definition 2 (Isomorphism graph)**<sup>3</sup> An isomorphism is a bijective function  $f: V(G) \rightarrow V(G')$ , such that:

- $v \in V(G), l_G(v) = l_{G'}(f(v))$ ,
- $(u, v) \in E(G), (f(u), f(v)) \in E(G')$  and  $l_G(u, v) = l_{G'}(f(u), f(v))$ .

**Definition 3 (Frequent subgraph)**<sup>3</sup> Given a graph dataset,  $D = \{G_1, G_2, \dots, G_n\}$  and a minimum support  $minSup$ . A graph  $G$  is a frequent subgraph in  $D$  with  $minSup$  if  $sup(G, D) \geq minSup$ , where  $sup(G, D) = |\{G_i \in D: G \text{ is isomorphism to a subgraph of } G_i\}|$ .

In the following section, I will discuss the concepts of DFS code and some properties that help to build gSpan algorithm.

Given an undirected connected graph  $G$ . The DFS tree of graph  $G$  is a tree built from the vertices and the edges of the graph  $G$  by DFS algorithm.<sup>10</sup> The DFS tree creates a linear order between vertices and edges of the graph in their order of visit.

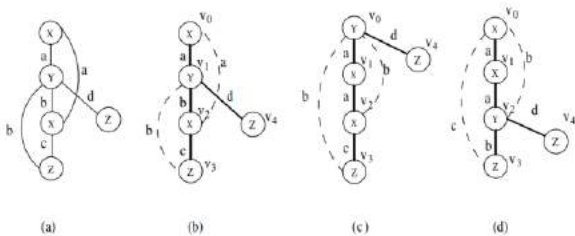


**Figure 1.** DFS tree and Forward/Backward edge<sup>3</sup>

**Definition 4. (DFS code)**<sup>3</sup>. Given a DFS tree  $T$  for a graph  $G$ , an edge sequence  $(e_i)$  such  $e_i < e_{i+1}$ , where  $i = 0, 1, \dots, |E(G)|-2$ ,  $(e_i)$  is called a DFS code, denoted as  $code(G, T)$ .

An edge  $e = (v_i, v_j)$  in a DFS code is a 5-tuple:  $(i, j, l_p, l_{(i,j)}, l_j)$ . Table 1 shows the corresponding DFS codes for Figure 1 (b), (c), (d).

**Table 1.** DFS codes for Figure 1 (b), (c), (d)

Edge no.	(Fig. 1b) $\alpha$	(Fig. 1c) $\beta$	(Fig. 1d) $\gamma$
0	(0,1,X,a,Y)	(0,1,Y,a,X)	(0,1,X,a,X)
1	(1,2,Y,b,X)	(1,2,X,a,X)	(1,2,X,a,Y)
2	(2,0,X,a,X)	(2,0,X,b,Y)	(2,0,Y,b,X)
3	(2,3,X,c,Z)	(2,3,X,c,Z)	(2,3,Y,b,Z)
4	(3,1,Z,b,Y)	(3,0,Z,b,Y)	(3,0,Z,c,X)
5	(1,4,Y,d,Z)	(0,4,Y,d,Z)	(2,4,Y,d,Z)

**Definition 5 (DFS code Lexicographic Order)**<sup>3</sup> If  $\alpha = code(G_\alpha, T_\alpha) = (a_0, a_1, \dots, a_m)$  and  $\beta = code(G_\beta, T_\beta) = (b_0, b_1, \dots, b_n)$  then  $\alpha \leq \beta$  if either of the following is true:

- $\exists t, 0 \leq t \leq \min(m, n), a_k = b_k$  for  $k < t, a_t < b_t$
- $a_k = b_k$  for  $0 \leq k \leq m$ , and  $n \geq m$ .

**Definition 6 (Minimum DFS code)**<sup>3</sup> Given a graph  $G, Z(G) = \{code(G, T) | T \text{ is a DFS tree for } G\}$ , based on DFS lexicographic order, the minimum one,  $min(Z(G))$ , is called *Minimum DFS code* of  $G$ , denoted as  $min(G)$ .

The minimum DFS code of a  $G$  graph is also called a labeling scheme for graph  $G$ . Based on this labeling, we have the result of isomorphism of the two graphs.

**Theorem 1<sup>3</sup>** Given two graphs  $G$  and  $G'$ ,  $G$  is isomorphism to  $G'$  if and only if  $min(G) = min(G')$ .

**Definition 7 (DFS code's Parent and Child)**<sup>3</sup> Given a DFS code  $\alpha = (a_0, a_1, \dots, a_m)$ , any DFS code valid  $\beta = (a_0, a_1, \dots, a_m, b)$  is called  $\alpha$ 's child, and  $\alpha$  is called  $\beta$ 's parent. We denote  $children(\alpha) = \{\beta | \text{is } \beta \text{'s parent}\}$ .

The growth from the DFS code  $\alpha$  to valid DFS code  $\beta$  is necessary for frequent subgraph mining. In fact, to construct a valid DFS code,  $b$  must be an edge which only grows from the vertices on the rightmost path. In figure 2 the graph shown in 2(a) has several potential children with one edge growth, which are shown in 2(b)-2(f) (assume the drakened vertices constitute the righthmost path).

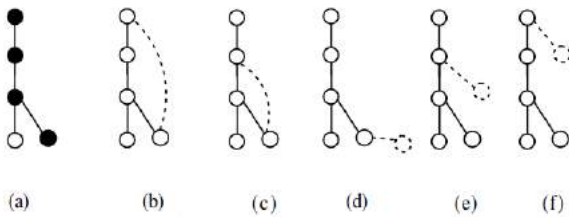


Figure 2. DFS code growing<sup>3</sup>

The DFS code together with the parent-child relationship forms a tree, called the *DFS code tree*. In the DFS code tree each node is a DFS code of a graph. The nodes at the  $i^{\text{th}}$  level are DFS codes of graphs with  $i-1$  edges. Figure 3 illustrates the DFS code tree.

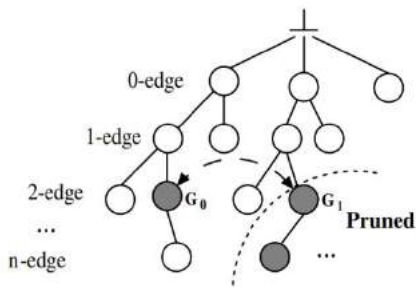


Figure 3. DFS code tree<sup>3</sup>

We can truncate the branches of the DFS code tree that do not contain the minimum DFS code with the following result:

**Theorem 2 (DFS code Growth)<sup>3</sup>** Given a DFS code  $\beta$ , if  $\alpha = \min(\beta)$ ,  $\alpha < \beta$ . Let  $D_\gamma = \{\eta \mid \eta < \gamma\}$ ,  $\forall \sigma \in \text{children}(\beta)$ ,  $\min(\sigma) \in D_\alpha \cup \text{children}(\alpha) \subseteq D_\beta$ .

From the above results, the gSpan algorithm starts from the 1-edge frequent subgraph and grows for more-edge graphs until the graph expands infrequently.

However, the gSpan algorithm complexity is an exponential function in the worst case scenario. Therefore, frequent subgraph mining on large graph sets is still a challenge.

To contribute to addressing this challenge, an approach is to build algorithms based on the MapReduce model to perform in parallel on the computer cluster to reduce execution time. MapReduce model is a parallel programming

model on cluster of computers proposed by Google<sup>11</sup>. Then Apache Hadoop is an open source platform that supports this programming model and is widely used in research and applications.

The FSM-H algorithm is an approach to frequent subgraphs mining on the MapReduce model. The FSM-H algorithm works on a graph set of data sets consisting of  $k$  parts, one on a data node. The multi-step iterative algorithm, at the  $i^{\text{th}}$  step, is the candidate  $i$ -edge subgraph from the  $i-1$ -edge frequent subgraph, then calculates the support for each candidate at each node and passes it to the reduce function summarizes and determines which subgraphs are often saved along with a list of graphs that contain it as input for the next step. The process is repeated until no more frequent subgraphs are discovered.

The FSM-H algorithm uses minimal DFS code to identify isomorphic subgraphs. However, the this algorithm has some limitations during the frequent subgraph mining: The generation of candidate  $i$ -edge subgraphs from  $i-1$ -edge frequent subgraphs is still redundant because it contains many duplicate (isomorphic) subgraphs. So data transfer and calculation are also more. For each  $i$ -edge subgraph in the candidate set, the algorithm finds the minimum DFS code to homogeneous subgraphs from each other, thereby sending the results to the reduce function. The algorithm to find the minimum DFS code is exponentially complex. If instead of finding the minimum DFS code by checking the DFS code is minimal, the computational complexity of the algorithm will be reduced if the DFS code is not minimal but the correctness of the algorithm is still guaranteed. To overcome these limitations, we improved the FSM-H algorithm based on the properties of DFS code as shown in the following section.

### 3. gSpanMR ALGORITHM

To overcome the limitations of the FSM-H algorithm, we use the following property in generating  $i$ -edge subgraph candidates from regular  $i-1$ -edge frequent subgraphs.

**Property 1** Given  $\alpha = (a_0, a_1, \dots, a_n)$  is a minimum DFS code of a graph  $G$ . If  $\beta = (a_0, a_1, \dots, a_n, b)$  is a minimum DFS code then the following is true:

- i)  $b$  is greater than or equal to  $a_0$ .
- ii) If  $b$  is a backward edge of the form  $(v_i, v_j), j < i$  then  $b$  is greater than or equal to the edge of  $\alpha$  that contains  $v_j$ .
- iii) If  $b$  is a forward edge of the form  $(v_i, v_j), j > i$  then  $b$  is greater than or equal to the edge of  $\alpha$  that contains  $v_i$ .

*Proof.*

Let  $G'$  be the graph of DFS code  $\beta$ .

i) Assume  $b < a_0$ . We build a DFS code  $\beta'$  of graph  $G'$  that  $b$  is the first edge of the DFS code. It is easy to see  $\beta' < \beta$ , which contradicts the hypothesis  $\beta$  is the minimum DFS code.

ii) If  $a_k$  ( $0 \leq k \leq n$ ) contains vertices  $v_j$  and  $a_k > b$  then DFS code  $\beta' = (a_0, a_1, \dots, a_{k-1}, b', a'_n, \dots, a'_{k+1}, a_k)$ , is a DFS code of  $G'$  and  $\beta' < \beta$  should conflict with the hypothesis  $\beta$  is the minimum DFS code of  $G'$ . Let  $b = (i, j, l_i, l_{(i,j)}, l_j)$  we denote  $b' = (j, i, l_j, l_{(i,j)}, l_i)$ .

iii) If  $b < a_k$  ( $0 \leq k \leq n$ ) then  $\beta' = (a_0, a_1, \dots, a_{k-1}, b, b_k, \dots, b_n)$  is a DFS code of  $G'$ , and  $\beta' < \beta$ , should conflict with the hypothesis is the minimum DFS code of  $G'$ .

We build an algorithm to generate DFS codes  $k+1$ -edge from minimum DFS code  $k$ -edge and graph  $G$ , based on property 1.

---

**Algorithm 1.** Generate DFS codes  $k+1$ -edge

---

*Input:* Minimum DFS code  $k$ -edge  $dfsMin$ , graph  $G$

*Output:*  $\{\beta \mid \beta \in children(dfsMin), \beta$  is a DFS code of a subgraph in  $G\}$

*Format:* **Candidate\_generation**( $dfsMin, G$ )

*Action:*

1.  $C = \emptyset$
2.  $rmp = \mathbf{rightMostPath}(dfsMin)$
3.  $vMax = rmp[0]$

4.  $minLabel = dfsMin[0].fromLabel$
  - // Backward edges
  5. **for each**  $v$  **in**  $rmp$ :
  6.  $e = (vMax, v)$
  7. **if**  $e$  **in**  $G$  **and**  $e$  **not in**  $dfsMin$  **then**
  8. **for each**  $e'$  **in**  $dfsMin$ :
  9. **if**  $e' > e$  **then continue**
  10.  $dfs = dfsMin \cup \{e\}$
  11.  $C = C \cup dfs$
  - // Forward edge from  $vMax$
  12. **for each**  $v$  **in**  $G.adjList(vMax)$ :
  13.  $e = (vMax, v)$
  14. **if**  $e$  **not in**  $dfsMin$  **and**  
 $label(e) \geq minLabel$  **then**
  15.  $dfs = dfsMin \cup \{e\}$
  16.  $C = C \cup dfs$
  - // Forward edges of the form  $(u, v)$ , where  $u$  in  $rmp$
  17. **for each**  $v$  **in**  $rmp, v \neq vMax$ :
  18. **for each**  $v'$  **in**  $G.adjList(v)$ :
  19.  $e = (v, v')$
  20. **if**  $e$  **not in**  $dfsMin$  **then**
  21. **for each**  $e'$  **in**  $dfsMin$ :
  22. **if**  $e' > e$  **then continue**
  23.  $dfs = dfsMin \cup \{e\}$
  24.  $C = C \cup dfs$
  25. **return**  $C$
- 

The correctness of the algorithm is confirmed by property 1. The time complexity of algorithm 1 in the worst case is  $O(k.m)$ , where  $k$  is the number of edges in  $dfsMin$ , and  $m = |E(G)|$ .

In the gSpanMR algorithm we check if a DFS code is the minimum DFS code? The algorithm is as follows:

---

**Algorithm 2.** Check the minimum DFS code.

---

*Input:* DFS code for check  $dfsCode$

*Output:* **True** if  $dfsCode$  is minimum, **False** otherwise

*Format:* **isMin**( $dfsCode$ ).

Action:

1.  $g = \text{to\_Graph}(dfsCode)$
2.  $minDFS = \emptyset$
3. **return tryIsMin**( $dfsCode, minDFS, 0$ )

Procedure **tryIsMin**( $dfsCode, minDFS, i$ ) checks whether the  $i^{\text{th}}$  edge of  $dfsCode$  is a edge in the minimum DFS code;  $minDFS$  is the minimum DFS code  $i-1$  edge.

**Sub tryIsMin**( $dfsCode, minDFS, i$ )

1. **if**  $i > \text{length}(dfsCode)$  **then return true**
2.  $list =$  List of smallest edges in  $g$  can grow for  $minDFS$
3. **for each**  $e$  **in**  $list$ :
4. **if**  $e < dfsCode[i]$  **then return False**
5.  $minDFS = minDFS \cup \{e\}$
6.  $chk = \text{tryIsMin}(dfsCode, minDFS, i+1)$
7. **if**  $chk = \text{False}$  **then return False**
8.  $minDFS = minDFS - \{e\}$

Algorithm 2 uses branch-and-bound method, so in practice it is better than the algorithm to find the minimum DFS code of a graph, although the worst case complexity of algorithm 2 is  $O(2^n)$ , where  $n$  is the number of edges of  $dfsCode$ .

Based on the gSpan algorithm and the approach of the FSM-H algorithm, we developed the gSpanMR algorithm with 3 phases:

Phase 1 (Preparation): this phase reads data from HDFS, explores frequent edges of a set of graphs and writes the results to HDFS to prepare for phase 2.

Phase 2 (Mining): this phase explores frequent  $k+1$ -edge subgraphs from frequent  $k$ -edge subgraphs. This phase consists of many steps starting from  $k = 0$  until no more frequent subgraphs are explored.

Phase 3 (Collection): this phase collects all sub-graphs often exploited in phase 2.

**Algorithm 3. gSpanMR**

*Input:*  $D$  is set of graphs, minimum support  $minSup$

*Output:* Set of frequent subgraphs of  $D$  with minimum support  $minSup$

Action:

// Phase 1

*key:* id of a graph

*value:* a graph

**Mapper\_Preparation**(Text  $key$ , Text  $value$ )

1.  $intermediate\_key = null$
2.  $intermediate\_value = \text{serialize}(value)$  // Convert graph into byte sequence
3. **omit**( $intermediate\_key, intermediate\_value$ )

*key:* a DFS Code

*values:* byte sequences of graphs

**Reducer\_Preparation**(DFSCode  $key$ , ByteWritable  $values$ )

1. **forall**  $value$  **in**  $values$ :
2. **write\_to\_file**( $key, value$ )

// Phase 2

*key:* a DFS code  $k$ -edge

*value:* byte sequence of graphs that contain key

**Mapper\_Mining**(DFSCode  $key$ , ByteWritable  $value$ )

1.  $listGraph = \text{convert_to_List_Graph}(value)$  //convert byte sequence to list of graphs
2.  $C = \emptyset$
3. **forall**  $g$  **in**  $listGraph$ :
4.  $C = C \cup \text{Candidate\_generation}(key, g)$

5. **forall**  $c$  **in**  $C$ :
6. **if**  $\text{isMin}(c)$ :

7.  $v = \text{serialize}(c.OL)$
8. **emit**( $c, v$ )

*key:* a DFS Code

*values:* byte sequences of graphs

**Reducer\_Mining**(DFSCode  $key$ , ByteWritable  $\langle values \rangle$ )

1. **forall**  $value$  **in**  $values$ :
2.  $support += \text{getsupport}(value)$
3. **if**  $support \geq minSup$ :
4. **forall**  $value$  **in**  $values$ :
5. **write\_to\_file**( $key, value$ )

// Phase 3

*key:* a DFS code  $k$ -edge

*value:* byte sequence of graphs that contain key



**Mapper\_Collection**(DFSCode *key*,  
ByteWritable *value*)

1. *gText* =

**convert\_DFSCode\_to\_Graph\_Text**(*key*)

//Convert DFS code to graph in format text

2. **emit**(*gText*, null)

*key*: a abugraph in format text

*values*: null

**Reducer\_Collection**(Text *key*, Text *values*)

1. **write\_to\_file**(*key*)

#### 4. IMPLEMENTATION AND EXPERIMENT

We have implemented the gSpanMR algorithm on the Hadoop platform in the Java programming language. We conducted experiments on a system of 5 PCs with CPU: Intel Core 2 Duo E8400 3.00GHz, RAM: 4GB, installed Ubuntu 14.04, Hadoop 2.7.3, including 1 MasterNode and 4 NameNode. Three datasets are created from *Graphgen* tool with the number of graphs are 5000, 7000 and 10000 graphs respectively, the number of vertices in the graph is from 20 to 40 vertices, the minimum support is 20%. Experimental results as shown in Table 2.

**Table 2.** Runtime of FSM-H and gSpanMR

Number of graphs	FSM-H	gSpanMR
5000	1050s	820s
7000	2134s	1721s
10000	3930s	3122s

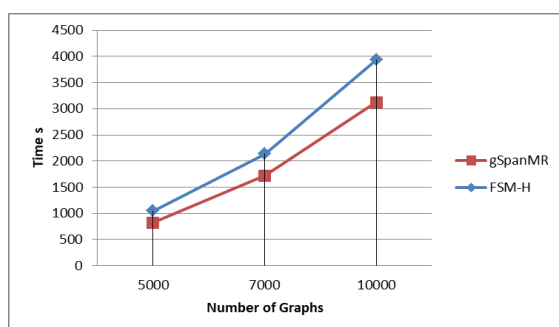


**Figure 4.** Experimental results comparing the execution time of FSM-H and gSpanMR

Through experimental results show that the execution time of the algorithm gSpanMR less FSM-H algorithm. The more the graphs increase, the more the difference in time increases due to the reduction of many subgraph candidates and the minimum DFS code test.

#### 5. CONCLUSIONS

With the improved subgraph candidates and testing the minimum DFS code in the gSpanMR algorithm, it has been shown to improve the time it takes to perform the frequent subgraph mining algorithm. In the future, we will continue to improve gSpanMR algorithm and implement gSpanMR algorithm on Spark environment to limit the reading and writing data in external memory.

#### ACKNOWLEDGEMENTS

*This study is conducted within the framework of science and technology projects at institutional level of Quy Nhon University under the project code T2019.625.20.*

#### REFERENCES

1. Inokuchi, T. Washio, and H. Motoda. *An apriori-based algorithm for mining frequent substructures from graph data*, 4<sup>th</sup> Eur. Conf. Principles Data Mining Knowl. Discov., PKDD, Lyon, France, September 13-16, 2000.
2. M. Kuramochi and G. Karypis. *Frequent subgraph discovery*, 1<sup>st</sup> IEEE International Conference on Data Mining, IEEE, San Jose, California, USA, 29 November - 2 December 2001.
3. Yan and J. Han. *gSpan: Graph-based substructure pattern mining*, Int. Conf. Data Min. IEEE, Maebashi City, Japan, 9-12 December 2002.
4. S. Nijssen, and J. Kok. *A quickstart in frequent structure mining can make a difference*, 10<sup>th</sup> ACM SIGKDD Int. Conf. Knowl. Discov. Data Mining, ACM, Seattle, WA, USA, 22-25 August, 2004.

5. V. Chaoji, M. Hasan, S. Salem, and M. Zaki. An integrated, generic approach to pattern mining: Data mining template library, *Data Mining Knowledge Discovery*, **2008**, 17(3), 457–495.
6. S. Chakravarthy, R. Beera, and R. Balachandran. *Db-subdue: Database approach to graph mining*, 8<sup>th</sup> Adv. Knowl. Discov. Data Mining, IEEE, Sydney, Australia, 26-28 May, 2004.
7. S. Chakravarthy and S. Pradhan. *Db-FSG: An SQL-based approach for frequent subgraph mining*, 19<sup>th</sup> Int. Conf. Database Expert Syst. Appl., IEEE, Turin, Italy, 1-5 September, 2008.
8. Srichandan and R. Sunderraman. *Oo-FSG: An object-oriented approach to mine frequent subgraphs*, 9<sup>th</sup> Australasian Data Mining Conf., IEEE, Ballarat, Australia, December, 2011.
9. Mansurul A. Bhuiyan and Mohammad Al Hasan. An Iterative MapReduce Based Frequent Subgraph Mining Algorithm, *IEEE Transactions on Knowledge and Data Engineering*, **2015**, 27(3), 608-620.
10. Cormen, H. Thomas, Leiserson, E. Charles, Rivest, L. Ronald. *Introduction to Algorithms*, 1<sup>st</sup> ed., MIT Press and McGraw-Hill, NewYork City, 1990.
11. J. Dean and S. Ghemawat. *Mapreduce: Simplified Data Processing on Large Clusters*, 6<sup>th</sup> Symposium on Operating System Design and Implementation, San Francisco, OSDI, December 6-8, 2004.

## Một kỹ thuật phát hiện u gan dựa trên mô hình chất liệu

Lê Thị Kim Nga<sup>1,\*</sup>, Đoàn Thị Xương<sup>2</sup>

<sup>1</sup>Viện Nghiên cứu ứng dụng khoa học và công nghệ, Trường Đại học Quy Nhơn, Việt Nam

<sup>2</sup>Thư viện, Trường Đại học Quy Nhơn, Việt Nam

Ngày nhận bài: 12/05/2020; Ngày nhận đăng: 14/06/2020

### TÓM TẮT

Việc phát hiện bất thường trên ảnh y tế nói chung và ảnh chụp cắt lớp vùng gan nói riêng là một vấn đề quan trọng được quan tâm nghiên cứu nhiều trong những năm gần đây tại Việt Nam. Bài báo trình bày một kỹ thuật phát hiện u gan trên ảnh vùng gan dựa trên mô hình chất liệu vùng gan, kết hợp với phân tích dữ liệu trên ảnh chụp cắt lớp vùng gan. Kỹ thuật đã được cài đặt thử nghiệm với bộ dữ liệu mẫu 3D-IRCADb-01 và dữ liệu thu thập thực tế tại Bệnh viện Đa khoa Bình Định.

**Từ khóa:** U gan, chất liệu, bất thường.

\*Tác giả liên hệ chính.

Email: kimnle@arist.edu.vn

# A technique to detect liver tumor based on texture model

Le Thi Kim Nga<sup>1,\*</sup>, Doan Thi Xuong<sup>2</sup>

<sup>1</sup>Research Institute for Applied Science and Technology, Quy Nhon University, Vietnam

<sup>2</sup>Library, Quy Nhon University, Vietnam

Received: 12/05/2020; Accepted: 14/06/2020

## ABSTRACT

The detection of abnormalities in medical images in general and tomography of liver areas in particular is an important issue of great research interest in recent years in Vietnam. The paper presents a technique for detecting liver tumors in the image of the liver based on the texture model of the liver region, combined with data analysis on the CT scan. The technique has been experimentally installed with 3D-IRCAdB-01 sample dataset and actual collected data at Binh Dinh General Hospital.

**Keywords:** *Liver tumor, texture, abnormal.*

## 1. INTRODUCTION

The socio-economic development leads to the increasing demand for health care. The research and application of high technologies and modern information technology in the field of health in order to improve the quality of human health care always attracts the attention of the community of professionals. In recent years, the development of image recognition technology and artificial intelligence based on deep learning, deep neural networks with large training datasets has led to a lot of research and development in the field of image processing. medical, especially in detecting abnormalities, liver tumors on the image of the liver areas. Research results in this direction open up the prospect, allowing for important advances in the diagnosis of liver diseases. According to statistics, about 750,000 people were diagnosed with liver cancer and nearly 696,000 people died from the disease<sup>1</sup> worldwide in 2008.

In diagnosing based on medical imaging, the study of processing, analyzing and identifying liver images is difficult because this is a complex object and it is difficult to observe details even with the human eye. CT images of the liver area have low contrast compared to the surrounding tissue. This contrast is altered by the influence of fat concentration in the liver. Another important point is that the shape of the liver has many variants. In addition, medical imaging data is private and is taken on specialized hospital equipment, so in fact, it is not simple to collect a large enough data to train deep learning model which meets diagnostic requirements.

To overcome the difficulties of liver image data, Lu et al<sup>2</sup> proposed an approach to segment the image of liver region through two steps: detecting and estimating the probability map for segmentation using 3D convolutional neural network; and next step is adjusting with graph cut. Authors built a completely automated

---

\*Corresponding author:

Email: kimnle@arist.edu.vn

process, without user control. The Hoogi et al<sup>2</sup> used the adaptive estimation method with active contour model in the liver segmentation and the test achieved good results on the dataset of 164 MRI images and 112 CT images of liver images with low contrast and noise.

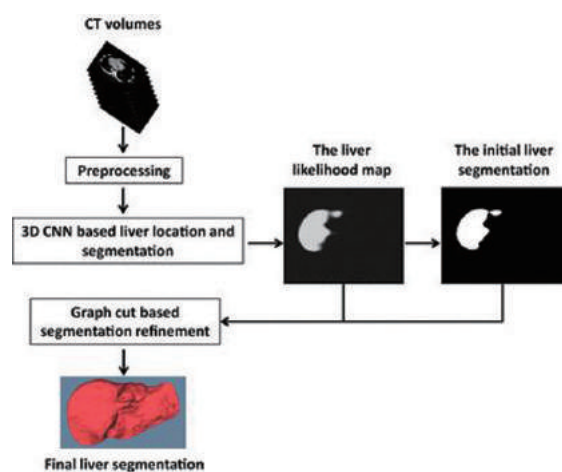


**Figure 1.** Processing steps of Lu et al<sup>3</sup>

The paper proposes a texture model approach in combination with data analysis on liver CT image. The texture model assumes the homogeneity in the image regions, meaning that all sub-regions within the liver image area will have the same liver texture. Thus, the idea is: randomly sample sub-regions of the liver image area and analyze them to find outlier, abnormal areas based on the assumption that in terms of image, abnormal areas, such as liver tumors appear in the liver image area, there will be certain differences in structure and contrast with the surrounding liver region. Part 2 of the paper will present technical details, including the following: limiting the area of the liver on the image, the sampling method and the classification. Part 3 will then describe the test results and evaluation comments.

## 2. ALGORITHM

### 2.1. Limit object area

Usually, in practical problems, the objects of interest do not always appear in a fixed position in the image. For example, when recognizing face in an image, the face image (the object of

interest) can appear at any location in the image, with different sizes and rotation. However, CT images have a fixed pose, the organs are usually located in certain areas with relatively stable arrangements between body parts. This also means that for each slice position, visceral objects on CT images usually appear in relatively stable positions on the image. Therefore, in the position of a specific slice image when you want to identify an internal object, such as the liver, kidneys, etc., it is possible to locate the corresponding area of the image object of interest on the image. Limiting the area of interest allows a significant reduction in search space, identifying objects, increasing processing speed and eliminating false detection.

To identify the target area of liver tumors, techniques to limit the area of interest can be used as follows:

**Limit coordinates:** To limit the position of the liver tumor, we will use the interval corresponding to the minimum and maximum limits in the x and y dimensions. More specifically, when there are pixels (x, y) in the liver object area, that is  $(x, y) \in [Xmin, Xmax] \times [Ymin, Ymax]$ . In there, these ranges are estimated based on the statistics of locations of liver objects in the CT images. This technique is quite simple, allowing quick implementation. However, the boundary is still quite large.

**Limit by mask image:** This technique uses binary images, on which white areas are able to appear liver tumors, black areas are not. In other words, if the pixel (x, y) on the slice image is a liver tumor, then the (x, y) point on the mask image must be a white pixel. This technique is quite simple and fast, allowing the boundary to be narrower than technique using coordinate.

**Limit by liver segmentation:** After segmentation, we are able to determine the specific boundary and circumference of the liver region on the image. The accuracy as well as the speed of limiting the image area of interest

depend directly on the accuracy and speed of the segmentation technique. In general, this technique closer to reality than the above two, but takes more time.

## 2.2. Sampling method

After localizing the liver boundary, the next step is sampling liver image areas, in other hand, is determining the list of sub-image areas within the liver object area. According to the texture approach, if the region is normal, there are no abnormalities, then all sub-image areas in the liver image area will have the same output value when performing classification. In the case of an abnormal liver area, there are sub-regions in the liver image that give values unlike most of the remaining sub-regions.

Sampling is performed by following these steps: Select a square in the liver image area, rotate at any angle and conduct random image flip transform.

The sampling is described as follows:

**Input :** I, M

**Output :** S

**Process:**

1.  $S := \emptyset$
2.  $\text{brect} := \text{bounding\_rectangle}(M)$
3. for each  $\text{wsize} \in [\text{MIN\_WND\_SIZE}, \text{MAX\_WND\_SIZE}]$
4. for each  $x \in [\text{brect.left}, \text{brect.right}]$
5. for each  $\text{wsize} \in [\text{brect.top}, \text{brect.bottom}]$
6.  $R := \text{rectangle}(x, y, \text{wsize}, \text{wsize})$
7. if ( $\text{is\_inside}(R, M)$ )
8.  $s := \text{calculate\_sample}(R, I)$
9.  $S := S \cup \{s\}$

In the description above, I is the slice image, M is the limited liver area. In programming, M is a binary image, with a white area corresponding to region may contain liver, the black area is not the liver area. The brect parameter is the limited area in the iteration step to select the sampling window, and  $[\text{MIN\_WND\_SIZE}, \text{MAX\_WND\_SIZE}]$  is a

limited size of the sampling window. The sample received is the input of the machine learning process. Before classifying, the system needs to be trained, using a machine learning model on the set U of training data.

Each training data sample s in the U set must be specifically labeled: normal or abnormal.  $U = \{ \langle s, l \rangle : s \in S, l \in \{0,1\} \}$ , where l is the label of training data sample s, 1 corresponds to normal, 0 is abnormal. The training dataset is constructed by experienced experts on liver images. For each sub-image region marked in the liver region M, depending on whether expert's opinion is abnormal or normal,  $\langle s, 0 \rangle$  or  $\langle s, 1 \rangle$  will be added accordingly to U.

## 2.3. Process sample

Taking the output of the sampling process as an input, the classifier will give conclusion corresponding to the state of liver is tumor or not. This is a binary classifier with input is sample, the output is a corresponding state. The classifier is based on the Resnet network architecture.<sup>4</sup> In the application made here, use Resnet because this network architecture is resistant to gradient signal loss during back propagation. Therefore, application designers can build deep networks with thousands of layers. Continuing with the array of Residual Block, the network is designed to add an output of fully connected layer, and using sigmoid function to determine two status values. To reduce the rate of false positives, after being classified, samples will be aggregated into a result mask image and proceeded to remove too small areas. This processing allows the elimination of noise results. On a sequence of CT images, this will not affect you as much. Tumor regions in slices at the beginning or end of the tumor may be mistakenly removed because they are too small, but later slices at a deeper position into tumor will not be removed. Therefore, results throughout the image sequence are not affected. If the sequence of images is sparse, this should be corrected accordingly.

**3. EXPERIMENT**

The technique is implemented with the support of open source libraries such as OpenCV, VTK and Tensorflow. The dataset is selected for testing is 3D-IRCADb-01.<sup>5</sup> The dataset consists of several sets of anonymous medical imaging of patients, in which organs are manually marked by experts. The dataset includes CT scans of 10 women and 10 men, each patient’s data was stored in one folder. The medical image data and the annotated data are stored in DICOM format.

In the experiment setting, data of 10 patients were selected as training data, data of 10 patients were selected as evaluation data. The information of the limited area was established based on annotated data of 10 cases. In particular, the coordinate boundary area is set to a rectangular area with {x: 36, y: 64, width: 447, height: 349}.



**Figure 2.** Image of limited region in case using coordinates and mask image

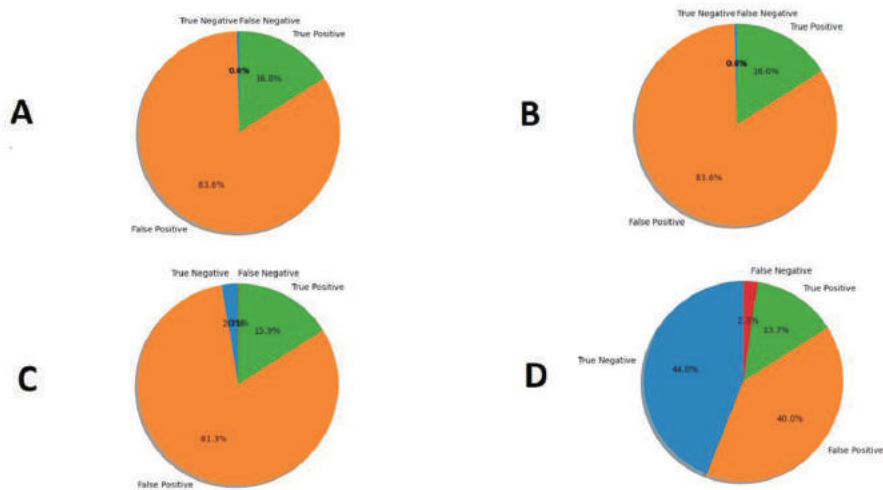


**Figure 4.** Conclusion rate in 4 limited cases: A. unlimited, B. limit coordinates, C. Limit by mask image, D. Limiting by liver segmentation

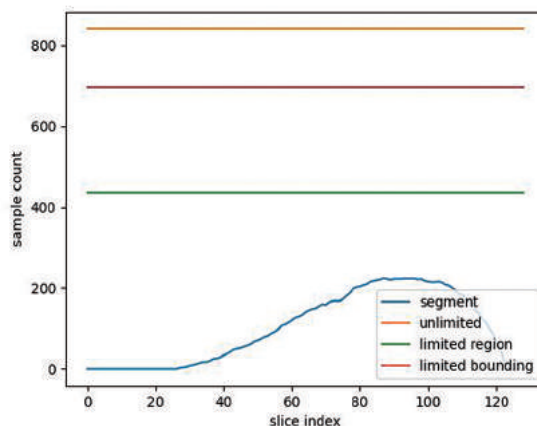


**Figure 3.** Diagram about sample amount in each slice of one patient: unlimited (Orange), limit coordinates (Red), Limit by mask image (Green), Limiting by liver segmentation (Blue)

It is easy to see that in the case of different limits, there will be different number of selected samples. This will affect the processing speed, because it is necessary to classify all input samples. From the results of assigning a status classification label to the samples, it is possible to evaluate whether the input image has liver tumor appearance. The testing of the input image will give conclusions, in one of 4 cases: True Positive, True Negative, False Positive, False Negative.

It is easy to see that, in the first case, the False Positive rate is quite high. This is quite understandable, since the classifier is trained on liver texture areas. When the limited region contains more area than the actual liver, the conclusions of the classifier in those outward

areas are more likely to be wrong, thus increasing the rate of false positives. However, in practice the results for these areas are acceptable, considering the circumstances in which a doctor can easily assess that the results are not of concern.

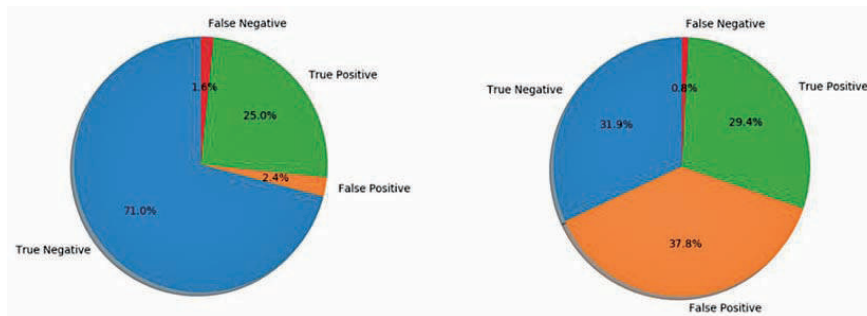


Figure 5. The rate of conclusions on data of two patients

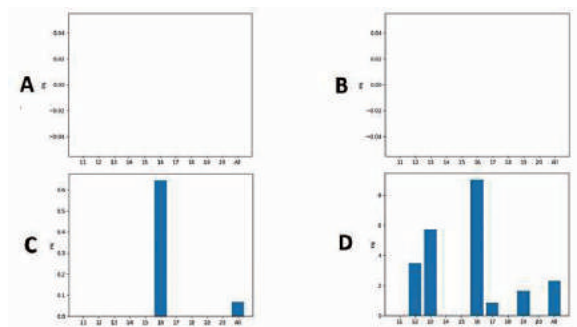


Figure 6. Statistics of False Negative per patient (%) A. unlimited, B. limit coordinates, C. Limit by mask image, D. Limiting by liver segmentation

When looking at the False Negative ratios in different cases, we find that the rates increase gradually on each case. The majority of the results were quite low and the highest case was in patient 16 data with about 9%. This result is partly due to post-processing of small sized areas. If we do not remove the small sized areas, the result is only 6.5%. Overall, however, this patient was not missed due to the positive True Positive ratio. The first two cases give false Negative ratios of zero. However, this does not reflect a good classification result, because it needs to be considered for many cases of non-liver data.

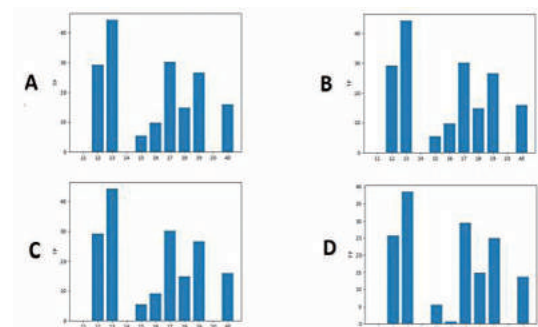


Figure 7. Statistics of True Positive per patient (%) A. unlimited, B. limit coordinates, C. Limit by mask image, D. Limiting by liver segmentation

In the results of the True Positive ratio, we find that the data is relatively stable among the region restriction cases. This is quite understandable. The discrepancy between the cases is mainly also affected in the post-processing step for small size areas. Overall, no patients were missed.

The algorithm was also tested with actual data at Binh Dinh General Hospital. Test data are abdominal CT images provided by the Department of Internal Medicine. Program uses the function of reading data, conducting a value conversion based on Hounsfield indicators and conducting the detection of abnormal areas, liver tumors. In order to limit the processing area, the program also integrated one technique to locate



liver area.<sup>6</sup> The data is taken on the basis of linking with data of QNPACS system.<sup>7</sup>

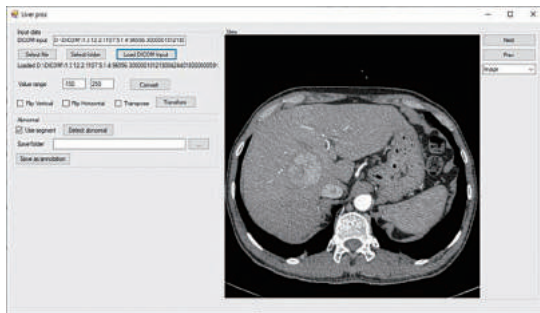


**Figure 8.** Program at Binh Dinh General Hospital

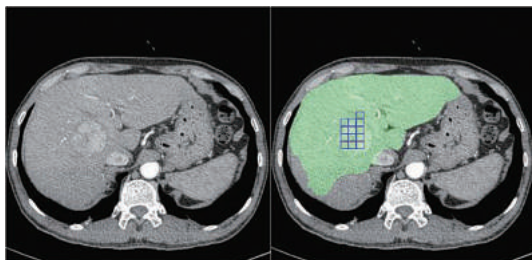


**Figure 9.** Result on a slice image of 52-year-old male patient has liver tumor

Green image area is liver object area, blue squares mark liver tumor. Result showed that the probability of detecting true position liver tumor within liver area is very high.

#### 4. CONCLUSION

Processing and detecting abnormalities in medical images in general and in liver images in particular is an important issue, based on the application of research results on machine vision and machine learning in practical problems. The paper presents the technique of analyzing, processing and detecting liver abnormalities on liver CT images using the model texture approach, combined with classification task.

The technique was tested on 3D-IRCADb-01 database and liver CT images were collected at Binh Dinh General Hospital. The results demonstrate the effectiveness of the proposed technique. This is an important basis for further improvement studies and more extensive testing.

#### REFERENCE

1. F. Lu, F. Wu, P. Hu, Z. Peng, & D. Kong, Automatic 3D liver location and segmentation via convolutional neural network and graph cut. *International journal of computer assisted radiology and surgery*, **2017**, 12(2), 171-182.
2. A. Hoogi, A. Subramaniam, R. Veerapaneni, & Rubin, D. L. Adaptive estimation of active contour parameters using convolutional neural networks and texture analysis. *IEEE transactions on medical imaging*, **2016**, 36(3), 781-791.
3. A. Jemal, F. Bray, M. M. Center, J. Ferlay, E. Ward, D. Forman Global cancer statistics. *CA Cancer J Clin*, **2011**, 61(2), 69–90.
4. K. He, X. Zhang, S. Ren, & J. Sun, Deep residual learning for image recognition, *In Proceedings of the IEEE conference on computer vision and pattern recognition*, **2016**, 770-778.
5. Database of CT liver image, <https://www.ircad.fr/research/3d-ircadb-01/>, Retrieved 29/3/2020.
6. Lê Thị Kim Nga, Huỳnh Lê Anh Vũ, Nguyễn Thị Kim Phượng. *Một kỹ thuật phát hiện đối tượng không cấu trúc trên ảnh dựa vào tiếp cận hồi quy*, Hội nghị quốc gia về CNTT&TT 2017.
7. Database of CT liver image in Binh Dinh, <https://aristqnu.com/san-pham/phan-mem-qnpacs> Retrieved 29/3/2020.



## Một kỹ thuật xác định điểm bao phục vụ đánh giá sự thay đổi của vùng bất thường trên ảnh y tế

Lê Thị Kim Nga<sup>1,\*</sup>, Đoàn Thị Xương<sup>2</sup>, Đoàn Thị Thu Cúc<sup>3</sup>

<sup>1</sup>Viện Nghiên cứu ứng dụng khoa học và công nghệ, Trường Đại học Quy Nhơn, Việt Nam

<sup>2</sup>Thư viện, Trường Đại học Quy Nhơn, Việt Nam

<sup>3</sup>Khoa Công nghệ thông tin, Trường Đại học Quy Nhơn, Việt Nam

Ngày nhận bài: 30/05/2020; Ngày nhận đăng: 30/06/2020

### TÓM TẮT

Việc đánh giá sự tăng trưởng hay giảm thiểu của vùng bất thường trên ảnh y tế nói chung và ảnh chụp cắt lớp nói riêng là một vấn đề quan trọng được quan tâm nghiên cứu nhiều trong những năm gần đây tại Việt Nam. Bài báo trình bày một kỹ thuật xác định điểm trên đường bao vùng bất thường để làm cơ sở sau này có thể đánh giá sự phát triển của vùng bất thường trên ảnh y tế. Kỹ thuật dựa trên việc phân tích kết cấu cục bộ tại lân cận đường bao vùng bất thường kết hợp với sử dụng mạng nơ ron tích chập và đã được cài đặt thử nghiệm và đánh giá dựa trên bộ dữ liệu mẫu 3D-IRCADb-01 với các vùng u gan.

**Từ khóa:** Khối u, vùng bất thường, chất liệu.

\*Tác giả liên hệ chính.

Email: kimnle@arist.edu.vn

# A technique of identifying the contour point to assess the change of abnormal areas on medical imaging

Le Thi Kim Nga<sup>1,\*</sup>, Doan Thi Xuong<sup>2</sup>, Doan Thi Thu Cuc<sup>3</sup>

<sup>1</sup>*Research Institute for Applied Science and Technology, Quy Nhon University, Vietnam*

<sup>2</sup>*Library, Quy Nhon University, Vietnam*

<sup>3</sup>*Faculty of Information Technology, Quy Nhon University, Vietnam*

*Received: 30/05/2020; Accepted: 30/06/2020*

## ABSTRACT

Assessing the growth or reduction of abnormal areas in medical imaging in general and tomography in particular is a greatly concerned and important research issue in recent years in Vietnam. The article presents a technique of identifying contour points of an abnormal area as a basis for later assessment of the development of abnormal area on medical imaging. The technique is based on the analysis of local structures in the vicinity of abnormal area boundaries combined with the use of convolutional neural networks and has been tested and evaluated based on 3D-IRCADb-01 sample data set with liver tumors.

**Keywords:** *Tumor, abnormalities, texture.*

## 1. INTRODUCTION

Medical imaging plays a vital role in diagnosis job of the doctors. Modern medicine today diagnoses not only by clinical symptoms but also by subclinical symptoms or so-called subclinical diagnosis. In particular, the diagnosis on medical imaging is a subclinical diagnosis based on images obtained from specialized imaging equipment, such as ultrasound, endoscopes, CT scanners (Computed Tomography), MRI (Magnetic Resonance Imaging), PET (Positron Emission Tomography) or SPECT (Single Photon Emission Computed Tomography) machines, etc. Each medical imaging device has its own advantages and decisive meaning in many diagnostic cases.

Being an important part, medical imaging is also a critical data type for information

technology research in health. An important issue with medical imaging is that abnormal areas, such as strange areas appearing in an image of organ, such as a lesion or tumor. In such cases, it is desirable not only to quickly and accurately detect that abnormal area, but also to track changes in that abnormal area over time. Being able to estimate changes in abnormal areas, whether growth or reduction, has an important implication for healthcare job of the doctors.

Normally, abnormal areas on medical imaging will not have a stable geometric structure. We can imagine with other objects, such as human face when looking straight and we can see that the geometric structure is quite stable and can be used as a basis for conducting research, but with areas of vegetation or unoccupied land appearing on remote sensing

---

\*Corresponding author:

Email: kimnle@arist.edu.vn

images are completely different. It is often tough to make assumptions or think of a common geometric structure for them. The abnormal area on medical imaging is similar. They appear quite randomly and have unpredictable shapes. Often image processing problems for this object type are detected and segmented. If we want to track changes in abnormal area, we need to analyze the boundary of the abnormal area on the basis of correlation with itself in the previous time.

In studies on the demarcation of the subject on medical imaging, Mikkel Stegmann

and Dorthe Pedersen<sup>1</sup> conducted a quantitative analysis on cardiac magnetic resonance imaging data. In this paper, the authors aim to estimate the ejection fraction in the left ventricle based on four-dimensional MRI data based on the Cootes algorithm expansion study of the Cootes group<sup>2</sup>. In the experiment, Mikkel Stegmann and Dorthe Pedersen used data of 12 patients with a model of 1560 points and achieved a deviation of  $-1.2 \rightarrow -3.3\%$  when compared to the results of the observers.

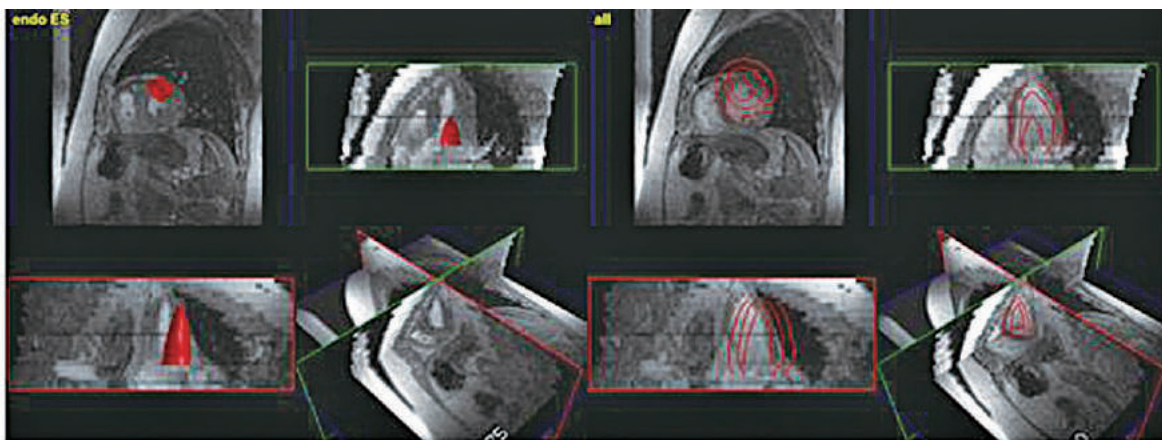


**Figure 1.** Some images of research results<sup>1</sup>

Zhao's team<sup>2</sup> again has a study of improved dynamic contour models with the combined use of local and global intensity data. In the study, the effect of Gaussian scroll image data with the original image will replace the original image

and the authors built a gradient flow model based on Euler-Lagrange equation. Accordingly, the research results are presented on both composite image data and medical imaging data.

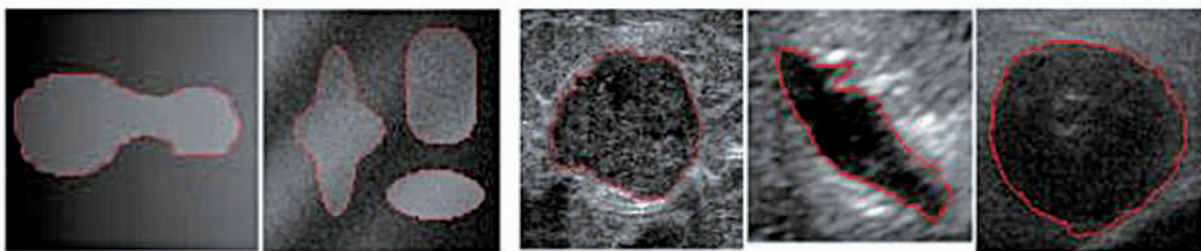


**Figure 2.** Results of Zhao team<sup>3</sup>: composite image (left) and medical image (right)

In a recent study, the Guha team<sup>4</sup> built a function to map a pair of input images into a deformed field using machine learning. The group performed functional parameterization via a convolutional neural network and performed network learning on an image data set. The team performed a test on a set of 3731 brain MRI data

from eight different published data sets, where each scan was sampled to a  $256 \times 256 \times 256$  and 1mm grid on voxel.

In this article, we present a technique of determining the points on a contour to assess the change of abnormal area based on the change of the abnormal area contour nearby, in other words,

transform from an adjacent boundary. The problem is about estimating the displacement of a set of boundary points sampled on the contour to find a new location for it. Section 2 will detail the proposed technical content while Section 3 will present experimental results and final conclusions.

## 2. IDENTIFYING THE CHANGE OF ABNORMAL AREA ON MEDICAL IMAGING

### 2.1. Abnormal area on medical imaging

On medical imaging, an abnormal area is an image area corresponding to the location of anomalies of the object in the image. For example, with CT scans of the liver region, tumor areas, lesions, etc., these can be considered abnormal areas. In this case, the paper assumes an abnormal area without holes. That is, any sub-region in the abnormal area is also an abnormal area. Thus an abnormal region may be represented by its boundary.

The boundary of an abnormal area is a border points list of this area. So, we can describe the boundary of abnormal area  $A$  on image  $I$  as follows:

$$A = \{P_i\}_{i=0}^{n-1}, P_i \in [0, I_{width} - 1] \times [0, I_{height} - 1]$$

Each point  $P_i$  is a point on the contour; two points in a row  $P_i P_{i+1}$  is an edge on the contour.

### 2.2. Regression problem at each point

The problem here is that we need to identify the abnormal area on the input image based on a state of the irregular region that has been assumed to be adjacent. That is, we need to define a new set of contour points based on a set of contour points that have been instantiated close enough. Because the abnormal area is an unstructured material object, the points on the contour all have the same role, whether they are  $P_i$  points or a certain point in the middle of any  $P_i P_{i+1}$  segment.

Considering that the abnormal area and the normal area both have certain material

characteristics, and the boundary of the abnormal area is the boundary between the two material areas, thus assuming a straight line intersects the boundary once, then points on that line will have two different characteristics. We use this statement to construct a regression problem at each point. Specifically, at any point near the boundary, we can evaluate the characteristics of surrounding materials to draw conclusions about the ability to move that point to the boundary. The regression performance at any point on the contour is the same. In order to increase the similarity between characteristics at points in different locations, we assume additional parameter of the point's direction. We expect that when the point stops at the boundary, the direction of the point will coincide with the normal of the contour at that point.

Algorithm of characteristics in points.

**Function:** sampling

**Input:** image,  $P$ ,  $N$ , angles, times, step

**Output:** sample

**Process:**

1.  $sample = \emptyset$
2. for each  $\alpha \in angles$ :
3.  $D = rotate(N, \alpha)$
4. for each  $t \in [1, time]$ :
5.  $S = P + D * t * step$
6.  $sample = sample \cup \{image.at(S)\}$

The algorithm performs specificity at the input point  $P$  on the *image*. The characteristic is calculated by sampling the pixel values in different directions in the list of *angles* sampling directions which are relative and depend on the current  $N$  direction of point  $P$ . In each direction, sampling was performed in *times*; each time was *step* apart. Initially, *sample* output characteristic is set to empty. For each angle  $\alpha$  in the set of *angles*, we calculate the  $D$  sampling direction by rotating the current  $N$  angle by the angle  $\alpha$ . With the calculated  $D$  sampling direction, we measure the sampling position  $S$  with each sampling and then integrate the pixel value at point  $S$  of the

image into the sample output characteristic. At the end of the process, a characteristic at point  $P$  can be obtained in  $N$  direction of the image.

With the characteristic at a point calculated according to the above rule, a regression model is needed to estimate the displacement parameter for a position on the contour. Thus, with a medical imaging data set labeled abnormal areas, we can build an input sample set to learn regression model. Supposing for an image that has been labeled an abnormal area, a data set can be generated based on it. Rules can be envisioned at each sampling as follows:

- Taking random point  $P$  on the contour and calculate  $N$  direction of  $P$ .
- Generating random points  $P_i$  adjacent to  $P$  and  $N_i$  of  $P_i$ .
- Using the characteristics of  $P_i$  and  $N_i$  with parameters that change from  $P_i, N_i$  to  $P, N$  as input samples for learning. Variable parameters include a rotation value and a step length.

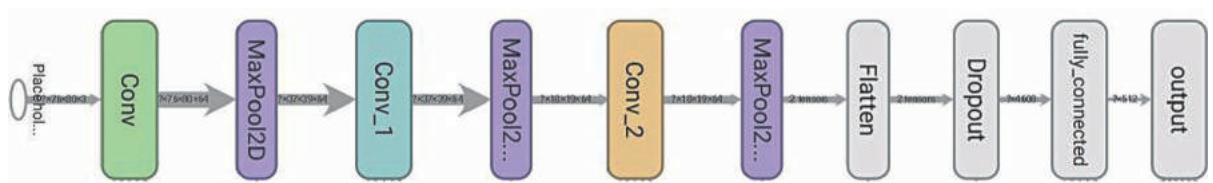


**Figure 3.** Structure of convolutional neural network

The deviation on the output per sample is calculated as the average of the deflections of each output value from the actually established value. Network training will be done through this deviation.

Later on, from the results of network construction, the assessment of abnormal area change can be carried out according to the following steps: to have the boundary of abnormal area at a given time, to figure the boundary of abnormal area at the moment and to assess the change. Having an abnormal area at the previous scan of the patient, we want to determine the change of that known abnormal area. The initial position is taken on the earlier boundary area. We need to identify the contour

- Variable parameters are normalized to paragraph [0, 1].

After several sampling iterations over a set of labeled medical images, we will build a specific learning data set. Note that the regression is performed for each point on the boundary, so to get the result boundary we need a postprocessing step that includes removing points that are too close together, inserting point when two consecutive points too far and handle cases where the updated points deviate to create an intersection.

**2.3. Building regression network**

With the point-to-point regression problem described along with how to build the learning data set from a set of medical images that have been labeled with an abnormal area, the next step is to design a machine learning model to solve the regression problem at each point. The machine learning model used is a convolutional neural network structured as shown below.

of the abnormal area on the current image through the regression of the sampled locations as described above. For each position, the regression model will give parameters to change the new position. After some steps, the new location will converge and the results will be located on the current contour. We can evaluate to increase or decrease accordingly depending on the density of positions on the contour. With the new contour, it is easy to assess the change of abnormal area compared to the previous time.

**3. EXPERIMENT**

The technology was tested and installed with the support of open source libraries OpenCV, VTK and Tensorflow. The data set selected for testing is 3D-IRCADb-01<sup>5</sup> and it consists of a number

of anonymous medical image sets of patients and manually marked internal organs by medical professionals. The data set included CT scans of

10 women and 10 men; each patient's data was stored in a folder. Medical imaging data and the mask data are stored in DICOM format.

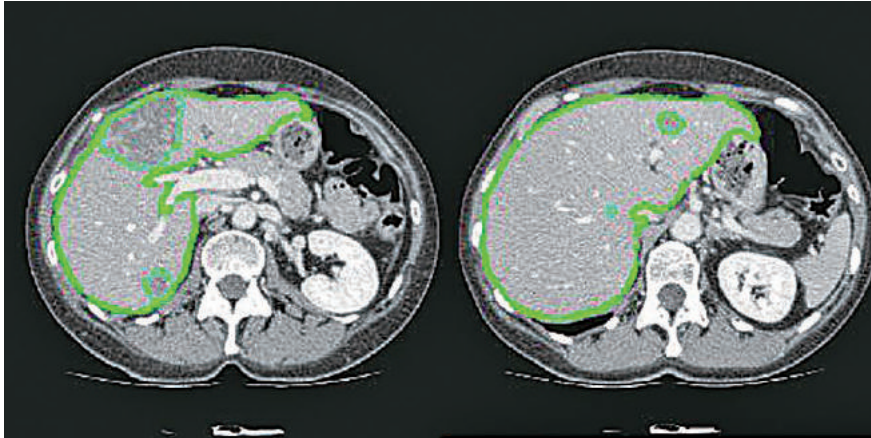


**Figure 4.** Illustrative data of 3D-IRCADb-01 set with liver area and abnormal area on liver

With slices with abnormal data, especially areas marked with liver tumors, we randomly generate data around the contours. The number of generated points is taken randomly and depends on the circumference of the abnormal

area. In the test to generate data, the number of surrounding sampling locations corresponding to an abnormal area is calculated by the circumference of the abnormal area multiplied by a random value in the segment  $[0.5, 2]$ .

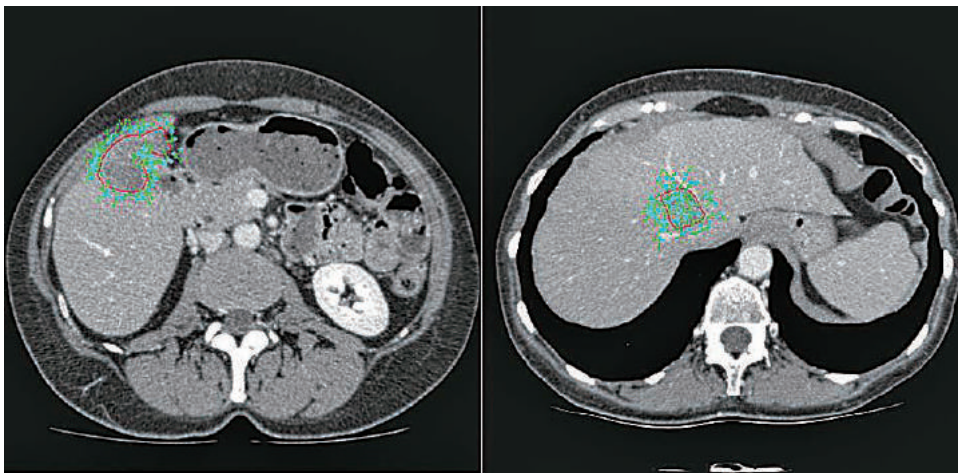


**Figure 5.** Illustration of random generation data around the boundary of the abnormal area: the abnormal area boundary is in red while the generated data samples consist of a position (in cyan) and the direction at that location (green arrow).

From the sampling around the contours of the abnormal areas, we get data sets for learning and evaluation of results. In the experiment with 3D-IRCADb-01 data, the number of data samples was taken as 161351, half of which will be for network learning and half will be used to assess model results during network learning.

The training program is installed and tested on the Google Colab platform; among them data has been pre-sampled. The deviation function is constructed by squaring the deviations from the regression value from included label value. This deviation function will be minimized during the training process.



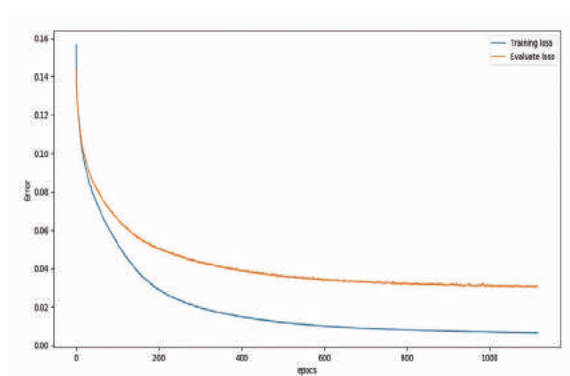


**Figure 6.** Chart updating training deviations in both training and evaluation

In addition, to facilitate evaluation, the article sets up the accuracy value. For each sample, it is considered true if each result value is less than 0.1 deviation from the corresponding value in the input label. On that basis, the article also calculates accuracy on training and assessment exercises during network learning.

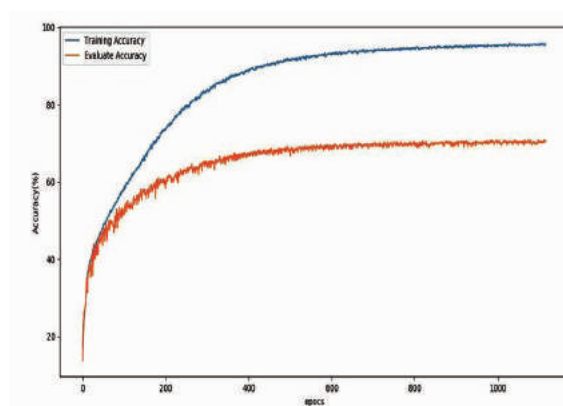


**Figure 7.** Chart updating training accuracy for both training and evaluation

On the basis of trained network, we apply it to build the function of updating the coordinates of points on the boundary of the abnormal area. This is the basic function to estimate the change of abnormal area compared to the previous state.

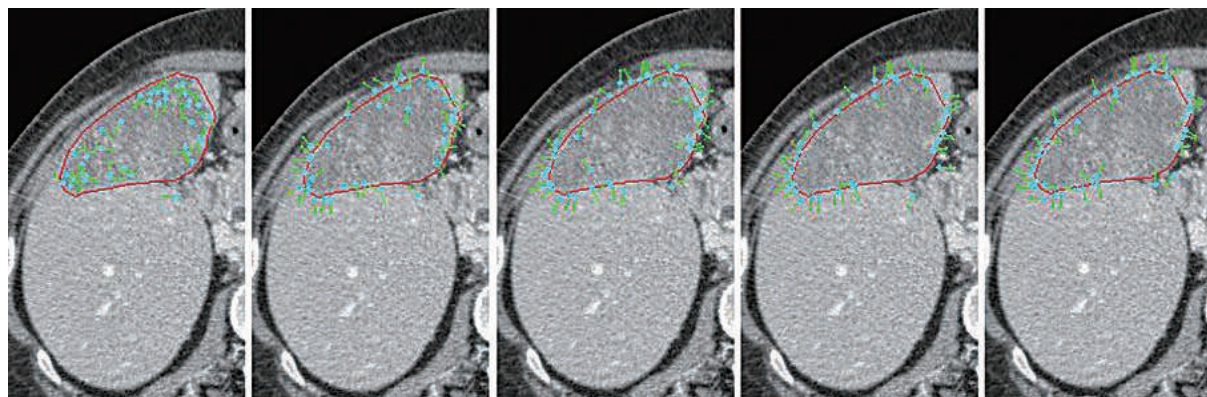


**Figure 8.** Process of updating the position of points on the contour of abnormal area

**4. CONCLUSION**

Identifying and assessing abnormal areas in medical imaging is generally an important issue, based on the application of research findings on machine vision and machine learning in practical problems. The article presents the technique of identifying points on the contour of abnormal area based on the analysis of local structures in the vicinity of the contour, in combination with machine learning regression. The technique has been tested on 3D-IRCADb-01 database and gained primary success. The outcomes demonstrate the effectiveness of the proposed

approach and technique. This is an essential basis for further improvement studies and more large-scale testing.

**REFERENCE**

1. Stegmann, B. Mikkel, and D. Pedersen. Bi-temporal 3D active appearance models with applications to unsupervised ejection fraction estimation, *Medical Imaging 2005: Image Processing, International Society for Optics and Photonics, 2005, 5747.*
2. T. F. Cootes, G. J. Edwards, and C. J. Taylor.

- Active appearance models, *ECCV*, **1998**, 2, 484-498.
3. Zhao, Wencheng, et al. Active contour model based on local and global Gaussian fitting energy for medical image segmentation, *Optik*, **2018**, 158, 1160-1169.
  4. Balakrishnan, Guha, et al. VoxelMorph: a learning framework for deformable medical image registration. *IEEE transactions on medical imaging*, **2019**, 38(8), 1788-1800.
  5. 3D-IRCADb01, <https://www.ircad.fr/research/3d-ircadb-01/>, Retrieved March 29, 2020.

## Ứng dụng công nghệ xử lý ảnh trong phân loại cà chua sau thu hoạch

Nguyễn Trường Duy<sup>1</sup>, Trần Đình Huy Đức<sup>1</sup>, Bùi Văn Vũ<sup>2,\*</sup>, Đỗ Văn Cần<sup>2</sup>

<sup>1</sup>Sinh viên ngành Kỹ thuật điện - Điện tử, Khoa Kỹ thuật và Công nghệ,  
Trường Đại học Quy Nhơn, Việt Nam

<sup>2</sup>Khoa Kỹ thuật và Công nghệ, Trường Đại học Quy Nhơn, Việt Nam

Ngày nhận bài: 29/05/2020; Ngày nhận đăng: 20/07/2020

### TÓM TẮT

Bài viết này trình bày về việc ứng dụng công nghệ xử lý ảnh trong việc phân loại cà chua theo màu sắc và kích thước quả. Việc xác định mức độ chín và kích thước của cà chua một cách tự động sẽ được đưa ra phân tích chi tiết và cụ thể trong bài báo này. Cụ thể, hệ thống sẽ thu thập hình ảnh từ máy ảnh được đặt trên băng chuyền. Hình ảnh sau khi được chụp bằng máy ảnh sẽ được đưa về bộ xử lý trung tâm để tính toán và phân tích. Các thuật toán về xác định biên và màu sắc của đối tượng sẽ được ứng dụng. Những quả cà chua không đạt yêu cầu sẽ được phát hiện dựa trên số điểm ảnh và kích thước đường biên của đối tượng được chụp. Mục tiêu của hệ thống này là để thay thế khâu phân loại cà chua theo hình thức thủ công vốn còn tồn tại các nhược điểm như độ chính xác chưa cao, năng suất lao động thấp.

**Keywords:** Xử lý ảnh, cà chua, màu sắc, kích thước, tự động.

\*Tác giả liên hệ chính.

Email: [bvvu@ft.edu.vn](mailto:bvvu@ft.edu.vn)

# Applying of image processing technology in classifying tomatoes after harvest

Nguyen Truong Duy<sup>1</sup>, Tran Dinh Huy Duc<sup>1</sup>, Bui Van Vu<sup>2,\*</sup>, Do Van Can<sup>2</sup>

<sup>1</sup>*Undergraduate student majoring in electrical and electronic engineering, Faculty of Engineering and Technology, Quy Nhon University, Vietnam*

<sup>2</sup>*Faculty of Engineering and Technology, Quy Nhon University, Vietnam*

*Received: 29/05/2020; Accepted: 20/07/2020*

## ABSTRACT

This paper applies image processing technology in classifying tomatoes by color and size. An automatic determination of ripeness and size of tomatoes will be analyzed in detail in this paper. Actually, the system will collect images from cameras placed on a conveyor belt. The images will be taken to the central processor for calculation and analysis. Algorithms is used to estimate the boundary and color of the object will be applied. Tomatoes that have low quality will be detected based on the number of pixels and border size of the subject being captured. The goal of this system is to replace manual grading of tomatoes that still have shortcomings such as low accuracy, low labor productivity.

**Keywords:** *Image processing, tomatoes, color, size, automatic.*

## 1. INTRODUCTION

Vietnam is a country with a high proportion of agricultural sectors. However, the labor productivity of this industry is not high. Therefore, the application of science and technology in the field of production and export of agricultural products is very necessary. Currently, the post-harvest classification of agricultural products, particularly tomatoes in our country, is mainly done by hand. When using human power, tasks that require high concentration and repetition make the eyes strained and tired, so it is difficult to guarantee accurately, especially in the case of high-frequency labor. These forms of manual labor need to be replaced by automatic or semi-automatic models to overcome the above weakness. This improves the accuracy, labor productivity and product quality so that Vietnam's agricultural products can compete

with the agricultural products of developed countries in the world.

Today, one of the technologies that is supposed to replace the manual classification of agricultural products after harvest is image processing.<sup>1-7</sup>

In this study, the author will apply image processing technology to classify tomatoes after harvest. The technology mentioned by the author can overcome the shortcomings of the visual classification of tomatoes used in our country today such as: high accuracy, high labor productivity, quality of production, good product. Different image processing algorithms will be used in author's study.<sup>8-12</sup>

## 2. STUDY METHODS AND TECHNIQUES

### 2.1. Method of classifying tomatoes according to its color

In order to classify the ripeness of tomatoes,

---

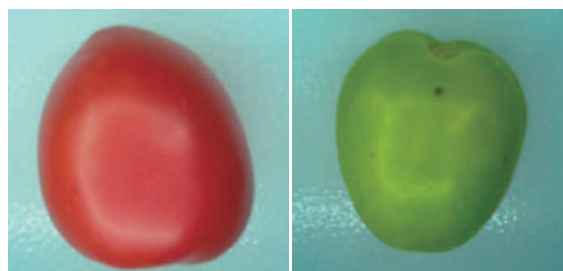
\*Corresponding author.

Email: [bvvu@ft.edu.vn](mailto:bvvu@ft.edu.vn)

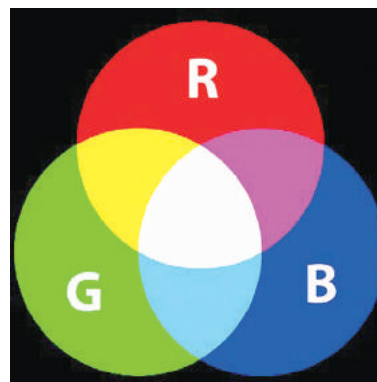
the system relies on the images obtained from the camera. First, images captured from the camera are converted to the HSV color space. Next, the image will be divided into 3 separate color channels H, S, V and then a series of comparison analysis algorithms are used to output the results. The analysis algorithm for tomato fruit color is shown in detail in Figure 1.<sup>4,12</sup>

Figure 2 shows a photo of tomatoes taken from a camera. This image is represented under the RGB color space.<sup>2,3,12,13</sup> RGB color spaces use a complementary pattern where red, green, and blue light are combined each other in different ways to form different colors.

The RGB color model is depicted in Figure 3. The advantage of the RGB model is that it is convenient for color correction, but this color model is not suitable for image processing. Therefore, the image needs to be converted to the HSV color space (figure 4).<sup>3,12,13,14</sup>



**Figure 2.** Tomato images were taken from the camera.



**Figure 3.** RGB color space.

To convert from RGB color space to HSV color space, formulas (1) - (5) are used.<sup>8,9</sup>

$$H = \arccos\left(\frac{\frac{1}{2}(2R - G - B)}{\sqrt{(R - G)^2 - (R - G)(G - B)}}\right) \quad (1)$$

$$H = H_1 \quad \text{if } B < G \quad (2)$$

$$H = 360^\circ - H_1 \quad \text{if } B > G \quad (3)$$

$$S = \frac{\max(R, G, B) - \min(R, G, B)}{\max(R, G, B)} \quad (4)$$

$$V = \frac{\max(R, G, B)}{255} \quad (5)$$

Where,

R, G, B: are values representing the intensity of red, green, and blue in the RGB color space, respectively (0 -255).

H: The value represents the color area.

S: value that represents color saturation.

V: value represents luminous intensity.

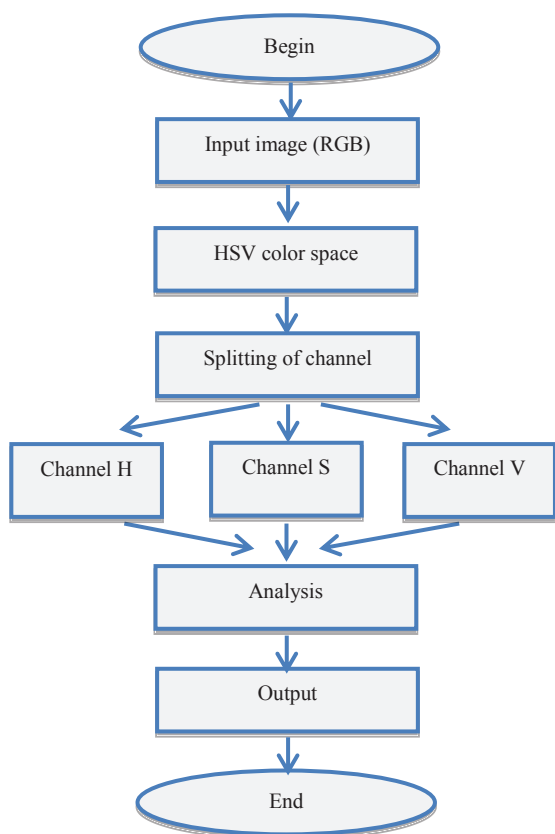


**Figure 1.** The algorithm determines the maturity level of the tomatoes.

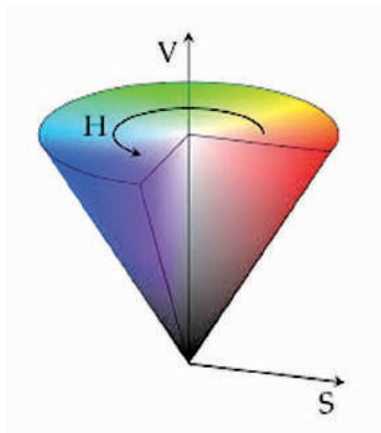


Figure 4. HSV color space.

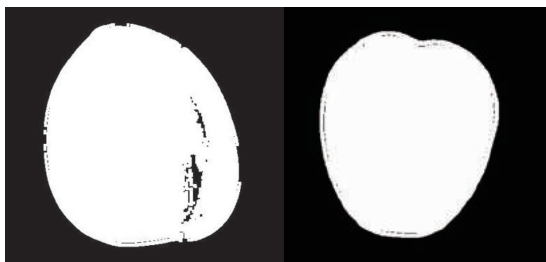


Figure 5. The binary image of the object.

After the object image is converted from the RGB color space to the HSV color space, we obtain the values of the color channels. From the values of these color channels, we obtain a binary image of the object (see Figure 5). Based on this binary image, we determine the number of pixels in the each object image, the number of white pixels of each color in the object image and the number of black pixels. Once these data are available, the author can determine the proportions of each color and use this result to determine the maturity level of the fruit.

**2.2. Method of classifying tomatoes according to fruit size**

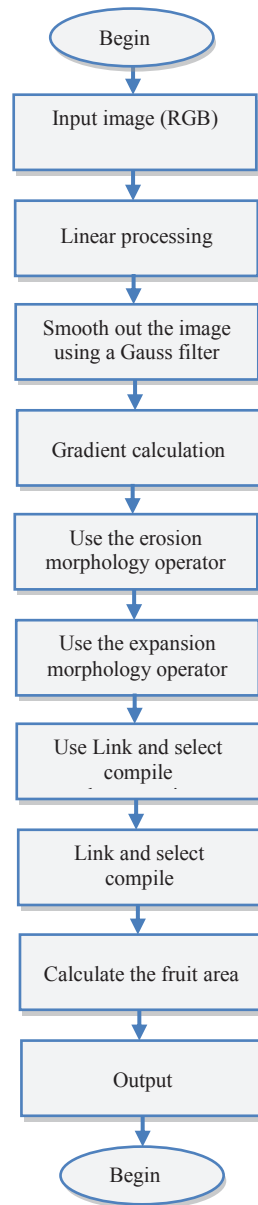


Figure 6. Diagram of the fruit size classification process.

To be able to remove tomatoes that do not satisfy the size requirements, the authors used a method of determining the boundary of the object image captured from the camera.<sup>10,11</sup> The size of the analyzed tomato is the area of the figure surrounded by the boundary.

Derived from related concepts about the boundary point and boundary,<sup>1</sup> there are two methods used to detect the boundary of an object. The first method is the direct method. This method aims to enhance the boundary

based on the variation in the pixel's luminance value. The direct method using mainly derivative techniques (Gradient, Sobel, Prewitt, Laplace, Canny, ...).<sup>1,7,15</sup> And, the second method is the indirect method. This method often relies on the surface texture of the image to divide the image into regions, the border between those regions is the boundary need to be detected. Indirect edge detection method is difficult to set up but works well when there is small variation in luminance.<sup>1,7,15</sup>

Here, the author uses the Canny boundary detection method, which is commonly used because it has the advantage of being less affected by noise.<sup>1</sup> The process diagram of fruit size determination is shown in Figure 6.<sup>11</sup> Canny boundary detection method is shown in formula (6) - (12).<sup>1,7,10,11</sup>

We have the derivative of a filtered image:  $\nabla f = \nabla(G \otimes I) = f_x + f_y$ , where  $f_x$  and  $f_y$  is the partial derivative of  $f$  in terms of  $x$  and  $y$  respectively.

Hence, we obtain formula (6):

$$\nabla f = \nabla(G \otimes I)_x + \nabla(G \otimes I)_y = \nabla(G_x \otimes I) + \nabla(G_y \otimes I) \quad (6)$$

Taking the partial derivative of  $G$  for  $x$  and  $y$ , we get:

$$G_x(x, y) = \frac{-x}{\sigma^2} e^{-\frac{(x^2+y^2)}{2\sigma^2}} \quad (7)$$

$$G_y(x, y) = \frac{-y}{\sigma^2} e^{-\frac{(x^2+y^2)}{2\sigma^2}} \quad (8)$$

Where,

$x, y$ : are directions

$\sigma$ : width control parameter

Furthermore, the Gaussian filter is decoupled so that convolutional charges can be performed separately for  $x$  and  $y$ . See equations (9) and (10):

$$G_x(x, y) = G_x(x) \otimes G(y) \quad (9)$$

$$G_y(x, y) = G_y(y) \otimes G(x) \quad (10)$$

From (6), (9) and (10), we have (11) and (12):

$$f_x(x, y) = G_x(x) \otimes G(y) \otimes I \quad (11)$$

$$f_y(x, y) = G_y(y) \otimes G(x) \otimes I \quad (12)$$

After Gaussian blurring, the image pixel values are extracted for low threshold and high threshold values. The authors use the Gradient operator to calculate the local gradient of amplitude and direction.

Assuming that  $g_1$  and  $g_2$  are gradients in  $x$  and  $y$  directions, respectively, then the amplitude of the gradient at the point  $(m, n)$  and the direction of the boundary at the point  $(m, n)$  are calculated by equations (13) and (14):<sup>1,11</sup>

$$A_0 = g(m, n) = \sqrt{g_1^2(m, n) + g_2^2(m, n)} \quad (13)$$

$$\theta_r(m, n) = \arctan \frac{g_2(m, n)}{g_1(m, n)} \quad (14)$$

After using the Gradient operator to calculate the local gradient, the authors use the erosion morphology operator to remove white noise.<sup>1</sup> White points with a low pixel value are removed. Because the morphology operator removes white noise, the thickness and size of the boundary will be reduced. Therefore, the authors continue to use the expansion morphology operator with the aim of increasing the size of the boundary after using noise and erosion removal algorithms. Now we get a curve connecting all continuous points of the same color or intensity. This curve is the boundary of the object. Figure 7 shows a picture of the tomato after marginal extraction.

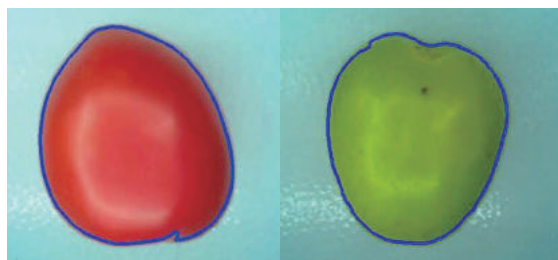


**Figure 7.** Photo after determining border.

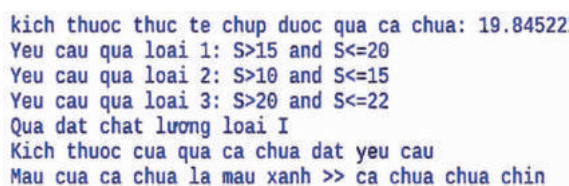


**Figure 8.** Cross-sectional area of above red tomato.

kích thước thực tế chụp được quả cà chua: 20.56933  
 Yêu cầu quả loại 1:  $S > 15$  and  $S \leq 20$   
 Yêu cầu quả loại 2:  $S > 10$  and  $S \leq 15$   
 Yêu cầu quả loại 3:  $S > 20$  and  $S \leq 22$   
 Quả đạt chất lượng loại III  
 Kích thước của quả cà chua đạt yêu cầu  
 Màu của cà chua là màu cam >> cà chua chưa chín

Figure 9. Cross-sectional area of above green tomato.

After we have the boundary of the object image, we compute the cross-sectional area of the fruit. The cross-sectional area of the fruit is here understood as the area delimited by the boundary of the object image. Figures 8 and 9 show cross-sectional area data of two tomatoes taken from the experimental model. Figure 8 shows data for red tomatoes (see Figure 7) and Figure 9 shows data for green tomatoes (see Figure 7).

2.3. Building of the system program

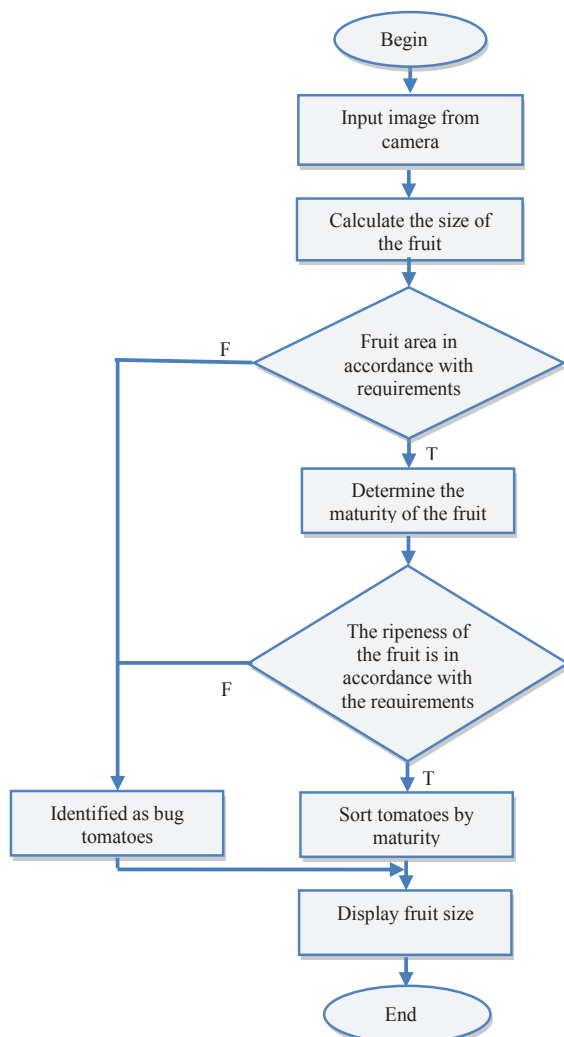


Figure 10. General system algorithm diagram.

From the analytical results in sections 2.1 and 2.2, a general algorithmic scheme is built for an automatic tomato classification system. This algorithmic automatic tomato classification scheme is shown in Figure 10.

From the general algorithm diagram in Figure 10, a block diagram of the classification system is proceed to build. The central controller of the system is raspberry, Arduino Uno, and PLC S7-200 devices (see Figure 11). From the diagram shown in Figure 11, authors select the types of equipment to build the experimental model as shown in Figure 12 and Figure 13.

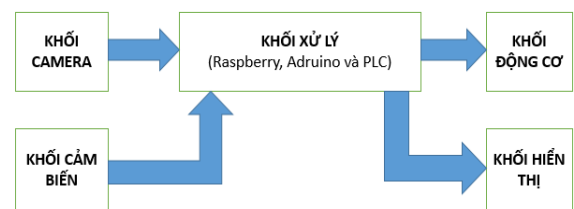


Figure 11. Diagram of the system's blocks.

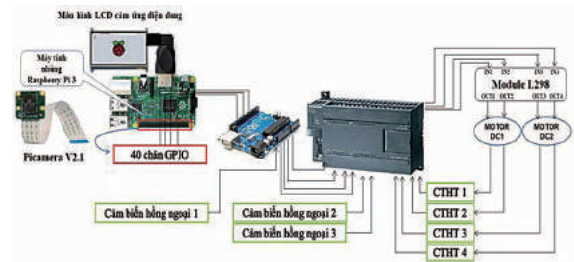


Figure 12. Diagram of controlling of the classification process.

2.4. Experimental results

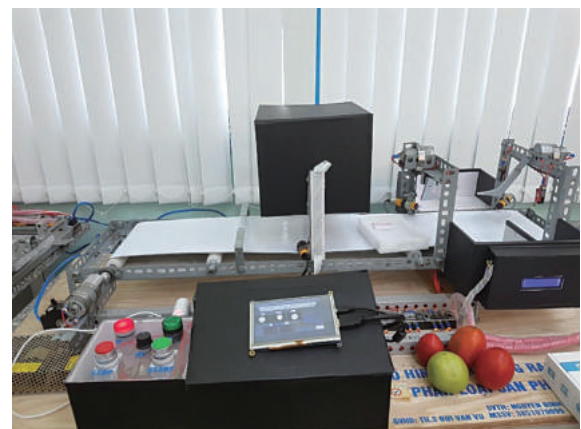


Figure 13. Experimental model.

The experimental model includes the following blocks:

a. Processing block



Kit Raspberry Pi 3 Model B +: Used to receive image signals from the camera, perform image processing according to pre-programmed program, and send signals to PLC.

PLC S200: Receiving signals from Raspberry and transmits signals to actuators of a sorting system.

*b. Camera block*

The Camera block has the function of collecting real-world image signals and converting them to electrical signals and sending data to the Raspberry Pi unit in the model using Raspberry Pi camera.

*c. Sensor block*

The sensor block used to detect the fruit has reached the position of the camera in the model uses infrared sensor E18-D80NK.

*d. Actuator block*

This unit receives signals from S7 -200 PLC to control the swing arms to bring products with different degrees of ripeness to different boxes.

*e. Display block*

The display block has the function of displaying information about the color and size of the fruit. In the model using a 7 inch LCD (Raspberry Pi) screen.

The entire product classification process is as follows:

**Step 1:** When starting up the system, the conveyor belt brings the sorted tomatoes to the camera's location. When the sensor detects that the fruit has reached the camera position. Raspberry will take the image signal of the object and process the image (see Figure 14).

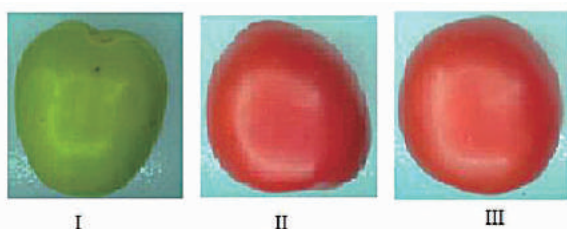


**Figure 14.** Experimental results taken from the camera

**Step 2:** An algorithm to determine the size of the fruit will be done by raspberry. The size of the fruit will be determined based on the area delimited by the boundary of the object's image. The experimental results of the boundary determination process are shown in Figure 15. In the system developed, the tomato subjects were classified into four groups based on fruit size. Particularly, Group 1, the fruit has a size of 15-20 (cm<sup>2</sup>); Group 2, the fruit has a size of 10-15 (cm<sup>2</sup>); Group 3, the fruit has a size of 20-22 (cm<sup>2</sup>), and Group 4, the fruit has a size of smaller than 10 (cm<sup>2</sup>) or larger than 22 (cm<sup>2</sup>) (see Figure 17, Figure 18 and Figure 19). In case of unsatisfied fruits (a size of smaller than 10 (cm<sup>2</sup>) or larger than 22 (cm<sup>2</sup>)), the system will sort immediately without any color determination. The fruits of these different groups are classified and put in different containers.

After classifying tomatoes according to fruit size, the system will determine the maturity level of the fruit based on the color of the fruit. In terms of color, the system only selects fruits from light red to red. Fruits of other colors are rejected because the fruit is still green or the fruit is overripe.

Figure 16 shows an experimental result taken from Raspberry's memory when determining the color of an object based on the number of white pixels of each color.

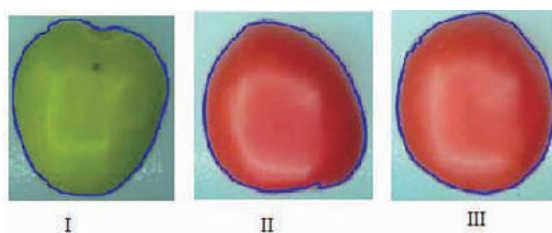


**Figure 15.** Experimental results of determining the object boundary.

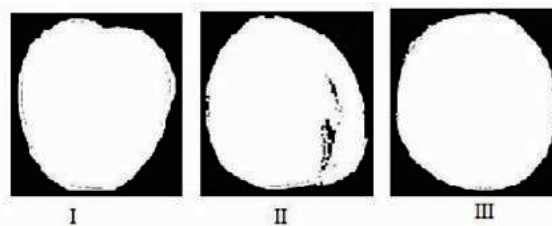


**Figure 16.** Experimental results of objects after converting to binary images.

**Step 3:** Display information on the LCD screen.

In this step, the maturity and fruit size information will be displayed on an LCD screen connected directly to the Raspberry (see Figures 17, 18, and 19).

Figure 17 shows the first tomato's data (see Figure 15) displayed on the Raspberry screen. This fruit is analyzed by the system as an unripe tomato. At the same time, the system also analyzes this fruit with a cross-sectional area of 19.84522 (cm<sup>2</sup>), while the experimental measured data was about 19 (cm<sup>2</sup>).

Figure 18 shows the second tomato's data (see Figure 15) displayed on a Raspberry screen. The fruit is analyzed by the system to be orange in color. At the same time, the system also analyzes this fruit with a cross-sectional area of 20.56933 (cm<sup>2</sup>), while the experimental measured data was about 21.4 (cm<sup>2</sup>).

Figure 19 shows the third tomato's data (see Figure 15) displayed on a Raspberry screen. This fruit was analyzed by the system to have a cross-sectional area of 25.32344 (cm<sup>2</sup>), while the experimental measured data was about 25.5 (cm<sup>2</sup>). Because in the program programmed for Raspberry, tomatoes are too big, larger than 22 (cm<sup>2</sup>), are removed without analyzing its color. Therefore, the system does not need to analyze its color for this fruit (see Figure 19).

```
kích thước thực tế chụp được quả cà chua: 19.84522
Yêu cầu quả loại 1: S>15 and S<=20
Yêu cầu quả loại 2: S>10 and S<=15
Yêu cầu quả loại 3: S>20 and S<=22
Quả đạt chất lượng loại I
Kích thước của quả cà chua đạt yêu cầu
Màu của cà chua là màu xanh >> cà chua chưa chín
```

**Figure 17.** Information display about maturity level and size of the first fruit.

```
kích thước thực tế chụp được quả cà chua: 20.56933
Yêu cầu quả loại 1: S>15 and S<=20
Yêu cầu quả loại 2: S>10 and S<=15
Yêu cầu quả loại 3: S>20 and S<=22
Quả đạt chất lượng loại III
Kích thước của quả cà chua đạt yêu cầu
Màu của cà chua là màu cam >> cà chua chưa chín
```

**Figure 18.** Information display about maturity level and size of the fruit.

```
kích thước thực tế chụp được quả cà chua: 25.32344
Yêu cầu quả loại 1: S>15 and S<=20
Yêu cầu quả loại 2: S>10 and S<=15
Yêu cầu quả loại 3: S>20 and S<=22
kích thước của quả cà chua không đạt yêu cầu
loại
```

**Figure 19.** Information display about maturity level and size of the third fruit.

The results of fruits' size analysis in Figures 17, 18, and 19 show that the built-in automatic tomato classifying system can determine the size of tomatoes with a maximum error of 5%.

In the study, the author has tested on 200 tomato samples on the experimental model built. The experimental results show that, in terms of color grading criteria, the system accurately classifies the colors of 200 experimental tomato samples. Regarding the criteria of product classification according to the size of the fruit, the system determines the size of the fruit with an error of not more than 1.32 (cm<sup>2</sup>).

Figure 20 shows analytical data of 10 samples per 200 samples of tomatoes that were tested. The statistics show that the maximum size error of the system is 1.32 (cm<sup>2</sup>) and there is no error in determining fruit color. Also, the process from taking pictures to getting classification results on raspberry for a tomato sample is approximately 0.6 seconds.

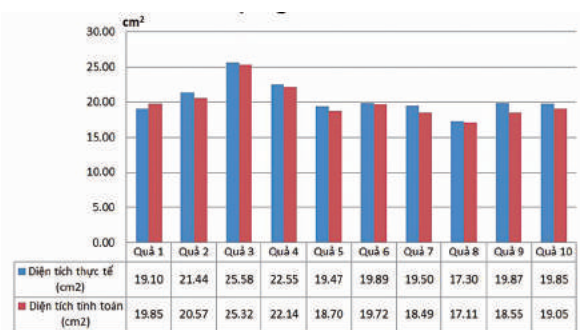


**Figure 20.** Analytical data of 10 tomato samples.

**3. CONCLUSION**

The paper presents the application of image processing technology in the automatic tomato grading system after harvest. In the paper, authors have applied image processing algorithms to identify the maturity level and size of tomatoes to classify. Tomatoes of different sizes and satisfactory maturity will be classified and sent to different containers. Beside, fruits that are too large or too small, or too ripe or green will be rejected by the system. Furthermore, the author

has also successfully built an experimental model of the system. The experimental results show that the system is stable, has high accuracy and high productivity.

#### 4. REFERENCES

1. Lương Mạnh Bá, Nguyễn Thanh Thủy. *Nhập môn xử lý ảnh số*, Nhà xuất bản Khoa học và Kỹ thuật, Hà Nội, 2006.
2. P. Koirala. *RGB Color Space*, Department of Computer Science and Statistics, University of Joensuu, 2017.
3. D. Cardani. *Adventures in hsv space*, *Laboratorio de Robótica*, Instituto Tecnológico Autónomo de México, 2001.
4. R. R. Mhaski, P.B. Chopade and M.P. Dale of MES College of Engineering. *Determination of Ripeness and Grading of Tomato using Image Analysis on Raspberry Pi*, International Conference on Communication, Control and Intelligent Systems (CCIS), 2015.
5. Nguyen Duc Thong; Nguyen Truong Thinh; Huynh Thanh Cong. *Mango Classification System Uses Image Processing Technology and Artificial Intelligence*, 2019 International Conference on System Science and Engineering (ICSSE), IEEE, 2019.
6. Andrés Felipe Sánchez-Aguiar, Alberto Mario Ceballos-Arroyo and Albeiro Espinosa-Bedoya. *Toward the recognition of non-defective coffee beans by means of digital image processing*, Symposium on Image Symposium on Image (22<sup>th</sup>), Signal Processing and Artificial Vision (STSIVA), 2019.
7. G. Xin, C. Ke, H. Xiaoguang. *An improved Canny edge detection algorithm for color image*, 10<sup>th</sup> International Conference on Industrial Informatics, 2012.
8. P. Li, Y. Huang and K. Yao. *Multi-algorithm Fusion of RGB and HSV Color Spaces for Image Enhancement*, In Proceedings of the International Conference on 37<sup>th</sup> Chinese Control Conference (CCC), 2018.
9. K.N. Plantaniotis and A.N. Ventsanopoulos. *Color image processing and applications*, Springer, 2000.
10. Vinh Du Mai, D. Miao, R. Wang and H. Zhang. *An Improved Method for Vietnam License Plate Location*, 2011 International Conference on Computation and Information Sciences, 2011.
11. Ali, M. H. Mouad, P. Yannawar, and A. T. Gaikwad. *Study of edge detection methods based on palmprint lines*, 2016 International Conference on Electrical, Electronics, and Optimization Techniques (ICEEOT), 2016.
12. P. Ganesan, V.Rajini, B.S. Sathish Khmar and Basha.Shaik. *HSV Color Space Based Segmentation of Region of Interest in Satellite Images*, International Conference on Control, Instrumentation, Communication and Computational Technologies (ICCICCT), 2014.
13. L. Feng, L. Xiaoyu, C. Yi. *An efficient detection method for rare colored capsule based on RGB and HSV color space*, International Conference on Granular Computing (GrC), 2014.
14. R. P. Salunkhe & A. A. Patil. *Image Processing for Mango Ripening Stage Detection: RGB and HSV method*, International Conference on Image Information Processing (3<sup>rd</sup>), 2015.
15. J. Zhang. *Edge detection in glass fragmentation images based on One Order Differential operator*, Second International Conference on Computer Engineering and Applications, 2010.



# Hệ thống giám sát và cảnh báo lũ lụt thời gian thực ứng dụng công nghệ LoRa cho lưu vực sông Côn - Hà Thanh, tỉnh Bình Định

Trần Văn Trung, Nguyễn Đức Thiện\*, Lê Song Toàn, Ngô Văn Tâm, Hồ Văn Phi

*Khoa Kỹ thuật và Công nghệ, Trường Đại học Quy Nhơn, Việt Nam*

*Ngày nhận bài: 09/07/2020 ; Ngày nhận đăng: 09/08/2020*

## TÓM TẮT

Trong bối cảnh của biến đổi khí hậu như hiện nay, lũ lụt đã và đang gây ra những thiệt hại nghiêm trọng đến tính mạng và tài sản của người dân trên toàn cầu nói chung, Việt Nam nói riêng, trong đó có Bình Định. Do vậy, việc xây dựng các hệ thống giám sát và cảnh báo lũ sớm với công nghệ hiện đại là yêu cầu hết sức cấp thiết. Trong bài báo này, các tác giả sẽ nghiên cứu và thiết kế một hệ thống giám sát và cảnh báo lũ lụt thời gian thực ứng dụng công nghệ LoRa kết hợp với nền tảng mã nguồn mở Thingsboard. Hệ thống này cho phép thu thập số liệu tại các khu vực khác nhau trên sông một cách đầy đủ, chính xác và kịp thời, nhằm phục vụ cho công tác dự báo và cảnh báo sớm. Hệ thống đề xuất được triển khai thử nghiệm trên lưu vực sông Côn - Hà Thanh, tỉnh Bình Định.

**Từ khóa:** *Giám sát và cảnh báo lũ lụt, thời gian thực, LoRa, IoT và Thingsboard.*

---

\*Liên hệ tác giả chính

Email: [nguyenducthien@qnu.edu.vn](mailto:nguyenducthien@qnu.edu.vn)

# A real-time flooding monitoring and warning system using LoRa technology in Kone and Ha Thanh river basin, Binh Dinh Province

Tran Van Trung, Nguyen Duc Thien\*, Le Song Toan, Ngo Van Tam, Ho Van Phi

*Faculty of Engineering and Technology, Quy Nhon University, Vietnam*

*Received: 09/07/2020; Accepted: 09/08/2020*

## ABSTRACT

In the context of the recent climate change, flooding has been causing serious damages to the human lives and their properties in the world in general, Vietnam in particular, including Binh Dinh province. Therefore, it is pivotal for local governments to build up real-time flooding monitoring and warning systems supported by modern technologies. Addressing to this aim, in this paper, we will study and design a new flooding monitoring and warning system based on a combination of the Long Range (LoRa) technology and an open-source platform of Thingsboard. The proposed system allows collecting effectively and sufficiently data from different locations on rivers in a timely manner, thus supporting the early flooding prediction and forecast processes. A testbed of the proposed system is then deployed in the Kone and Ha Thanh river basin, Binh Dinh Province.

**Keywords:** *Flooding monitoring and warning, Realtime, LoRa, IoT and Thingsboard.*

## 1. INTRODUCTION

Flooding has been causing serious damages to the lives and property of people around the world. According to the Center for Research on the Epidemiology of Disasters - EM-DAT Database (<https://www.emdat.be/>), over the period 2000 - 2018, water-related disasters accounts for 90% of total global natural disasters, of which floods account for about 54%. During the same period, human losses amounted to 93,470 and economic losses to nearly 500 billion USD.<sup>1</sup>

One of the biggest challenges of mitigation of flooding damages to communities is how to provide local residences with warnings of natural disasters in a timely manner. In June 2015, the United Nations adopted the Sendai Framework for Disaster Risk Reduction 2015 - 2030.<sup>2</sup> The Sendai Framework is considered as an effective

approach for flooding risk management.<sup>2,3</sup> Especially, the Sendai Framework emphasises roles of Flooding Early Warning Systems (FEWS) and recognises that the FEWS is an important prerequisite to collect data accurately and promptly in different regions and areas. These data are expected to effectively serve the forecast and early warning of weather and climatic extremes<sup>3,4</sup>.

In the current global climate change context, flooding is becoming more dangerous and unpredictable. Vietnam, a country located in the monsoon tropics and one of the five "storm centers" of the Asia-Pacific region has been facing various types of natural disasters with increasing severity. Notably, the Southern Central Coastal regions such as Binh Dinh, Phu Yen, Khanh Hoa, Ninh Thuan were severely affected.

---

\*Corresponding author:

Email: [nguyenducthien@qnu.edu.vn](mailto:nguyenducthien@qnu.edu.vn)

Binh Dinh has a natural area of 6,039 km<sup>2</sup> with a coastline of more than 135 km and a population of 1,486,918 people<sup>5</sup>. The whole province lies neatly on the eastern side of the Truong Son mountain range, with steep and complicated terrain. The slope direction is mainly from West to East, hills and plains alternate to form separate regions and basins under the major river systems including Lai Giang, Kone, La Tinh and Ha Thanh. Due to the influence of natural geographic factors, topography, geology, and climate, Binh Dinh and the Kone - Ha Thanh river basin in particular are often influenced by heavy flooding, causing serious damages to the local residences, property, infrastructure and environment. In this circumstance, the main mission of Binh Dinh authority is to implement early flood monitoring and warning systems in order to mitigate damages caused by floodings.

Towards the above goal, under the sponsorship of the German International Cooperation Organization - GIZ<sup>6</sup> and Rockefeller<sup>7</sup>, Binh Dinh authority deployed an early flood warning system on the Kone - Ha Thanh river basin in 2016. In 2018, The Provincial Steering Committee for Disaster Prevention and Search and Rescue built up a rainfall and flooding data transmission and management system in the Kone - Ha Thanh area<sup>8</sup>. A disaster prevention information system introduced by Hitachi was also deployed in Binh Dinh<sup>9</sup>. The above systems are responsible for collecting data from hydro-meteorological stations, monitoring and sending them to a headquarter via available telecommunication infrastructures. Based upon analysing collected data, adequate warnings will be sent to the authorities or the local people through the mass media. After a period of operation, however, the efficiency achieved from the above systems is not high as expected and there are several following limitations:

- In the existing systems, devices using the standards of WiFi and mobile technologies (i.e., 2G, 3G, or 4G) are powered by available electricity grids. In fact, when floodings happen,

it is very difficult to maintain electricity sources to ensure the continuous operation of stations and transmission lines, especially in mountainous and remote areas;

- Due to the disruption of communication systems (i.e., broken or swept away broadcasting stations), communication between the authorities and residents in flooded areas is limited, making it difficult for search and rescue activities;

- The number of stations deployed in the area is small and the density of stations is low (e.g., the Rockefeller warning system in the Kone - Ha Thanh river basin has from 4 to 7 stations). As a result, there is a lack of the collected data which is influencing the accuracy of warnings and forecasting models;

- The large-scale deployment of the FEWS requires high costs. Furthermore, these systems are copyrighted systems in terms of hardware and software. Therefore, it is difficult for the local authorities to deploy in a large scale.

To solve these limitations, studying and implementing new solutions and technologies for flooding monitoring and early warning are essential. In recent years, Internet-of-Things (IoT) and Low Power Wide Area Network (LPWAN) like Wireless Sensor Networks (WSN), Long Range (LoRa) are emerging as potential technologies for FEWS<sup>10</sup>. Compared to solutions used in the existing systems<sup>6-9</sup>, LoRa or WSN can be deployed with open source platforms, hardware and software costs are fairly low. In particular, the LoRa or WSN-based devices can operate in a long time, up to 3 - 10 years by using only AA batteries. Therefore, LPWAN solutions are attracting the attention of the scientific community and industries. Some typical real-time flood warning systems using LoRa or WSN have been proposed, such as Advantech's flood warning system<sup>11</sup>, Libelium<sup>12</sup>, Semtech<sup>13</sup>, Flood-Network<sup>14</sup>, or StormSense<sup>15</sup>. These systems ensure the full range of features of a flood warning system with user-friendly interfaces. However, the biggest limitation of

the above solutions is the cost of installation and operation. Typically, each toolkit with two or three sensor nodes costs from 5.000 to 7.000 Euros, which is too expensive for the local authorities to deploy in a large scale.

Meanwhile, there are not many FEWS combined with these new technologies in the domestic market. Recently, there is an intelligent flood warning system VFASS<sup>16</sup> allowing to collect data using the LoRa technology and broadcast warnings. However, it has not integrated with tools of visualisation and data management, making it difficult for flooding management.

As analysed above, the deployment of flooding monitoring and warning system upon a combination of IoT and LWPAN is necessary. In this work, the authors will design and implement a real-time flood monitoring and warning system based on LoRa technology combined with an open source platform Thingsboard. The system model proposed in this paper is expected to solve the above limitations. The system will be then deployed and evaluated in some frequently flooded areas of the Kone - Ha Thanh river basin.

The rest of the article includes the following sections. Section 2 describes background of flooding monitoring and warning systems, LoRa technology and the open source platform Thingsboard. Session 3 introduces the proposed real-time flooding monitoring and warning system. The implementation and evaluations of the proposed model are illustrated in Section 4. The conclusion of the paper is presented in Section 5.

## 2. BACKGROUND

### 2.1. An overview of FEWS

There are many different definitions of the FEWS. According to the United Nations Office's definition of disaster risk reduction, FEWS is *"an integrated system of hazard monitoring, forecasting and prediction, disaster risk assessment, communication and preparedness*

*activities systems and processes that enable individuals, communities, governments, businesses and others to take timely actions to reduce disaster risks in advance of hazardous events"*<sup>3</sup>. The architecture of FEWS includes basic functional components as described in Figure 1:

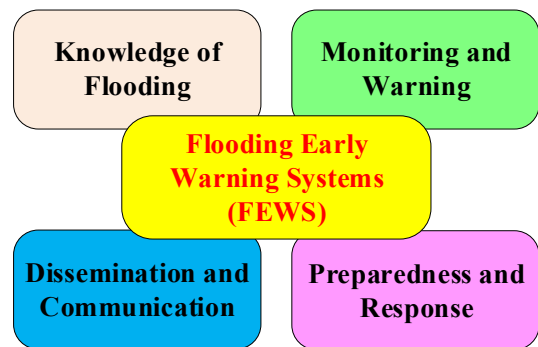


Figure 1. The architecture of FEWS<sup>3</sup>

In this paper, the authors focus on monitoring and warning components. By the end, we will design, build and implement a flooding monitoring and warning system by using the LoRa technology.

### 2.2. LoRa technology

LoRa (Long Range) is a wireless standard designed for LPWAN to connect devices with low bandwidth and data rates requirements, while focusing on coverage efficiency as well as energy efficiency. The LoRaWAN standard developed by the LoRa Alliance defines the Medium Access Control (MAC) layer and the LPWAN network architecture using the LoRa modulation method at the physical layer as shown in Figure 2. The operational frequency spectrum of the LoRa is from 430 MHz to 915 MHz. LoRa is one of the communication technologies in the low power long range connection group. LoRa works in the physical layer of LoRaWAN architecture Semtech<sup>10</sup>. LoRa technology allows data transmission at distances up to several kilometers without the need for power amplifiers, thereby saving energy consumption when transmitting/receiving data and can operate for a long time before replacing the battery.



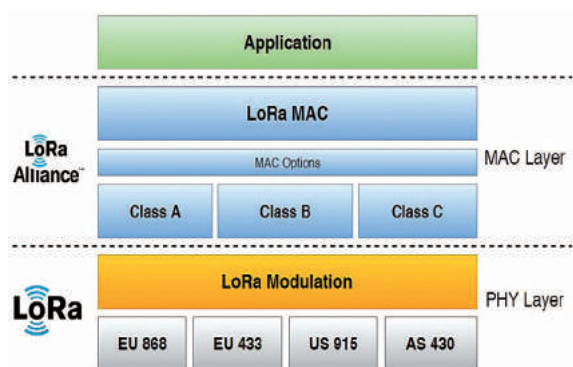


Figure 2. LoRa technology và LoRaWAN<sup>10</sup>

LoRa uses a Chirp Spread Spectrum (CSS) modulation technique. The data will be hashed with high-frequency pulses to produce a signal with a frequency range higher than that of the original data (called chipped). These high-frequency signals are encoded in sequences of Chirp signals (sinusoidal signals whose frequency changes over time). The CSS principle allows for less complexity and improves the accuracy of the receiver circuit so that data can be decoded and reprocessed. Furthermore, LoRa can transmit at a long distance without using a high transmission power level, even when the signal power is lower than ambient noise.

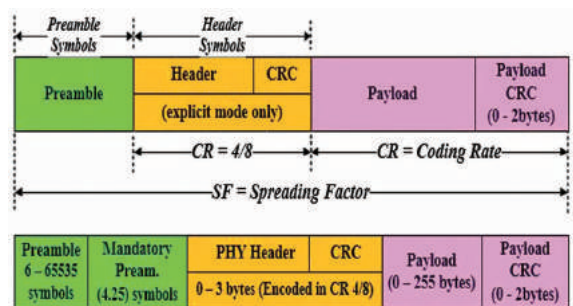


Figure 3. LoRa packet structure<sup>10, 17</sup>

The LoRa packet structure is depicted in Figure 3 and includes the following information:

- Header: contains information about the size of the download (Payload) and PayloadCRC or not.
- Payload: is the length of the application data that needs to transmit.
- Spreading Factor (SF): determines the number of Chirp signal chains when encoding

the frequency-modulated signal. The value of SF varies from 7 to 12. The larger SF value is, the data transmission time is longer and the transmission distance is extended.

- Bandwidth (BW): defines the frequency range at which the Chirp signal can change. The higher the bandwidth is, the shorter chipped signal encoding time will be. In this circumstance, the data transmission time is reduced, and the transmission distance is also shortened. The three common bandwidth levels for LoRa are 125 kHz, 250 kHz, and 500 kHz.

- Coding Rate (CR): is the number of bits that are automatically added to each payload in a LoRa packet by the LoRa chipset to help the receiver circuit to restore some of the data bits if there is an error in the reception process. The higher the CR, the more likely it is to receive the correct data; but the LoRa chip has to send more data.

SF, BW, CR are three basic and important parameters of LoRa chipset. SF and BW will affect the time and distance of data transmission; CR only influences data transmission time. Depending on specific application requirements in terms of distance, data delivery rate, the values of SF, BW and CR can be selected to optimise transmissions over LoRa.

### 2.3. IoT open sources platform - Thingsboard

In order to store, manage, and display data collected in monitoring and warning models, the selection of the right IoT platform is important<sup>17,18</sup>. The IoT platform will perform the main functions such as: connecting devices, collecting, monitoring, managing and analysing data. Recently, many open source and commercial platforms have been proposed to meet the growing needs of IoT applications. Compared with the open source platforms Thingio, Sitewhere, WSO2, Kaa IoT, DeviceHive, Zetta, and Blynk. Thingsboard is considered a very effective platform to solve the need for collection, processing, and data visualization and device management<sup>17</sup>. Thingsboard includes some basic features as follows:

- Telemetry data collection: support telemetry data collection and storage in a reliable way. The collected data can be accessed using a custom website or server-side API;

- Data visualisation: Thingsboard provides many utilities to visualise data collected in real-time;

- Device management: Thingsboard offers abilities to register, manage devices as well as track devices' properties. Thingsboard also allows server-side applications to send control commands to devices via APIs;

- Dashboard: This functionality allows to display data and control devices remotely in real-time;

- Warning management: Thingsboard provides tools to initiate and manage alerts related to entities in the system, especially real-time alarm monitoring. To connect devices and exchange data, Thingsboard uses industry standard IoT protocols, typically MQTT (Message Queuing Telemetry Transport). MQTT is a Publish-Subscribe messaging protocol, uses low bandwidth, so it is an efficient protocol for IoT applications. In a system using the MQTT protocol, multiple clients connect to a server (called the MQTT Broker). Each client will subscribe to monitoring information channels (topic) or post data to that information channel<sup>18</sup>.

**3. A PROPOSED REAL-TIME FLOODING MONITORING AND WARNING SYSTEM**

**3.1. System model**

In the paper, the authors build a real-time flood monitoring and warning system based on the combination of LoRa technology<sup>10</sup> and the Thingsboard open source platform<sup>17</sup>. The basic idea of the system is to remotely collect important data, such as: rainfall level  $L$  (mm), water level  $H$  (m) and water flow rate  $V$  (m<sup>3</sup>/s). These data will be sent to the processing center and displayed in real time to serve for analytical monitoring and alert decision-making.

- Gateway (GW): is a central device that converts two wireless transmission protocols, LoRa and WiFi. GW will collect data from Nodes (or measuring points). These data will be updated on ThingsBoard MQTT Server to display to users via website interface and on smart phone. At the same time, GW sends control signals from MQTT Server to the Nodes to execute warning commands. In this paper, Nodes 1 and 2 can operate like monitoring nodes as well as controlling nodes (through the I/O pins available connecting to speakers or other warning devices).

- Monitoring nodes: are the terminals. The nodes are responsible for measuring values of rainfall, flow rate and river water level. Data is then sent

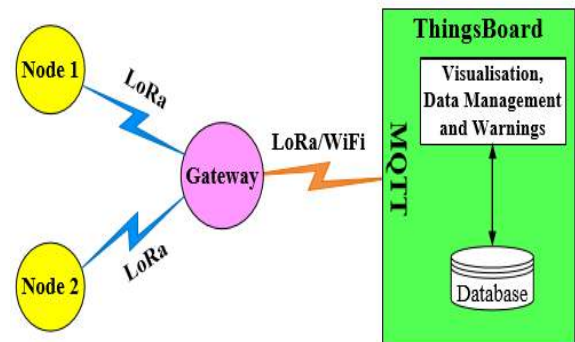


**Figure 4.** Proposed system model

to GW for further processing. The nodes communicate with GW over the LoRa protocol.

- User interaction: User is provided with an account to be able to access data on MQTT Server, monitor and control via website and smart phone interface.

- Thingsboard: This platform receives data from GW, processes and visualises it. Based on the proposed warning algorithm, Thingsboard will make the appropriate warning decisions and send the control command to GW to execute the warning process.

**3.2. Proposed monitoring and warning algorithm**

The proposed algorithm's flowchart is described in Figure 5. Warning decisions are released relied

on the analysis and evaluation of data stored on Thingsboard. Setting threshold values of  $L$ ,  $H$ ,  $V$  in the Thingsboard platform is dependent on the actual topographic conditions at the considering checkpoints and the authorities' regulations:

- *The threshold value of rainfall  $L$ :*  
Parameter  $L$  is determined using the regulation<sup>19</sup>

o Medium rain alarm:  $L1 = 50\text{mm}$  within 24 hours;

o Heavy rain alarm:  $L2 = 100\text{mm}$  within 24 hours;

o Very heavy rain alarm:  $L3 = \text{over } 100\text{mm}$  within 24 hours;

- *The threshold value of river water level  $H$ :* The value determined using the regulation<sup>20</sup>:

o Level 1:  $H1 = 6\text{m}$ ;

o Level 2:  $H2 = 7\text{m}$ ;

o Level 3:  $H3 = 8\text{m}$ .

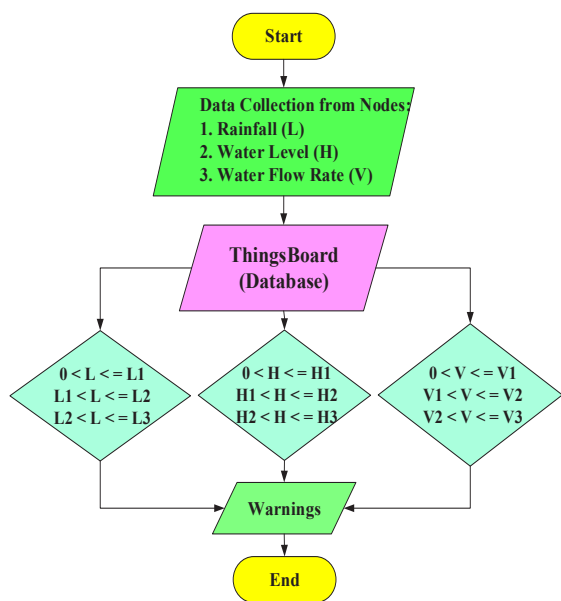


**Figure 5. Algorithm flowchart of flood warning process**

- *The threshold value of flow rate  $V$ :*  
Assuming that the parameters are set as follows:

o Level 1 alarm:  $V1 = 5 \text{ m}^3/\text{s}$ ;

o Level 2 alarm:  $V2 = 10 \text{ m}^3/\text{s}$ ;

o Level 3 alarm:  $V3 = 15 \text{ m}^3/\text{s}$ .

The proposed algorithm is executed by comparing parameters of  $L$ ,  $H$ ,  $V$  with threshold parameters ( $L1$ ,  $L2$ ,  $L3$ ), ( $H1$ ,  $H2$ ,  $H3$ ) and ( $V1$ ,  $V2$ ,  $V3$ ) independently through the use of the "or" ( $\parallel$ ) operator. There are three levels of warning:

- *Level 1 alarm:*

$$(0 \leq L \leq L1) \parallel (0 \leq H \leq H1) \parallel (0 \leq V \leq V1)$$

- *Level 2 alarm:*

$$(L1 \leq L \leq L2) \parallel (H1 \leq H \leq H2) \parallel (V1 \leq V \leq V2)$$

- *Level 3 alarm:*

$$(L2 \leq L \leq L3) \parallel (H2 \leq H \leq H3) \parallel (V2 \leq V \leq V3)$$

## 4. IMPLEMENTATION AND RESULTS

### 4.1. Proposed system implementation

This section will introduce the implementation of the proposed system in the Kone - Ha Thanh River area passing the Nha Phu spillway. Figure 6 shows the experimental model with 02 Nodes and 01 GW:

- Nodes use LoRa configuration and are integrated with sensors to collect information of rainfall, flow rate and river water level. Nodes are distributed at two different locations: Node 2 is located above the spillway surface and Node 1 is located 1000m from the spillway.

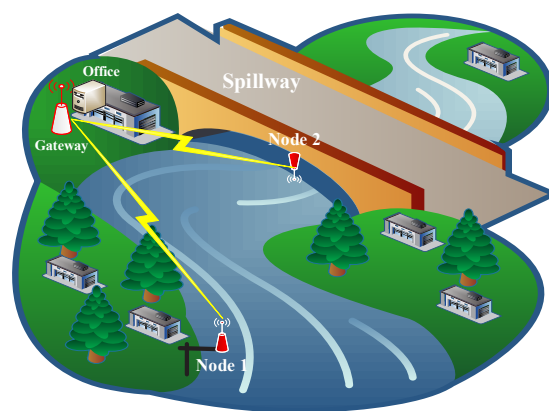


**Figure 6. A deployment of the proposed system at Nha Phu spillway, Kone - Ha Thanh river basin.**

- GW is set up in the office or at the house. Data at GW will be sent to Thingsboard.

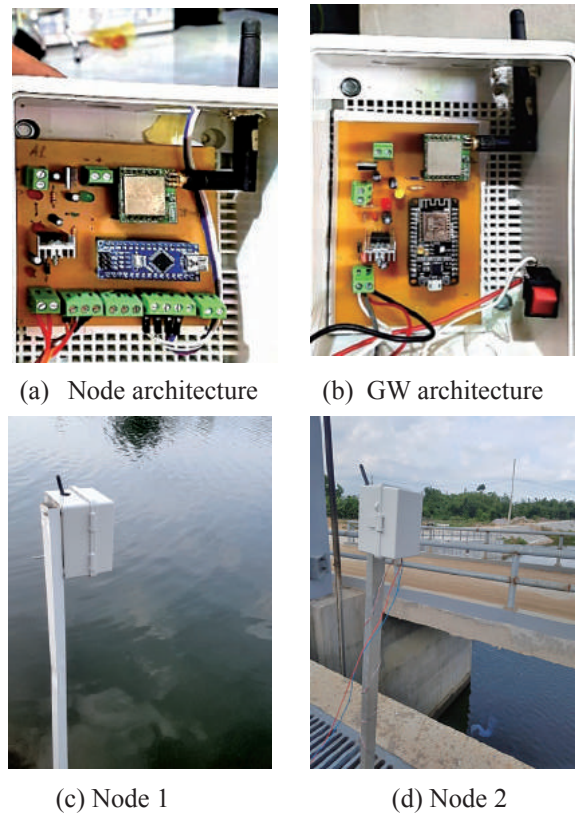
**4.2. Results**

The parameters of the implementation are shown in Table 1. Figures 7 (a) and (b) describe the internal structure of sensor Nodes and GW respectively. At the same time, the actual implementation of Nodes and GW is illustrated in Figures 7 (c) and (d).

**Table 1.** Parameters of experimental model

Parameter	Symbol	Value
Frequency	$F$	433MHz
Spectrum factor SF	$SF$	7, 9, 12
Encoded rate	$CR$	5/8
Bandwidth	$BW$	125KHz
Transmitted power	$T_x$	14dBm
Rainfall sensor		Holman WS5070W
Water flow sensor		YFS201
Water level sensor		HC-04
Microcontroller – Node		Arduino Nano
Microcontroller – GW		ESP32
LoRa Node		Air4 (SX1278)
Distance Node - GW	$D$	1000 m

Figure 8 shows an interface for monitoring data collected from Node 1 and 2 on the Thingsboard platform. In addition, Thingsboard also allows for monitoring the quality of the transmission links between the Nodes and GW by using received signal strength indicator (RSSI) and signal to noise (SNR) ratio. The results in Figure 8 (b) show that the Thingsboard platform not only effectively supports flood warning data visualisation, but also enables monitoring of the operability and reliability of the Nodes.



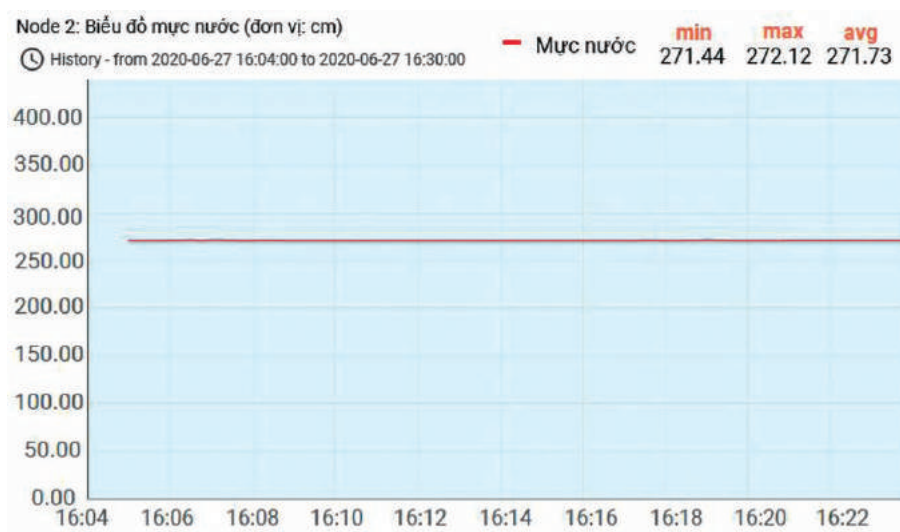
**Hình 7.** Structures of Nodes and GW

**5. CONCLUSION**

In the paper, we have proposed and implemented a real-time flood monitoring and warning model using LoRa technology at a low cost (~ 150 Euro). The system works well with the open source platform Thingsboard and is capable of integrating various communication technologies such as LoRa and WiFi. Relying on the functionality of visualisation, the proposed system allows users to access and monitor flooding parameters directly and easily. As a result, the proposed system is expected to widely deploy in reality.

Các thông số Node 2							
Time stamp ↓	Mức nước (cm)	Lượng mưa (mm)	Nhiệt độ (độ C)	Độ ẩm (%)	Kích thước gói tin (byte)	RSSI (dBm)	SNR
2020-06-27 16:31:55	271.84	0.00	35.00	69	44.00	-44.00	9.50
2020-06-27 16:31:45	271.94	0.00	35.00	70	44.00	-44.00	9.00
2020-06-27 16:31:35	271.84	0.00	35.00	70	44.00	-44.00	10.00
2020-06-27 16:31:25	272.01	0.00	35.00	70	44.00	-45.00	9.75
2020-06-27 16:31:15	272.02	0.00	35.00	70	44.00	-44.00	9.75
2020-06-27 16:30:45	271.97	0.00	35.00	70	44.00	-44.00	10.25
2020-06-27 16:30:35	271.95	0.00	35.00	70	44.00	-44.00	9.00
2020-06-27 16:30:25	271.94	0.00	35.00	70	44.00	-44.00	9.75
2020-06-27 16:30:05	271.94	0.00	35.00	70	44.00	-45.00	9.75
2020-06-27 16:29:55	271.95	0.00	35.00	70	44.00	-43.00	10.50

(a) Rainfall, water level, temperature and humidity data, and signal level received at Node



(b) River water level

**Figure 8.** Monitored data at Node 2

**ACKNOWLEDGEMENT**

*This research is conducted within the framework of the student scientific research project for the academic year 2019 - 2020 under the project code S2019.598.35.*

**REFERENCES**

1. D. Perera, O. Seidou, J. Agnihotri, M. Rasmy, V. Smakhtin, P. Coulibaly, H. Mehmood. *Flood Early Warning Systems: A Review Of Benefits, Challenges And Prospects*, United Nations

- University Institute for Water, Environment and Health, 2019.
2. United Nations Office for Disaster Risk Reduction, *Sendai Framework for Disaster Risk Reduction 2015 – 2030*, 2015.
3. The United Nations World Water Development, *Water and climate change*, UNESCO 2020
4. *Platform for the Promotion of Early Warning*, ISDDR (International Strategy for Disaster Risk Reduction), 2006.
5. <https://cucthongke.binhdinhh.gov.vn/vi/news/>

- ting-hinh-kinh-te-xa-hoi/ket-qua-so-bo-tong-dieu-tra-dan-so-va-nha-o-nam-2019-ting-binh-dinh-co-1-486-9-nghin-dan-xep-thu-20-ca-nuoc-ve-quy-mo-dan-so-99.html, accessed on 10/6/2020.
6. *Implementing Early Flood Warning Project: Contributing to response to storms and floods*, <[http://www.baobinhdinh.com.vn/viewer.aspx?macm=5&macmp=5&mabb=37642&no\\_redirect=true](http://www.baobinhdinh.com.vn/viewer.aspx?macm=5&macmp=5&mabb=37642&no_redirect=true)>, accessed on 10/6/2020.
  7. The Rockefeller Foundation, Asian Cities Climate Change Resilience Network (ACCCRN), Asia Office Bangkok - Thailand, 2013 <<https://www.rockefellerfoundation.org/wp-content/uploads/8ff925b8-2254-4b71-a7fb-6082464b844e-accrn-cities.pdf>>, accessed on 10/6/2020.
  8. <https://pcttbinhdinh.gov.vn/thong-tin-ban-do/ban-do-he-thong-quan-trac-mua-muc-nuoc-2417.html>, accessed on 10/6/2020.
  9. Hitachi Ltd., "Disaster prevention information system", 2013.
  10. <https://lorawan-alliance.org/sites/default/files/2018-07/lorawan1.0.3.pdf>, accessed on 10/6/2020.
  11. <https://www.advantech.com/resources/case-study/d02fa2f6-a668-4611-91ca-2956161fe569#app=all|pd=industrial%20communication>, accessed on 10/6/2020.
  12. <http://www.libelium.com/early-flood-detection-and-warning-system-in-argentina-developed-with-libelium-sensors-technology/>, accessed on 10/6/2020.
  13. LoRa technology: Flood sensor monitoring with real time data, <<https://www.semtech.com/uploads/technology/LoRa/app-briefs/Semtech-UseCase-GreenStream-FINAL-web.pdf>>, accessed on 10/6/2020.
  14. <<https://flood.network/>>, accessed on 10/6/2020.
  15. J. D. Loftis, S. Katragadda, S. Rhee and C. Nguyen, "StormSense: A Blueprint for Coastal Flood Forecast Information & Automated Alert Messaging Systems," IEEE SCOPE-GCTC, Porto, 2018.
  16. <https://www.watec.vn/>, accessed on 10/6/2020.
  17. ThingsBoard Open source IoT Platform, <https://thingsboard.io/>, accessed on 10/6/2020.
  18. A. A. Ismail, H. S. Hamza, and A. M. Kotb. *Performance Evaluation of Open Source IoT Platforms*, IEEE Global Conference on Internet of Things (GCIoT), Egypt, 2018.
  19. Decision 46/2014/QĐ-TTg, dated 15 August 2014, "Regulations on forecasting, warning and communicating natural disasters".
  20. Decision 05/2020/QĐ-TTg, dated 31 January 2020, "Regulating water levels corresponding to flood alarming levels on rivers nationwide".

# Ảnh hưởng của độ mặn đến sinh trưởng và sống sót của cá rô đầu vuông (*Anabas testudineus*) ở giai đoạn cá hương đến cá giống

Phùng Thị Hồng Diên<sup>1\*</sup>, Võ Văn Chí<sup>2</sup>

<sup>1</sup> Trường THPT Số 1 Phù Mỹ, huyện Phù Mỹ, tỉnh Bình Định, Việt Nam

<sup>2</sup> Khoa Khoa học Tự nhiên, Trường Đại học Quy Nhơn, Việt Nam

Ngày nhận bài: 27/04/2020; Ngày nhận đăng: 18/05/2020

## TÓM TẮT

Thí nghiệm này được thực hiện nhằm đánh giá khả năng thích nghi độ mặn của cá rô đầu vuông. Cá có khối lượng trung bình 1,5g được lựa chọn để bố trí nuôi ở các độ mặn 0, 5, 10 và 15‰. Cá được nuôi trong các bể 1m<sup>3</sup> với mật độ 200 con/bể. Các chỉ tiêu về sinh trưởng và tỷ lệ sống của cá được khảo sát định kỳ 10 ngày một lần. Kết quả cho thấy, ở độ mặn 5‰ cá sinh trưởng tốt, tương đương với môi trường nước ngọt (0‰). Ngược lại, khi độ mặn tăng lên 10‰ và 15‰ thì sinh trưởng của cá có xu hướng giảm dần. Tỷ lệ sống của cá đạt từ 86,67 - 95,67%, trong đó cá sống sót tốt nhất ở 0‰ và 5‰. Từ những kết quả này có thể nhận định rằng, mặc dù có sự khác nhau về sinh trưởng và sống sót của cá rô đầu vuông giữa các độ mặn thí nghiệm nhưng nhìn chung cá có thể thích nghi tốt ở khoảng độ mặn 0 -15‰, đặc biệt là ở độ mặn thấp ( $\leq 5‰$ ).

**Từ khóa:** *Anabas testudineus*, cá rô đầu vuông, độ mặn, sự thích nghi.

---

\*Tác giả liên hệ chính.

Email: hongdienpm1@gmail.com

# Effects of salinity on growth and survival of square head climbing perch (*Anabas testudineus*) in the early juvenile to juvenile stage

Phung Thi Hong Dien<sup>1,\*</sup>, Vo Van Chi<sup>2</sup>

<sup>1</sup>Phu My No.1 high school, Phu My district, Binh Dinh province, Vietnam

<sup>2</sup>Faculty of Natural Sciences, Quy Nhon University, Vietnam

Received: 27/04/2020; Accepted: 18/05/2020

## ABSTRACT

This study was conducted to assess salinity adaptation of square head climbing perch. Fish with average body weight of 1.5g were selected to rear at the salinities of 0‰, 5‰, 10‰ and 15‰. Fish were cultured in tanks (1m<sup>3</sup>) with the density of 200 individuals/tank. The growth and survival of fish were examined every ten days. The results showed that fish well grew at both salinity of 0‰ and 5‰ while its growth gradually decreased with increasing the salinity from 10‰ to 15‰. Survival rate of fish was from 86,67% to 95,67% and its highest values were obtained at the salinity of 0‰ and 5‰. Based on the results of this study, it is believed that despite different growth and survival of fish between the experimental salinities, in general square head climbing perch can well adapt to the salinity range of 0 - 15‰, especially at low salinity ( $\leq 5\%$ ).

**Keywords:** *Anabas testudineus*, square head climbing perch, salinity, adaptation.

## 1. INTRODUCTION

Agricultural production plays an important role in the economic development of Binh Dinh as well as South Central Coastal provinces. However, recently, because of impacts of climate change, lots of agricultural lands in Tuy Phuoc, Phu Cat, Phu My and Hoai Nhon districts have become alum and saline lands that are not effective for production or cannot be used for rice production. To deal with this situation, farmers in above districts have tended to used these lands for aquaculture. Therefore, it is essential to find aquatic species adaptable for environmental conditions in these areas.

Square head climbing perch (*Anabas testudineus* Bloch, 1792) is a variable fish species from climbing perch. This species can grow twice to three times faster than climbing perch and can adapt well to different environmental conditions. Moreover, the production of square head climbing perch can bring high economic benefit. Ngo Huu Toan and Nguyen Van Khanh<sup>1,2</sup> indicated that square head climbing perch can well adapt to different salinities, so it can be selected to culture in brackish waters. However, these authors only conducted the study on this fish species in juvenile stage, therefore its salinity adaption in early juvenile stage has not been

---

\*Corresponding author:

Email: hongdienpm1@gmail.com



known yet. Examining the salinity adaption of square head climbing perch in such early stages is very important for the following reasons: (1) can help promote survival and growth of fish when it is cultured in brackish waters later; (2) the bases that help culturists directly rear early juvenile stage to juvenile stage of this fish in brackish ponds to support the grow-out culture in the same condition to reduce the input cost compared to buying juveniles. The study “Effects of salinity on growth and survival of square head climbing perch (*Anabas testudineus*) in the early juvenile stage” was carried out for these above reasons.

**2. SUBJECT AND METHODS**

**2.1. Subject**

The early juveniles of square head climbing perch (*Anabas testudineus*) were bought from My Chau experimental farming for aquaculture, Phu My - Binh Dinh.

**2.2. Methods**

*2.2.1. Experimental design*

The strong early juvenile fish with average body weight of 1.5g and total length of 22mm were selected for the experiment. Fish were cultured in the composite tanks (1m<sup>3</sup>) within 30 days with density of 200 individuals/tank and divided into 4 saline treatments as NT1 (0‰ - control), NT2 (5‰), NT3 (10‰), NT4 (15‰) with 3 replicates. We chose salinity range of 0 - 15‰ to do the experiment because this is usually used to examine salinity adaption of freshwater fish.<sup>1,2,3,4,5</sup> The freshwater from the underground well and marine water from the sea at My Duc community were used to mix to the experimental salinity levels using method Pearson square.

Fish were fed by floating pelleted feed (SKRETTING) with size of 0.5 - 1mm and 42% protein. Fish were fed 6 - 10% body weight twice a day at 7 - 8 am and 4 - 5 pm. Water was exchanged 25% every 10 days during the

experiment. The tank bottom was daily cleared by manually siphoning out and corresponding amount of water was supplemented.

*2.2.2. Water parameters examination*

Temperature was daily examined using the thermometer with the accuracy of 1°C.

pH was daily examined using the electronic equipment HANNA with the accuracy of 0.01.

DO was daily examined using the electronic equipment HANNA with the accuracy of 0.01.

Salinity was examined using the salinity refractometer with the accuracy of 1‰.

*2.2.3. Fish growth and survival examination*

- Growth of fish: Body weight and total length of fish were measured every 10 days to examine growth of fish.

- Absolute growth rate for body weight and total length of fish were determined by the formula:

$$A = \frac{W_1 - W_0}{t_1 - t_0}$$

In which:

A: Absolute growth rate for body weight (g/day) and total length (mm/day) of fish.

W<sub>0</sub>: Body weight (g) or total length (mm) at time t<sub>1</sub>

W<sub>1</sub>: Body weight (g) or total length (mm) at time t<sub>2</sub>

t<sub>1</sub> - t<sub>0</sub>: Time period between two examinations (day).

- Survival of fish were examined every 10 days using the formula:

$$S\% = \frac{S2}{S1} \times 100$$

In which:

S1: Number of fish at the beginning

S2: Number of fish at the end

### 2.3. Data analysis

Microsoft Excel 2010 was used to calculate the average value and standard deviation. We used one way ANOVA to examine the difference of studied parameters between experimental treatments using SPSS 20.0.

## 3. RESULTS AND DISCUSSION

### 3.1. Water parameters

**Table 1.** The water parameters in the experimental tanks

Treatments	Temperature (°C)			pH			DO (mg/l)		
	Min	Max	Average	Min	Max	Average	Min	Max	Average
NT1	24.0	31.0	27.42	6.5	6.9	6.81	4.5	6.0	5.22
NT2	24.0	31.0	27.37	6.8	7.2	7.09	4.5	6.0	5.28
NT3	24.0	31.0	27.38	7.0	7.4	7.12	4.5	6.0	5.25
NT4	24.0	31.0	27.38	7.3	7.7	7.13	4.5	6.0	5.20

Remarks: *Min: minimum value; Max: maximum value; Average: average value*

The experiment was conducted in a house, so water temperature between the treatments were relatively stable, that was lowest at 24°C, highest at 31°C and average at 27.37 – 27.42°C. This temperature range is suitable for growth and development of tropical aquatic organisms.<sup>5</sup>

pH of water fluctuated from 6.5 to 7.7 and increased with salinity raising in the treatments. Specifically, average value of pH was lowest (6.81) in NT1 (salinity of 0‰) and highest (7.13) in NT4 (salinity of 15‰). Such variation is due to pH of freshwater lower than that of marine water, therefore the higher salinity of the mixture of two kinds of water is, the higher pH can obtain. According to Nguyen Thanh Phuong et al.,<sup>6</sup> climbing perch can inhabit in waters with pH from 5 to 10, but optimal pH for it is from 6 to 9. Square head climbing perch has similar

Water parameters such as temperature, pH, DO are the basic ones to assess the water quality in aquaculture. When these parameter are suitable for aquatic animals in general and fish in particular, they will grow and develop and thus the results of study are accurate. The water parameters in the experimental tanks were showed in Table 1.

behaviors to climbing perch, so it will also adapt well to this pH range. Thus, pH of water in the experimental tanks is suitable for growth and development of square head climbing perch.

Concentration of DO was from 4.5 - 6 mg/l, that is suitable for fish,<sup>8</sup> and this was not greatly different between treatments.

In summary, environmental parameters in experimental tanks are suitable for square head climbing perch, so experimental results are not affected.

### 3.2. Effects of salinity on growth of fish

#### 3.2.1. Effects of salinity on cumulative weight growth of fish

Cumulative weight growth of fish in four treatments as NT1, NT2, NT3 and NT4 is expressed in Table 2.

**Table 2.** Cumulative weight growth (g) of square head climbing perch

Treatment	Progressed time of rearing			
	Day 0	Day 10	Day 20	Day 30
NT1	1.50 ± 0.12 <sup>a</sup>	1.88 ± 0.10 <sup>a</sup>	2.41 ± 0.13 <sup>a</sup>	3.03 ± 0.14 <sup>a</sup>
NT2	1.50 ± 0.12 <sup>a</sup>	1.87 ± 0.10 <sup>a</sup>	2.42 ± 0.11 <sup>a</sup>	3.02 ± 0.13 <sup>a</sup>
NT3	1.50 ± 0.12 <sup>a</sup>	1.85 ± 0.11 <sup>b</sup>	2.29 ± 0.11 <sup>b</sup>	2.77 ± 0.13 <sup>b</sup>
NT4	1.50 ± 0.12 <sup>a</sup>	1.83 ± 0.11 <sup>c</sup>	2.25 ± 0.13 <sup>c</sup>	2.71 ± 0.12 <sup>c</sup>

Remark: in the same column, the different letters indicate significant difference ( $p < 0.05$ ).

The results showed that weight of fish increased according to rearing time. Particularly, fish weighing 1.5g at the beginning of experiment grew to 2.71 – 3.03g after 30 days of rearing.

Weight of fish between NT1 and NT2 was not significant different ( $p > 0.05$ ) at day 10, day 20 and day 30 but higher than that in NT3 và NT4 ( $p < 0.05$ ). Weight of fish in NT4 was lowest ( $p < 0.05$ ). Particularly, at the end of the experiment (day 30) weight of fish in NT1 and NT2 were 3.03g and 3.02g respectively while this in NT3 and NT4 were 2.77g and 2.71g. Therefore, it can be said that cumulative weight growth of early juveniles of square head climbing perch reared at salinity of 5‰ is similar to that of fish raised in freshwater. However, if fish are reared at higher salinity levels as 10‰ and 15‰, its cumulative weight growth tends to decrease.

The similar results are also reported in

some studies. Nguyen Van Kiem and Trang Van Phuoc<sup>4</sup> reared snakeskin gourami (*Trichogaster pectoralis*) at salinity range of 0 - 13‰ and showed that there was no difference of body weight of fish at the end of the experiment between the experimental salinity levels as 0‰, 5‰ and 7‰ but weight of fish gradually decrease with increasing salinity. Similarly, weight of climbing perch with initial weight of 7 - 8g reared at salinities of 0 - 15‰ was highest at 0‰ và 3‰ and lowest at 12‰ and 15‰ after 90 days.<sup>3</sup> Thus, it can be seen that square head climbing perch as well as snakeskin gourami and climbing perch can only grow well in low saline waters.

*3.2.2. Effects of salinity on cumulative length growth of fish*

Cumulative length growth of fish in four treatments is expressed in Table 3.

**Table 3.** Cumulative length growth (mm) of square head climbing perch

Treatment	Progressed time of rearing			
	Day 0	Day 10	Day 20	Day 30
NT1	22.00 ± 0.04 <sup>a</sup>	30.33 ± 1.62 <sup>a</sup>	39.33 ± 1.76 <sup>a</sup>	48.92 ± 1.94 <sup>a</sup>
NT2	22.00 ± 0.04 <sup>a</sup>	30.32 ± 1.68 <sup>a</sup>	39.26 ± 1.62 <sup>a</sup>	48.80 ± 2.07 <sup>a</sup>
NT3	22.00 ± 0.04 <sup>a</sup>	29.18 ± 1.82 <sup>b</sup>	36.98 ± 2.03 <sup>b</sup>	45.11 ± 2.13 <sup>b</sup>
NT4	22.00 ± 0.04 <sup>a</sup>	29.09 ± 1.73 <sup>b</sup>	36.64 ± 1.86 <sup>b</sup>	44.62 ± 2.26 <sup>b</sup>

Remark: in the same column, the different letters indicate significant difference ( $p < 0.05$ ).

Similar to cumulative weight growth, length of fish also increased according to rearing time. Particularly, initial length of fish was 22mm and after 30 days of rearing, total length of fish increased to 48.92mm in NT1, 48.8mm in NT2, 45.11mm in NT3 and 44.62mm in NT4.

Total length of fish in NT1 and NT2 was always higher than that in NT3 and NT4 at day 10, day 20 and day 30 ( $p < 0.05$ ). However, there was no significant difference of total length of fish between NT1 and NT2 as well as NT3 and NT4 ( $p > 0.05$ ). Particularly, at the end of the experiment, total length of fish in NT1 was 30.33mm similar to that in NT2 (30.32mm) while total length of fish in NT3 was 29.18mm similar to that in NT4 (29.09mm). Therefore, it can be said that cumulative length growth of early juveniles of square head climbing perch

reared at salinity of 5‰ is similar to that of fish raised in freshwater. However, if fish are reared at higher salinities as 10‰ and 15‰, its cumulative length growth tends to decrease. Our results are not similar to the findings of Le Thi Phuong Mai et al.<sup>5</sup> on snakeskin gourami (*Trichogaster pectoralis*), that showed that length of fish was highest after 90 days of rearing at salinity of 9‰ compared to 0‰, 3‰ and 6‰. However, in the experiment of these authors, survival of fish reared at 9‰ was lowest so fish can grow fast because of low density.

### 3.2.3. Effects of salinity on absolute growth rate for body weight of fish

Based on cumulative weight growth of fish, we calculated its absolute growth rate for body weight in the experimental treatments and the results are showed in Table 4.

**Table 4.** Absolute growth rate for body weight of fish (g/day)

Treatment	Time period of rearing			
	Day 0 - day 10	Day 10 - day 20	Day 20 - day 30	Day 0 - day 30
NT1	0.038 ± 0.001 <sup>a</sup>	0.053 ± 0.001 <sup>a</sup>	0.061 ± 0.009 <sup>a</sup>	0.051 ± 0.004 <sup>a</sup>
NT2	0.037 ± 0.001 <sup>a</sup>	0.055 ± 0.001 <sup>a</sup>	0.060 ± 0.009 <sup>a</sup>	0.051 ± 0.004 <sup>a</sup>
NT3	0.035 ± 0.001 <sup>b</sup>	0.044 ± 0.001 <sup>b</sup>	0.048 ± 0.009 <sup>b</sup>	0.042 ± 0.004 <sup>b</sup>
NT4	0.034 ± 0.001 <sup>b</sup>	0.041 ± 0.001 <sup>c</sup>	0.046 ± 0.009 <sup>c</sup>	0.040 ± 0.004 <sup>c</sup>

Remark: in the same column, the different letters indicate significant difference ( $p < 0.05$ ).

In general, absolute growth rate for body weight of fish gradually increased according to time periods of rearing (Table 4). This give a speculation that fish can well grow in next rearing periods.

Absolute growth rate for body weight of fish was different between treatments. In the period of day 0 to day 10 of rearing, this in NT1 and NT2 was significantly higher than that in NT3 and NT4 ( $p < 0.05$ ) but there was no difference of this between NT1 and NT2 as well as between NT3 and NT4 ( $p > 0.05$ ). In the period of day 10 to day 20 and day 20 to day 30 of rearing, absolute growth rate for body weight of fish in NT1 and NT2 was not significantly

different ( $p > 0.05$ ) and was highest, however this in NT3 and NT4 was different and the lowest value was seen in NT4 ( $p < 0.05$ ).

For pooled results of 30 days of rearing, treatment NT1 (salinity of 0‰) and NT2 (salinity of 5‰) still showed the superior absolute growth rate for body weight compared to NT3 (salinity of 10‰) and NT4 (salinity of 15‰) ( $p < 0.05$ ), of which growth rate of fish in NT4 was lowest. Therefore, like cumulative weight growth, absolute growth rate for body weight of early juveniles of square head climbing perch reared at salinity of 5‰ is similar to that of fish raised in freshwater. However, if fish are reared at higher salinity levels as 10‰ and 15‰,

its growth tends to be lower. Unlike, Ngo Huu Toan and Nguyen Van Khanh<sup>2</sup> reported that absolute growth rate for body weight of square head climbing perch in grow-out culture at the salinity levels of 0, 4‰, 8‰ and 12‰ was not different. The different results between this study and our study may be due to different ontogenetic stages of experimental fish; we conducted the experiment on early juveniles (1.5g in initial body weight) while these author did on juveniles

(2.28g in initial body weight). Therefore, it can be speculated that salinity adaptation of different ontogenetic stages of square head climbing perch is different.

*3.2.4. Effects of salinity on absolute growth rate for total length of fish*

Based on cumulative length growth of fish, we calculated its absolute growth rate for total length in the experimental treatments and the results are showed in Table 5.

**Bảng 5.** Absolute growth rate for total length of fish (mm/day)

Treatment	Time period of rearing			
	Day 0 - day 10	Day 10 - day 20	Day 20 - day 30	Day 0 - day 30
NT1	0.83 ± 0.16 <sup>a</sup>	0.90 ± 0.23 <sup>a</sup>	0.96 ± 0.16 <sup>a</sup>	0.90 ± 0.06 <sup>a</sup>
NT2	0.83 ± 0.17 <sup>a</sup>	0.89 ± 0.21 <sup>a</sup>	0.95 ± 0.19 <sup>a</sup>	0.89 ± 0.07 <sup>a</sup>
NT3	0.72 ± 0.18 <sup>b</sup>	0.78 ± 0.14 <sup>b</sup>	0.81 ± 0.19 <sup>b</sup>	0.77 ± 0.07 <sup>b</sup>
NT4	0.71 ± 0.17 <sup>b</sup>	0.76 ± 0.14 <sup>b</sup>	0.80 ± 0.17 <sup>b</sup>	0.75 ± 0.08 <sup>b</sup>

*Remark: in the same column, the different letters indicate significant difference (p < 0.05).*

In general, absolute growth rate for total length of fish gradually increased according to time periods of rearing (Table 5). This give a speculation that length growth of fish can rapidly increase in next rearing periods.

Absolute growth rate for total length of fish was different between treatments. In all periods of rearing, this in NT1 and NT2 was significantly higher than that in NT3 and NT4 (p < 0.05) but there was no difference of this between NT1 and NT2 as well as between NT3 and NT4 (p > 0.05).

For pooled results of 30 days of rearing, treatment NT1 (salinity of 0‰) and NT2 (salinity of 5‰) still showed the superior absolute growth rate for total length compared to NT3 (salinity of 10‰) and NT4 (salinity of 15‰) (p < 0.05). Therefore, it can be said that absolute growth

rate for total length of early juveniles of square head climbing perch reared at salinity of 5‰ is similar to that of fish raised in freshwater. However, if fish are reared at higher salinity levels as 10‰ and 15‰, its absolute growth rate for total length is lower.

The similar results are also found in grow-out culture of this fish; absolute growth rate for total length is highest at salinity of 0‰ and 4‰, followed by salinity of 8‰ and 12‰ and lowest at 16‰<sup>2</sup>. Thus, it can be seen that absolute growth rate for total length of square head climbing perch gradually reduces when fish are cultured in salinity more than 5‰.

**3.3. Effects of salinity on survival of fish**

Survival of fish in the treatments is showed in Table 6.

**Table 6.** Survival (%) of square head climbing perch in the stage of early juvenile to juvenile

Treatment	Time period of rearing			
	Day 0 - day 10	Day 10 - day 20	Day 20 - day 30	Day 0 - day 30
NT1	98.30 <sup>a</sup>	98.47 <sup>a</sup>	98.80 <sup>a</sup>	95.67 <sup>a</sup>
NT2	98.00 <sup>a</sup>	98.64 <sup>a</sup>	98.97 <sup>a</sup>	95.67 <sup>a</sup>
NT3	93.33 <sup>b</sup>	96.25 <sup>b</sup>	98.51 <sup>a</sup>	88.00 <sup>b</sup>
NT4	92.50 <sup>b</sup>	96.03 <sup>b</sup>	97.98 <sup>a</sup>	86.67 <sup>b</sup>

Remark: in the same column, the different letters indicate significant difference ( $p < 0.05$ ).

In general, survival of fish in the experimental treatments was high ( $> 86\%$ ), which indicates that fish well adapted to the culture environment. Survival of fish in this study is much higher than that of snakeskin gourami reared at salinities of 0 - 13‰ (2.45 - 82.31%)<sup>4</sup>.

Survival of fish tended to increase according to rearing periods (Table 6), which implies that fish gradually adapt to the culture environment in the experimental tanks. However, there was the difference of survival of fish between treatments. In two first periods of rearing (day 0 - day 10 and day 10 - day 20), survival of fish in NT1 and NT2 was higher than that in NT3 and NT4 ( $p < 0.05$ ). This indicates that fish reared in high salinities (10‰ and 15‰) died more than those cultured in freshwater and 5‰. It is speculated that fish did not immediately adapt to high salinity because of the osmotic pressure difference between the body and the environment. In contrast, in the period of day 20 - day 30 of rearing, survival of fish between treatments did not differ ( $p > 0.05$ ), implying that fish well adapted to the environmental conditions in the experimental tanks.

The accumulative results of 30 days of rearing showed that survival of fish in NT1 - 0‰ and NT2 - 5‰ (95.67%) was higher than that in NT3 - 10‰ (88%) and NT4 - 15‰ (86.67%) ( $p < 0.05$ ). There was no difference of survival of fish between NT1 and NT2 as well as NT3 and NT4 ( $p > 0.05$ ). The similar results are also

reported by Do Thi Thanh Huong et al. (2013)<sup>3</sup> on climbing perch with initial body weight of 7 - 8g; after 90 days of rearing, survival of fish was highest at 0‰ (97.5%) and 3‰ (96.7%) and gradually decreased at 9‰, 12‰ and 15‰. Nguyen Van Kiem và Trang Van Phuoc<sup>4</sup> also showed that survival of snakeskin gourami was highest at salinities of 0‰ and 3‰ (80.45 - 82.31%) and gradually decreased at salinities of 5‰, 7‰, 9‰, 11‰ and 13‰. Therefore, square head climbing perch, climbing perch or snakeskin gourami can survive well at low saline waters and when water salinity increases the rate for fish survival reduces.

#### 4. CONCLUSION

Our results show that square head climbing can adapt well to the salinity up to 15‰ in the stage of early juvenile to juvenile. However, uniquely, growth and survival of fish reared at salinity of 5‰ are similar to that at freshwater while these of fish gradually decrease at the higher salinity levels. Therefore, it can be concluded that juveniles of fish in the mentioned stage can be cultured at waters with salinity  $\leq 15\%$  but it is better to rear it at salinity  $\leq 5\%$ .

#### REFERENCES

1. Ngo Huu Toan, Nguyen Van Khanh. Saline adaptation of square head climbing perch (*Anabas testudineus* Bloch. 1792), *Science and Technology Journal of Agriculture and Rural Development*, **2013**, 2, 87-91.

2. Ngo Huu Toan, Nguyen Van Khanh. Effects of salinity on growth and survival of climbing perch (*Anabas testudineus* Bloch, 1792), *Science and Technology Journal of Agriculture and Rural Development*, **2014**, 4, 137-143.
3. Do Thi Thanh Huong, Tran Viet Toan, Nguyen Thi Kim Ha. Effects of salinity on osmoregulation and growth of climbing perch (*Anabas testudineus*), *Journal of Science - Can Tho university*, **2013**, 26, 55-63.
4. Nguyen Van Kiem, Trang Van Phuoc. The effects of salinity on growth and osmoregulation of Snakeskin gourami (*Trichogaster pectoralis* Regan, 1910), *Journal of Science - Can Tho university*, **2011**, 19b, 219-224.
5. Le Thi Phuong Mai, Vo Nam Son, Do Thi Thanh Huong, Duong Van Ni, Tran Ngoc Hai. Evaluation of impacts salinity to snakeskin gourami (*Trichogaster pectoralis*) and ability of farming in salinity intrusion condition by climate change in Hau Giang province, *Journal of Science - Can Tho university*, **2016**, 43, 133-142.
6. Le Nhu Xuan, Duong Nhut Long, Tu Thanh Dung, Nguyen Van Kiem, Pham Minh Thanh, Bui Minh Tam. *Biology and culture techniques of some freshwater fish species*, An Giang Department of Science, Technology and Environment, 2000.
7. Nguyen Thanh Phuong, Tran Ngoc Hai, Duong Nhut Long. *Aquaculture textbook*, Can Tho university, 2009.
8. Nguyen Van Kiem. *Artificial reproduction techniques of some fish species reared in the Mekong Delta*, Can Tho university, 1999.





## **Đặc điểm sinh học dinh dưỡng của cá Thát lát (*Notopterus notopterus*) phân bố tại đầm Trà Ổ, tỉnh Bình Định**

**Đặng Thị Thạch Trúc<sup>1,2\*</sup>, Võ Văn Chí<sup>1</sup>**

*<sup>1</sup>Khoa Khoa học tự nhiên, Trường Đại học Quy Nhơn, Việt Nam*

*<sup>2</sup>Trung tâm Giáo dục nghề nghiệp - Giáo dục thường xuyên, huyện Phù Mỹ, tỉnh Bình Định, Việt Nam*

*Ngày nhận bài: 03/07/2020; Ngày nhận đăng: 04/08/2020*

### **TÓM TẮT**

Nghiên cứu này được thực hiện để xác định đặc điểm sinh học dinh dưỡng của cá Thát lát (*Notopterus notopterus*) phân bố tại đầm Trà Ổ, tỉnh Bình Định. Mẫu cá được thu định kỳ hàng tháng để phân tích hình thái giải phẫu hệ tiêu hóa, chỉ số sinh trắc ruột (RLG) và thức ăn tự nhiên của cá. Hình thái cấu tạo của hệ tiêu hóa của cá (răng nhỏ nhọn, lưỡi có răng sắc nhọn, dạ dày lớn, ruột ngắn) và chỉ số sinh trắc ruột (RLG) (dao động từ 0,3 đến 0,36) cho thấy cá có tính ăn thiên về động vật. Thành phần thức ăn tự nhiên của cá gồm có giáp xác, ấu trùng côn trùng, rễ thực vật thủy sinh và mùn đáy, trong đó tần số xuất hiện của thức ăn động vật là rất cao (95,8%). Như vậy, có thể nói rằng, cá Thát lát có tính ăn tạp nhưng thiên về động vật.

**Từ khóa:** Cá Thát lát, hệ tiêu hóa, tập tính ăn, thức ăn tự nhiên.

---

*\*Tác giả liên hệ chính.*

*Email: thachtruc95@gmail.com*

# Feeding Biology of Bronze featherback (*Notopterus notopterus*) distributed in Tra O lagoon, Binh Dinh province

Dang Thi Thach Truc<sup>1,2\*</sup>, Vo Van Chi<sup>1</sup>

<sup>1</sup>Faculty of Natural Sciences, Quy Nhon University, Vietnam

<sup>2</sup>Center for Vocational Training - Continuing Education, Phu My district, Binh Dinh province, Vietnam

Received: 03/07/2020; Accepted: 04/08/2020

## ABSTRACT

This study was conducted to determine the feeding biology of Bronze featherback (*Notopterus notopterus*) distributed in Tra O lagoon, Binh Dinh province. Fish samples were monthly collected to analyze anatomical morphology of digestive system, the relative length of the gut (RLG) and natural food of fish. The morphological characteristics of the fish's digestive system (small sharp - pointed teeth, sharp teeth on the tongue, big stomach, short intestines) and the relative length of the gut (from 0.3 to 0.36) indicate that this kind of fish is carnivorous. The natural food composition of fish included crustaceans, larvae of insects, aquatic plant roots and humus, of which the occurrence frequency of food which are animals was very high (95.8%). Thus, it can be said that Bronze featherback is an omnivore but focusing on animals.

**Keywords:** *Bronze featherback, digestive system, feeding behavior, natural food.*

## 1. INTRODUCTION

Tra O lagoon is a natural freshwater lagoon, having characteristics of the coastal lagoon system in Central Vietnam. The lagoon covers an area of about 1600 hectares. It supplies the local community with a large amount of aquatic products every year, many of which have high economic value that take a part to solve living needs of majority of coastal residents and contribute to the general socio-economic development of the locality and Binh Dinh province.

Bronze featherback distributed in this lagoon is one of economically valuable species considered. This fish species has delicious meat, especially plasticity of its meat, so it is often used to produce fish cakes, which is a special food in Phu My district in particular

and Binh Dinh province in general. Therefore, the consuming demand of Bronze featherback inhabiting in Tra O lagoon is increasing. This is the cause of overexploitation, which leads to seriously decrease the mass of this fish in the wild and the commercial size of this fish is smaller and smaller. Thus, carrying out the complete and systematic studies on the basic biological characteristics of Bronze featherback, especially feeding biology, is essential to contribute to the effective conservation of this economically valuable species. In addition, studying on feeding biology of Bronze featherback will supply the important base for grow-out culture and breeding of this species to meet the market requirement and reduce pressure of exploitation for fish resources, as well as to diversify new cultured species in the locality.

---

\*Corresponding author:

Email: thachtruc95@gmail.com

**2. SUBJECT AND METHODS**

**2.1. Subject**

Bronze featherback (*Notopterus notopterus*) distributed in Tra O lagoon, Binh Dinh province.

**2.2. Methods**

*2.2.1. Sampling and treating fish samples*

Fish with different sizes were collected every month in Tra O lagoon. Based on size of fish collected, we divided fish into 3 groups: <15 cm, 15 - 18 cm and > 18 cm.

After being collected, the fish were frozen and brought to the Animal Science Laboratory, Faculty of Natural Sciences, Quy Nhon University to analyse within the day or fixed in 5 - 10% formol solution for later analysis.

*2.2.2. Examining the digestive system and feeding habit of fish*

Describing the characteristics of the digestive system (focusing on organs such as mouth, teeth, gill rakers, intestine) by observing of morphological and anatomical characteristics.

Examining feeding habit of fish: Based on the relative length of the gut (RLG) according to Al-Hussainy.<sup>1</sup>

$$RLG = \frac{Li}{L}$$

Where: + Li: Length of the gut of fish (cm)  
+ L: Total length of fish (cm).

*2.2.3. Analysing natural food of fish*

We dissected fish to analyze natural food in fish stomachs or intestines. Stereomicroscope and optical microscope were used to analyze and identify prey items of fish. Then, these prey items were classified to the lowest possible taxon based on classification documents.<sup>2,3</sup>

- We determined occurrence frequency (%O) of each of food item using formula of Hyslop:<sup>4</sup>

$$Oi\% = \left( \frac{\text{Number of stomach containing prey } i}{\text{Total number of analysed stomach}} \right) \times 100$$

**3. RESULTS AND DISCUSSION**

**3.1. Digestive system and feeding habit of fish**

According to our observation, the digestive system of Bronze featherback also included organs like most other fish species. To identify feeding habit of this fish, we focussed on describing some of the following organs:

- **Mouth:** Mouth is relatively large, with a short flat snout; maxilla extended to anterior eye orbit (Figure 1).

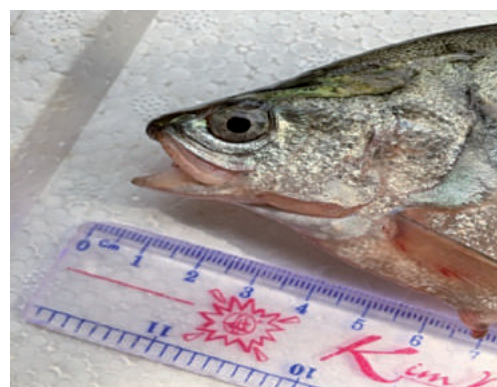


**Figure 1.** Morphology of mouth of Bronze featherback

- **Teeth:** There are small pointed teeth with rough teeth surface on both jaws (Figure 2). According to Nguyen Bach Loan,<sup>5</sup> fish that eat small animals often have small, smooth teeth. Thus, based on the described teeth characteristics, Bronze featherback can be a predator.

- **Tongue:** The tongue is well developed and movable, that had sharp teeth on the tip (Figure 2). Such morphological characteristics of the tongue show the adaptation of the fish as carnivorous behavior; it can be said that tongue is used to hold or tear prey when the fish eat.

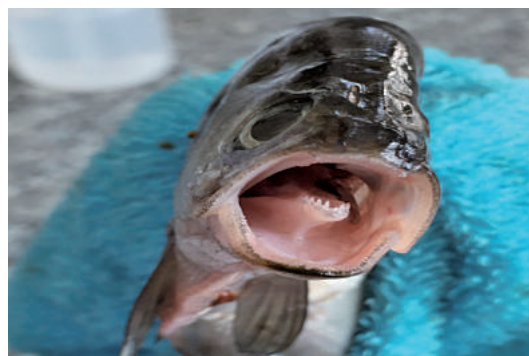


**Figure 2.** Morphology of teeth and tongue of Bronze featherback

- **Gill rakers:** As our observations, Bronze featherback has four separate pairs of gill arch. Each gill arch has 2 rows of white gill rakers. For the first gill arch, a row of gill rakers is rod-shaped, short, thin, relatively pointed and sparse, that has its bottom attached to gill arch and its tip directed to the mouth cavity while another row of gill rakers was spiny knobs. For other gill arches, both rows of gill rakers are spiny knobs (Figure 3). According to Vu Trung Tang and Nguyen Dinh Mao,<sup>6</sup> the shape and size of gill rakers of the fish are often suitable for their feeding behavior. Fish eating small animals have thin, and sparse gill rakers while gill arches of fish eating large animals have sharp spines or their gill rakers form spiny knobs.<sup>5</sup> Thus, based on the morphological characteristics of gill rakers, it can be said that Bronze featherback can be a carnivore.

- **Esophagus:** Esophagus is linked to the pharynx, that moves food into the stomach. The esophagus of Bronze featherback is short, tubular, easily stretched and its wall is thick (Figure 4).

- **Stomach:** Stomach, that contains food and release digestive enzymes to digest food, is connected to the esophagus. Stomach of bronze featherback is bag-shaped, relatively large and its wall is thick (Figure 4).

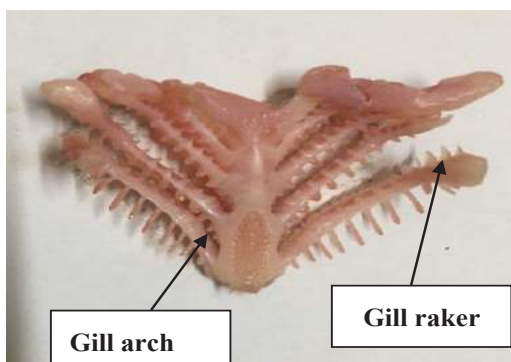


**Figure 3.** Morphology of gill arches and gill rakers of Bronze featherback

- **Intestine:** Intestine is the end part of the digestive tract, that connects the stomach and the anus of fish. It releases digestive enzymes and absorbs nutrients. The intestine of Bronze

featherback is relatively short, large at the beginning, and has folds (Figure 4).

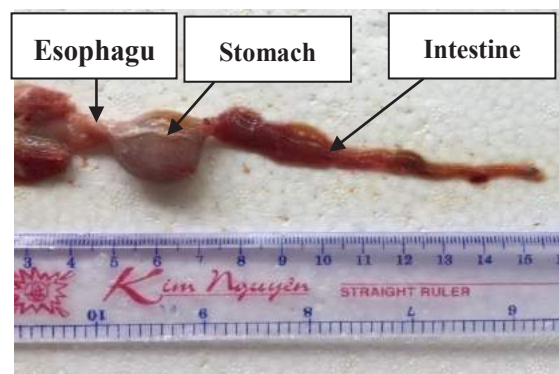


**Figure 4.** Morphology of stomach and intestine of Bronze featherback

The length of fish gut depends on natural food that they consume and this increases with increasing rate of plant in fish diet.<sup>7</sup> Therefore, to determine more accurately feeding habit of fish, we calculated the correlation index between the gut length (Li) and total length of fish (L) (The relative length of the gut - RLG). Results recorded on 228 individuals of fish with 3 size classes are shown in Table 1.

Bronze featherback has relatively low value of RLG that is from 0.30 to 0.36 (Table 1). According to Nikolsky,<sup>8</sup> carnivorous fish usually have RLG <1. Therefore, it can be said that Bronze featherback is also a carnivore. The results in Table 1 also show that RLG varied between different size classes of fish. Specifically, RLG of size class of fish > 18cm (0.36) is higher than this of size class 15 - 18cm (0.35) and size class <15cm (0.30). This shift can be the adaptability of fish in each ontogenetic stage.

**Table 1.** RLG of Bronze featherback

Size class of fish (cm)	Length of gut - Li (cm)	Total length of fish - L (cm)	RLG
< 15 cm	4.0 ± 0.13	13.6 ± 0.12	0.30
15 - 18 cm	5.7 ± 0.08	16.5 ± 0.07	0.35
> 18 cm	7.0 ± 0.16	19.5 ± 0.15	0.36

Based on analysed results of morphological characteristics of digestive system and RLG,

it can be seen that Bronze featherback is a carnivore. However, to more exactly examine feeding habit of this fish, we analyzed the composition of natural food in their stomach. The results are shown in the next section.

**3.2. Natural food of fish**

As it is impossible to directly observe feeding behavior of fish in the wild, the best way to determine feeding habit of the fish is to analyze the composition of food in their gut or stomach.<sup>7</sup>

The results of analysing natural food composition in the stomachs containing food of 216 fish individuals are shown in Table 2.

It can be seen from Table 2 that the natural food of Bronze featherback includes humus, aquatic plant roots, crustaceans, larvae of insects. Crustacean has highest occurrence frequency (63,4%), followed by humus (44,0%), larvae of insects (32,4%) and aquatic plant roots (19,9%). For larvae of insects, family Petaluridae (order Odonata) appears with the highest frequency (13,4%) while family Philopotamidae (order Trichoptera) has the lowest occurrence frequency (5,1%).

According to Vu Trung Tang and Nguyen Dinh Mao,<sup>6</sup> for omnivores that eat both plants and animals and also humus, there are those eating more animals than plants, and others eating more plants than animals. It can be seen that animals take 95,8% while plants only hold nearly 20% of the occurrence frequency in natural food composition of Bronze featherback. Thus, combining the results of analysis of natural food composition and the morphological and anatomical characteristics of the digestive system, it can be concluded that Bronze featherback is an omnivorous fish but focuses on animals.

**Table 2.** The natural food composition of Bronze featherback

<b>Food composition</b>	<b>Occurrence frequency (%O)</b>
<b>Humus</b>	<b>44.0</b>
<b>Aquatic plant roots</b>	<b>19.9</b>
<b>Crustaceans</b>	<b>63.4</b>
<b>Larvae of insects</b>	<b>32.4</b>
Order <i>Trichoptera</i>	5.1
- Family <i>Philopotamidae</i>	
Order <i>Odonata</i>	13.4
- Family <i>Petaluridae</i>	
Order <i>Odonata</i>	6.9
- Family <i>Lestidae</i>	
Order <i>Diptera</i>	6.9
- Family <i>Chironomidae</i>	

**4. CONCLUSION**

Bronze featherback has the relatively large mouth, small pointed teeth; there are sharp pointed teeth on tongue; there are two types of gill rakers: rod-shaped, short, thin, and sparse gill rakers and knob-shaped gill rakers.

Stomach of its relatively big and bag-shaped. Intestine is relatively short and has folds. The relative length of the gut (RLG) is from 0.3 to 0.36.

The morphological and anatomical characteristics of digestive system and RLG value show that Bronze featherback is a carnivore.

The natural food composition of this fish includes humus, aquatic plant roots, crustaceans, larvae of insects. Animals are dominant prey that take 95,8% of occurrence frequency.

Based on all findings of this study, it can be said that Bronze featherback is an omnivore but tends to be a carnivore.

**REFERENCE**

1. Al-Husainy, A.H. On the functional morphology of the alimentary tract of some fishes in relation to differences in their feeding habits, *Quarterly Journal of Microscopical Science*, **1949**, 9(2), 190-240.
2. Nguyen Xuan Quynh, C. Pinder, S. Tilling. *Identification of freshwater invertebrates common in Vietnam*, Hanoi National University Publishing House, Hanoi, 2001. (in Vietnamese).
3. Đặng Ngọc Thanh, Hồ Thanh Hải. *Shrimps, crabs in Vietnam (Palaemonidae, Atyidae, Parathelphusidae, Potamidae)*, Natural Sciences and Technology Publishing House, Hà Nội, 2012. (in Vietnamese).
4. Hyslop E.J. Stomach contents analysis: a review of methods and their application, *Journal of Fish Biology*, **1980**, 17, 411-429.
5. Nguyễn Thị Bạch Loan. *Ichthyology I*, Faculty of Fisheries, Cần Thơ University, 2003. (in Vietnamese).
6. Vũ Trung Tạng, Nguyễn Đình Mao. *Ichthyology*, Agriculture Publishing House, Hồ Chí Minh, 2005. (in Vietnamese).
7. Phạm Thanh Liêm and Trần Đặc Đình. *Methods for studying fish biology*, Cần Thơ University, 2004. (in Vietnamese).
8. G. V. Nikolski. *Ecology of fishes*, Academic press, London, 1963.

## Ảnh hưởng của pH đến quá trình hấp phụ - xúc tác quang của $WS_2$

Nguyễn Thị Thanh Bích<sup>1</sup>, Nguyễn Đức Nhân<sup>1</sup>, Huỳnh Hữu Điền<sup>1</sup>,  
Nguyễn Tông Yên Như<sup>1</sup>, Phạm Thị Yên Nhi<sup>1</sup>, Nguyễn Văn Phúc<sup>2</sup>,  
Trương Duy Hướng<sup>2</sup>, Võ Viễn<sup>2,\*</sup>

<sup>1</sup>Khoa Sư phạm, Trường Đại học Quy Nhơn, Việt Nam

<sup>2</sup>Viện Nghiên cứu ứng dụng Khoa học và công nghệ, Trường Đại học Quy Nhơn, Việt Nam

Ngày nhận bài: 18/03/2020; Ngày nhận đăng: 18/04/2020

### TÓM TẮT

Trong nghiên cứu này, vật liệu vonfram disulfua đã được điều chế bằng cách nung hỗn hợp  $H_2WO_4$  và thiourea với tỷ lệ khối lượng 1:5 trong dòng khí Ar ở 650 °C trong 1 giờ và được ký hiệu là  $WS_2$ . Sản phẩm được đặc trưng phổ nhiễu xạ tia X, phổ hồng ngoại, phổ tán sắc năng lượng tia X, ảnh kính hiển vi điện tử quét và phổ phân xạ khuếch tán từ ngoại khả kiến. Kết quả cho thấy mẫu tổng hợp được có cấu trúc đặc trưng của  $WS_2$ . Khả năng hấp phụ và xúc tác quang của vật liệu  $WS_2$  được đánh giá qua phản ứng phân hủy thuốc nhuộm cation (rhodamine B) ở khoảng pH từ 1,5 đến 8,0, kết quả cho thấy sự giảm nồng độ RhB trên vật liệu  $WS_2$  khi tăng pH dung dịch từ 1,5 đến 8,0 do ảnh hưởng của sự hấp phụ hơn là quá trình phân hủy hóa học. Đặc biệt ở pH = 4, tương tác tĩnh điện giữa bề mặt của vật liệu mang điện tích âm và thuốc nhuộm cation mạnh nhất, dẫn đến hiệu suất hấp phụ và quang xúc tác đạt tối đa tương ứng 66,98% và 20,88% sau 8 giờ thử nghiệm.

**Từ khóa:**  $WS_2$ , hấp phụ, xúc tác quang, pH, Rhodamine B.

---

\*Tác giả liên hệ chính.

Email: vovien@qnu.edu.vn

## Effect of pH on adsorption - photocatalysis of tungsten disulfide

Nguyen Thi Thanh Bich<sup>1</sup>, Nguyen Duc Nhan<sup>1</sup>, Huynh Huu Dien<sup>1</sup>, Nguyen Tong Yen Nhu<sup>1</sup>,  
Pham Thi Yen Nhi<sup>1</sup>, Nguyen Van Phuc<sup>2</sup>, Truong Duy Huong<sup>2</sup>, Vo Vien<sup>2,\*</sup>

<sup>1</sup>Faculty of Education, Quy Nhon University, Vietnam

<sup>2</sup>Applied research Institute for science and technology, Quy Nhon University, Vietnam

Received: 18/03/2020; Accepted: 18/04/2020

### ABSTRACT

In this work, the tungsten disulfide material was prepared by calcining mixture of  $H_2WO_4$  and thiourea with weigh ratio of 1:5 in Ar gas at 650°C for 1h, and denoted as  $WS_2$ . The obtained product was characterized by X-ray diffraction (XRD), infrared spectra (IR), energy-dispersive X-ray spectroscopy (EDS), scan electron microscopy (SEM) and UV-Vis diffuse reflectance spectroscopy (UV-Vis). The relevant characterizations indicated that the main composition of sample is tungsten disulfide. The integrated adsorption and photodegradation of the cationic dye (rhodamine B) on  $WS_2$  was evaluated in a pH range of 1.5 - 8.0, which showed that the decline of RhB degradation rate on  $WS_2$  when increasing solution pH from 1.5 to 8 due to adsorption rather than the photodegradation process. Specifically at pH of 4, the strongest electrostatic interaction between the negatively charged surface of the material and cationic dye resulted in a highest adsorption and photocatalytic efficiency up to 66.98% and 20.88%, respectively, after investigating time of 8 hours.

**Keywords:**  $WS_2$ , adsorption, photocatalysis, pH, Rhodamine B.

### 1. INTRODUCTION

Environmental pollution caused by organic toxic pollutants has become a global concern. In order to solve this problem, a variety of advanced oxidation processes have been widely used, and photocatalysis is now attracting a considerable attention for various applications. Beside metal oxide-based photocatalysts such as  $TiO_2$ ,  $ZnO$ ,  $WO_3$ ,  $Cu_2O$ , etc., the layered-structure materials transition metal dichalcogenides (TMDs) such as  $MoS_2$  and  $WS_2$  having a band gap of 1.8 eV have been become a promising candidate for photocatalyst.<sup>1-4</sup>

Layered  $MoS_2$  with different nanostructures like nanowires, nanorods, and nanotubes, the monolayer and multilayer structures have been also synthesized.<sup>5-10</sup> The layered structure of  $MoS_2$  crystals, with hexagonal arrangement of atoms by covalent bonds in a sequence of S–Mo–S through weak Van der Waals interactions could be suitable for solar cells, photonics, optoelectronics, and catalysts applications.<sup>5,6</sup> Similar to  $MoS_2$  in terms of crystal structure and chemical property,  $WS_2$  also has a narrow band gap making this material could work as a photocatalyst to decompose organic molecules under visible light.<sup>1,3,10,12</sup>

\*Corresponding author.

Email: vovien@qnu.edu.vn



Various reports show that a nano-photocatalyst possessing a high specific surface area performs not only an excellent photocatalytic activity but also a strong adsorption capacity to pollutants.<sup>13,14</sup> Furthermore, the adsorption process can strongly affect the photocatalytic efficiency of decomposing pollutants due to the fact that both the adsorption and the photoinduced reactive species mainly occur on the surface of the material.<sup>14,16</sup> Most available photocatalytic studies have ignored or ejected the adsorption kinetics by assuming the adsorption - desorption interaction reaching the equilibrium, then considering the decrease in the concentration of pollutants is due to photocatalytic process.<sup>17,19</sup> However, the adsorption-desorption equilibrium cannot be achieved in the photocatalytic reaction due to the activation of radicals, which causes the concentration of the adsorbent on the catalyst to decrease continuously when illuminated.<sup>20</sup> Meanwhile, few studies have been published involving the effects of adsorption on photocatalytic degradation to remove pollutants. Recently, Luo et al. showed that adsorption process can promote the decomposition of Red 120 dye on the g-C<sub>3</sub>N<sub>4</sub> catalyst with the proposed Elovich kinematic model.<sup>21</sup> This paper focuses on the synergy between adsorption and photocatalysis of a typical catalyst, WS<sub>2</sub>. To consider the adsorption capacity, in this study, we changed the pH of the reaction solution and used Rhodamine B (RhB) as a target molecule.

## 2. EXPERIMENT

### 2.1. Chemicals

The chemicals used in the synthesis were H<sub>2</sub>WO<sub>4</sub>, (NH<sub>2</sub>)<sub>2</sub>CS, rhodamine B purchased from Xilong Chemical Co. Ltd. (China) with the purity over 99% and no further modification.

### 2.2. Preparation of material

The WS<sub>2</sub> material was synthesized via a facile solid-state reaction by the following procedure: a mixture of tungstic acid and thiourea with weigh ratio of 1:5 was added to a solvent of 10 mL of distilled water and 30 mL of C<sub>2</sub>H<sub>5</sub>OH with stirring at 40 °C. After 5 hours, the solid

was collected and then dried for 12 hours at 80°C. The obtained solid was finely ground and transferred to a ceramic cup, covered closely with aluminum foil, and then annealed at 650°C for 2 h under Ar gas. The resulting material was rinsed several times with distilled water and C<sub>2</sub>H<sub>5</sub>OH, then dried at 80 °C for 12 hours, and denoted as WS<sub>2</sub>.

### 2.3. Material characterization

Powder X-ray diffraction (XRD) patterns of sample were recorded by a D8 Advance Xray diffractometer with Cu K $\alpha$  radiation ( $\lambda = 1.540\text{\AA}$ ) at 30 kV and 0.01 A. Infrared spectra (IR) of material were measured by IRPrestige-21 (Shimadzu). The SEM image and energy-dispersive X-ray spectroscopy (EDS) of sample were recorded on Nova Nano SEM 450. UV-Vis diffuse reflectance spectroscopy (UV-Vis-DRS) was carried out on Cary 5000 (Varian, Australia).

### 2.4. Determination of pH<sub>pzc</sub>

Point of zero charge (pH<sub>pzc</sub>) of WS<sub>2</sub> material was determined by titration method of measuring pH of 0.1M NaCl solution at 30 °C. In detail, initial pH values (pH<sub>i</sub>) of 50 mL of 0.1M NaCl solution were adjusted from 1.0 to 12.0 by addition of HCl or NaOH. To the solutions, 0.03 grams of WS<sub>2</sub> were added and stirred for 24 hours. The suspensions were separated and the pH final values (pH<sub>f</sub>) were measured. The point of zero charge was pH<sub>i</sub> when pH<sub>i</sub> = pH<sub>f</sub>. The pH value of the solutions is measured on the HANA HI2211 pH meter.

### 2.5. Photocatalytic activity evaluation

The adsorption and photocatalytic activity of WS<sub>2</sub> was evaluated by the removal efficiency of rhodamine B (RhB) in aqueous solution at the dark and under the light of LED (220V- 30W). The concentration change of RhB was measured on UV-Vis spectrophotometer (CECIL CE2011) at the wavelength of 553 nm.

The efficiency (h) is calculated by the following expression:

$$h = \frac{C_o - C_t}{C_o} 100 (\%)$$

Where  $C_0$  and  $C_t$  are the initial concentrations and the concentrations of rhodamine B solution (mg/L) at time  $t$  (hour).

### 3. RESULTS AND DISCUSSION

The crystal structure and phase of  $WS_2$  sample were analyzed by XRD. As seen in Figure 1, the XRD pattern of  $WS_2$  exhibits main peaks at  $2\theta = 14.3^\circ; 32.8^\circ; 39.5^\circ; 43.9^\circ; 58.4^\circ$  and  $69.1^\circ$  corresponding to the (002), (101), (103), (006), (110) and (201) planes, respectively. The peaks match well with the reference of  $WS_2$  (JPCDS card No. 002-0131), confirming that the  $WS_2$  has a hexagonal crystalline structure. The intensity of the (002) reflection for  $WS_2$  at  $2\theta = 14.3$  shows the characterization of multi-layered  $WS_2$  and high order of the material. The d-spacing was calculated base on the (002) plane using Vulf-Bragg equation to be  $d_{002} = \frac{\lambda}{2\sin\theta} = 6.2 \text{ \AA}$ , which is consistent with the previous published articles.<sup>3,22</sup>

The bonding vibrations in the molecular structure of  $WS_2$  sample were further confirmed by IR spectra and shown in Figure 2. The band at  $3445 \text{ cm}^{-1}$  is attributed to the OH vibration of adsorbed water, while the observed peaks in the region of  $500 \text{ cm}^{-1} - 690 \text{ cm}^{-1}$  are attributed to W-S bond and band at  $960 \text{ cm}^{-1}$  is due to the S-S bond.<sup>3</sup>

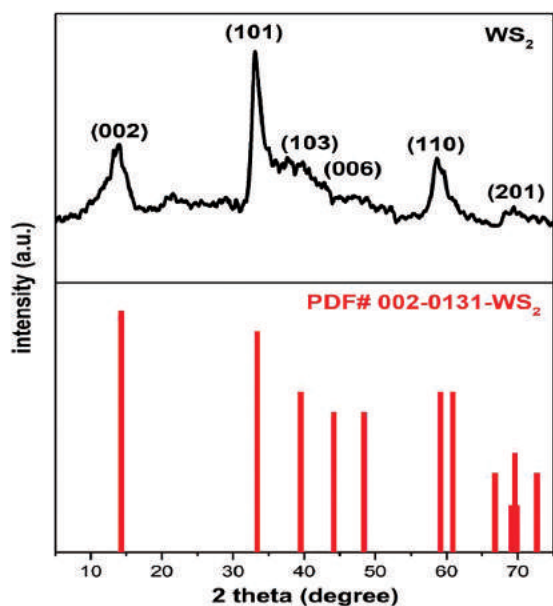


Figure 1. XRD pattern of  $WS_2$ .

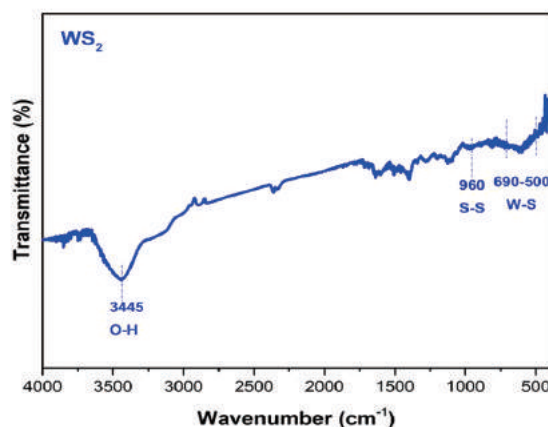


Figure 2. IR spectra of  $WS_2$ .

The EDS analysis of  $WS_2$  in Figure 3 shows that W and S are main elements of the material. However, the presence of C and N with insignificant content may come from decomposition of the precursors.

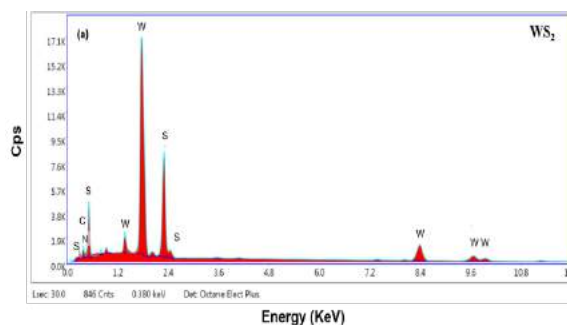


Figure 3. EDS patterns of  $WS_2$ .

The morphology of  $WS_2$  was also characterized using SEM. Figure 4 shows that  $WS_2$  is shaped like hydrangea flowers, formed from sheets.

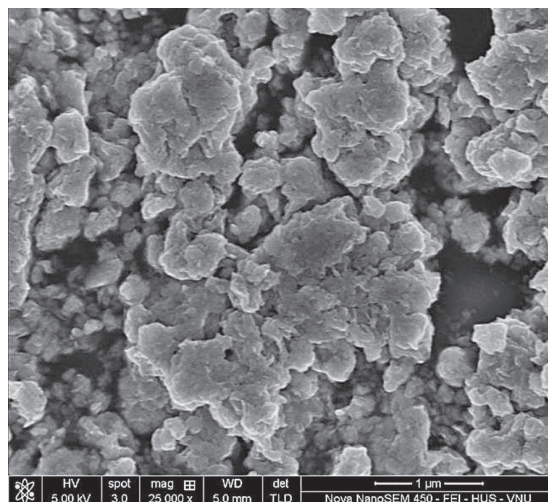
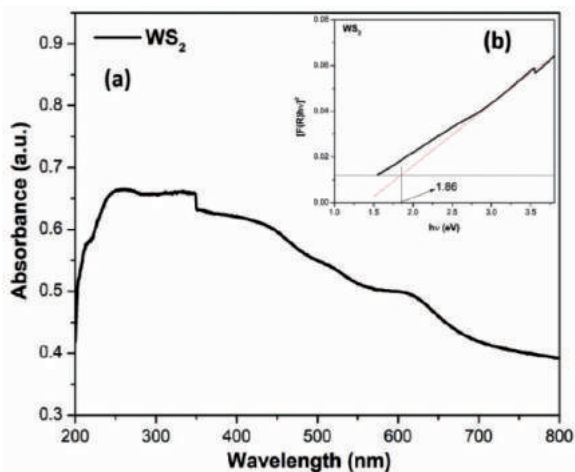


Figure 4. SEM image of  $WS_2$ .

The optical properties of WS<sub>2</sub> was characterized by UV-Vis diffuse reflectance spectroscopy and shown in Figure 5.



**Figure 5.** (a) UV-vis spectrum of WS<sub>2</sub> and (b, inset) optical band gap ( $E_g$ ) of WS<sub>2</sub>.

The results show that WS<sub>2</sub> had an absorption band that stretched from the peak in the near ultraviolet region, strong absorption edge and spread to visible light region. The band gap energy of WS<sub>2</sub> is determined via the Kubelka-Munk<sup>23</sup> equation  $[F(R) / hv]^2 \sim (\alpha hv)^2 \sim (hv - E_g)$  with a value of 1.86 eV.<sup>3</sup> This result is consistent with the previous published article.<sup>1,4</sup> With this bandgap energy, WS<sub>2</sub> may exhibit a good photocatalytic performance under visible light.

The effect of the solution pH on the RhB treatment efficiency is mainly due to the change in form of existing RhB molecule and catalyst surface charge in different pH environments. The problem in photocatalysis is distinguishing the adsorption and photocatalytic contribution throughout the total reduction in reactant concentration. The decrease in concentration in dark considered only adsorption (HP), while under light considered including adsorption and catalysis (HP + XT). From there, the difference between these two values ( $\Delta\{(HP + XT) - HP\}$ ) may be considered photocatalyst performance of the material. The conversion of RhB after 8 hours of stirring in dark and after 8 hours under led light is shown in Figures 6, 7, 8 and Table 1.

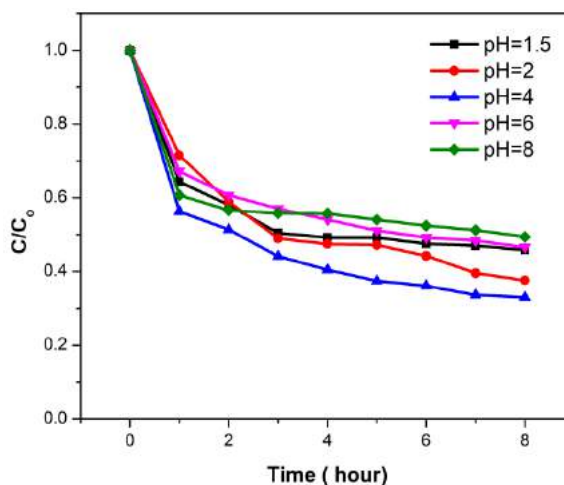


**Figure 6.** Adsorption efficiency of RhB after 8 hours reaction in dark on WS<sub>2</sub> ( $m_{WS_2} = 0.03$  g;  $V_{RhB} = 150$  mL;  $C_{RhB} = 30$  mg/L).

The results showed that at pH = 4, the adsorption efficiency of RhB on WS<sub>2</sub> was the highest (HP = 66.98%), with  $\Delta\{(HP + XT) - HP\}$  reached 20.88%. The adsorption efficiency decreased in lower pH values (pH = 1.5; 2) or higher pH values (pH = 6, 8), resulting in photocatalytic efficiency at these pH values were also lower than that at pH = 4. This can be explained by electrostatic interactions between the charged surface of WS<sub>2</sub> and the positively charged cationic dye. The  $pH_{pzc}$  of WS<sub>2</sub> is shown in Figure 9, estimated to be  $\sim 1.5$ . In aqueous solutions, when  $pH < pH_{pzc}$ , the surface charge of WS<sub>2</sub> is positive, while it is negative when  $pH > pH_{pzc}$ . Meanwhile, RhB as a cationic dye dissociate to chloride ions (Cl<sup>-</sup>) and cation ammonium in aqueous solution (Figure 10). In the range of the pH above  $pH_{pzc}$ , the WS<sub>2</sub> surface carries negative charges, which benefits the adsorption of cationic dyes onto WS<sub>2</sub> through electrostatic interaction. Therefore, the adsorption rates were improved with changing pH values from 1.5 to 4 since the number of negatively charged sites were increased with increasing pH values at this range. At higher pH values, however, specifically at 6 and 8, the -COOH group of RhB began dissociating for negative charges. Therefore, it increases the thrust force on the WS<sub>2</sub> surface, resulting in decreased adsorption capacity when further increasing

pH values.<sup>24</sup> On the other hand, the observed results show that the photodegradation ability of WS<sub>2</sub> declined dramatically with the increase of solution pH from 4 to 8. In a photocatalytic process, ·OH is believed to be a strong oxidant for decomposition of organic pollutants and is the main active species at neutral or high pH levels.<sup>25</sup> Moreover, ·OH is much easier produced at high pH value, resulting in the enhancement of photocatalytic efficiency.<sup>26,27</sup> As a result, there is a synergistic relationship between adsorption and photocatalysis, in which, adsorption will give good photocatalytic results due to free radicals reacting with organic compounds in the form of adsorption on the catalysts surface rather than they in solution. This result is also observed in the previously published article.<sup>21</sup>

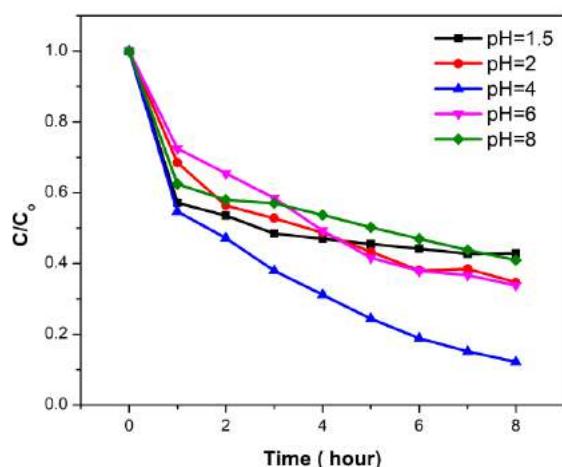


**Figure 7.** Photocatalytic efficiency of RhB after 8 hours reaction under led light on WS<sub>2</sub> ( $m_{WS_2} = 0.03$  g;  $V_{RhB} = 150$  mL;  $C_{RhB} = 30$  mg/L, LED light 220V-30W).

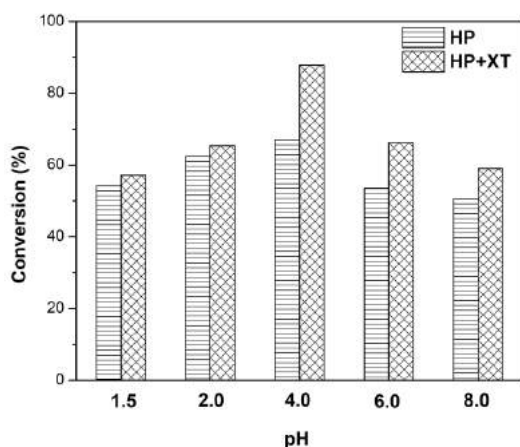


**Figure 8.** The conversion of RhB after 8 hours reaction in dark and under led light on WS<sub>2</sub>.

**Table 1.** The conversion of RhB after 8 hours reaction in dark and under led light on WS<sub>2</sub>.

pH	Conversion of RhB (%)		
	HP	(HP + XT)	$\Delta$ (HP+XT) - HP
1.5	54.18	57.11	2.93
2.0	62.40	65.34	2.94
4.0	<b>66.98</b>	<b>87.86</b>	<b>20.88</b>
6.0	53.45	66.24	12.79
8.0	50.59	59.03	8.44

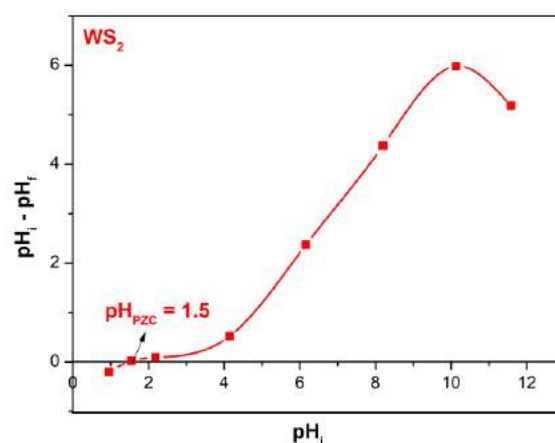


**Figure 9.** The point of zero charge of WS<sub>2</sub>.

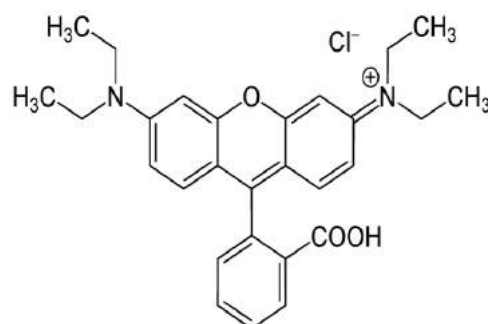


**Figure 10.** Chemical structure of rhodamine B.

#### 4. CONCLUSIONS

The WS<sub>2</sub> material was synthesized via a facile solid-state calcination of mixture containing H<sub>2</sub>WO<sub>4</sub> and thiourea in Ar gas. The synthesized WS<sub>2</sub> material has good adsorption and photodegradation capability towards the cationic dye (rhodamine B) at a wide pH ranges from 1.5 to 8. Especially at pH = 4, the electrostatic interaction between the negatively charged surface of the material and cationic

dye is strongest with a maximum efficiency of 66.98% after in dark for 8 hours and the highest photocatalytic efficiency of 20.88%. There is a synergistic relationship between adsorption and photocatalysis, in which, a high adsorption would give a better photocatalytic results due to free radicals reacting with organic compounds in the form of adsorption on the catalyst surface rather than them in the bulk of solution. Based on the obtained results, WS<sub>2</sub> can be a candidate for organic pollution treatment in the environment. However, further studies should be conducted including modification of the WS<sub>2</sub> material by doping or coupling with other materials in order to change its surface and electrochemical properties.

**ACKNOWLEDGEMENT:** *This research is conducted within the framework of the student scientific research project for the academic year 2019 - 2020 under the project code S2019.576.13.*

#### REFERENCES

1. M. S. Akple, J. Low, S. Wageh, A. Ahmed Al-Ghamdi, J. Yu, J. Zhang. Enhanced visible light photocatalytic H<sub>2</sub>-production of g-C<sub>3</sub>N<sub>4</sub>/WS<sub>2</sub> composite heterostructures, *Applied Surface Science*, **2015**, 358, 196–203.
2. M. Li, L. Zhang, X. Fan, M. Wu, Y. Du, M. Wang, Q. Kong, L. Zhang, J. Shi. Dual synergetic effects in MoS<sub>2</sub>/pyridine-modified g-C<sub>3</sub>N<sub>4</sub> composite for highly active and stable photocatalytic hydrogen evolution under visible light, *Applied Catalysis B: Environmental*, **2016**, 190, 36–43.
3. S. V. P. Vattikuti, C. Byon, V. Chitturi. Selective hydrothermally synthesis of hexagonal WS<sub>2</sub> platelets and their photocatalytic performance under visible light irradiation, *Superlattices and Microstructures*, **2016**, 94, 39-50.
4. Y. Sang, Z. Zhao, M. Zhao, P. Hao, Y. Leng, H. Liu. From UV to Near-Infrared, WS<sub>2</sub> Nanosheet: A Novel Photocatalyst for Full Solar Light Spectrum Photodegradation, *Adv. Mater.*, **2014**, 1-7.
5. S. G. Alexander, S. B. Ivan, D. L. Natalia, I. B. Mikhail, Y. A. Mikhail. Structural properties and phase transition of exfoliated-restacked molybdenum disulfide, *J. Phys. Chem. C*, **2013**, 117, 8509-8515.
6. S. V. P. Vattikuti, C. Byon, V. Chitturi. Synthesis of MoS<sub>2</sub> multi-wall nanotubes using wet chemical method with H<sub>2</sub>O<sub>2</sub> as growth promoter, *Superlattice. Microst.*, **2015**, 85, 124–132.
7. S. V. P. Vattikuti, C. Byon, C. V. Reddy, J. Shim, B. Venkatesh. Co-precipitation synthesis and characterization of faceted MoS<sub>2</sub> nanorods with controllable morphologies, *Appl. Phys. A*, **2015**, 119, 813–823.
8. X. Wang, Z. Zhang, Y. Chen, Y. Qu, Y. Lai, J. Li. Morphology-controlled synthesis of MoS<sub>2</sub> nanostructures with different lithium storage properties, *J. Alloy. Compd.*, **2014**, 600, 84– 90.
9. Z. Zeng, Z. Yin, X. Huang. Single-layer semiconducting nanosheets: High-yield preparation and device fabrication, *Angewandte Chemie.*, **2011**, 50, 11093–11097.
10. Y. Wu, Z. Liu, J. Chen, X. Cai, P. Na. Hydrothermal fabrication of hyacinth flower-like WS<sub>2</sub> nanorods and their photocatalytic properties, *Materials Letters*, **2017**, 189, 282–285.
11. Y. Ma, J. Li, E. Liu, J. Wan, X. Hu, J. Fan. High efficiency for H<sub>2</sub> evolution and NO removal over the Ag nanoparticles bridged g-C<sub>3</sub>N<sub>4</sub> and WS<sub>2</sub> heterojunction photocatalysts, *Applied Catalysis B: Environmental*, **2017**, 219, 467-478.
12. Y. Hou, Y. Zhu, Y. Xu, X. Wang. Photocatalytic hydrogen production over carbon nitride loaded with WS<sub>2</sub> as cocatalyst under visible light, *Applied Catalysis B: Environmental*, **2014**, 156-157, 122–127.
13. M. I. Zaki, N. E. Fouad, G. A. H. Mekhemer, T. C. Jagadale, S. B. Ogale. TiO<sub>2</sub> nanoparticle size dependence of porosity, adsorption and catalytic activity, *Colloid Surf. A*, **2011**, 385, 195–200.
14. W. Zou, B. Gao, Y. Ok, L. Dong. Integrated adsorption and photocatalytic degradation of volatile organic compounds (VOCs) using carbon-based nanocomposites: a critical review, *Chemosphere*, **2019**, 218, 845–859.

15. D. Friedmann, C. Mendive, D. Bahnemann. TiO<sub>2</sub> for water treatment: parameters affecting the kinetics and mechanisms of photocatalysis, *Appl. Catal. B: Environ.*, **2010**, *99*, 398–406.
16. C. B. Mendive, T. Bredow, A. Feldhoff, M. Blesa, D. Bahnemann. Adsorption of oxalate on rutile particles in aqueous solutions: a spectroscopic, electron-microscopic and theoretical study, *Phys. Chem. Chem. Phys.*, **2008**, *10*, 1960–1974.
17. C. Martínez, M. L. Canle, M. I. Fernández, J. A. Santaballa, J. Faria. Kinetics and mechanism of aqueous degradation of carbamazepine by heterogeneous photocatalysis using nanocrystalline TiO<sub>2</sub>, ZnO and multi-walled carbon nanotubes–anatase composites, *Appl. Catal. B: Environ.*, **2011**, *102*, 563–571.
18. H. S. Son, S. J. Lee, I. H. Cho, K. D. Zoh. Kinetics and mechanism of TNT degradation in TiO<sub>2</sub> photocatalysis, *Chemosphere*, **2004**, *57*, 309–317.
19. P. Ji, J. Zhang, F. Chen, M. Anpo. Study of adsorption and degradation of acid orange 7 on the surface of CeO<sub>2</sub> under visible light irradiation, *Appl. Catal. B: Environ.*, **2009**, *85*, 148–154.
20. G. Xue, H. Liu, Q. Chen, C. Hills, M. Tyrer, F. Innocent. Synergy between surface adsorption and photocatalysis during degradation of humic acid on TiO<sub>2</sub>/activated carbon composites, *J. Hazard. Mater.*, **2011**, *186*, 765–772.
21. Y. Luo, X. Wei, B. Gao, W. Zou, Y. Zheng, Y. Yang, Y. Zhang, Q. Tong, L. Dong. Synergistic adsorption-photocatalysis processes of graphitic carbon nitrate (g-C<sub>3</sub>N<sub>4</sub>) for contaminant removal: Kinetics, models, and mechanisms. *Chemical Engineering Journal*, **2019**, 122019(1-7).
22. Y. Q. Zhu, T. Sekine, K. S. Brigatti, S. Firth, R. Tenne, R. Rosentsveig, H.W. Kroto, D. R. M. Walton. Shock-Wave Resistance of WS<sub>2</sub> Nanotubes, *Journal of the American Chemical Society*, **2003**, *125*(5), 1329–1333.
23. P. Kubelka, F. Munk. Ein Beitrag zur Optik der Farbanstriche, *Zeits. f. Techn. Physik*, **1931**, *12*, 593–601.
24. P. Qin, Y. Yang, X. Zhang, J. Niu, H. Yang, S. Tian, J. Zhu, M. Lu. Highly efficient, rapid, and simultaneous removal of cationic dyes from aqueous solution using monodispersed mesoporous silica nanoparticles as the adsorbent, *Nanomaterials*, **2017**, *8*(1), 4(1-14).
25. Z. Shourong, H. Qingguo, Z. Jun, W. Bingkun. A study on dye photoremoval in TiO<sub>2</sub> suspension solution, *Journal of Photochemistry and Photobiology A: Chemistry*, **1997**, *108*(2-3), 235–238.
26. C. Galindo, P. Jacques, A. Kalt. Photodegradation of the aminoazobenzene acid orange 52 by three advanced oxidation processes: UV/H<sub>2</sub>O<sub>2</sub>, UV/TiO<sub>2</sub> and VIS/TiO<sub>2</sub>, *Journal of Photochemistry and Photobiology A: Chemistry*, **2000**, *130*(1), 35–47.
27. I. K. Konstantinou, T. A. Albanis. TiO<sub>2</sub>-assisted photocatalytic degradation of azo dyes in aqueous solution: kinetic and mechanistic investigations, *Applied Catalysis B: Environmental*, **2004**, *49*(1), 1–14.

## CONTENTS

1.	An application of Linearization Theorem to the problem on Tauberian convergence in weighted space of Gâteaux holomorphic functions <b>Duong Thanh Vy</b> .....	6
2.	Holomorphic extensions of weakly holomorphic functions in weighted spaces of holomorphic functions <b>Nguyen Van Dai</b> .....	18
3.	Some inequalities for matrix polynomials <b>Pham Quang Hung, Pham Nu Ngoc Diep</b> .....	28
4.	A frequent subgraph mining algorithm on the MapReduce model <b>Tran Thien Thanh, Tran Thi Lien, Nguyen Thi Kim Phuong</b> .....	36
5.	A technique to detect liver tumor based on texture model <b>Le Thi Kim Nga, Doan Thi Xuong</b> .....	44
6.	A technique of identifying the contour point to assess the change of abnormal areas on medical imaging <b>Le Thi Kim Nga, Doan Thi Xuong, Doan Thi Thu Cuc</b> .....	52
7.	Applying of image processing technology in classifying tomatoes after harvest <b>Nguyen Truong Duy, Tran Dinh Huy Duc, Bui Van Vu, Do Van Can</b> .....	60
8.	A Real-time flooding monitoring and warning system using LoRa technology in Kone and Ha Thanh river basin, Binh Dinh Province <b>Tran Van Trung, Nguyen Duc Thien, Le Song Toan, Ngo Van Tam, Ho Van Phi</b> .....	70
9.	Effects of salinity on growth and survival of square head climbing perch ( <i>Anabas testudineus</i> ) in the early juvenile to juvenile stage <b>Phung Thi Hong Dien, Vo Van Chi</b> .....	80

10. Feeding Biology of Bronze featherback (*Notopterus notopterus*) distributed in Tra O lagoon, Binh Dinh province  
**Dang Thi Thach Truc, Vo Van Chi**..... 90
  
11. Effect of pH on adsorption - photocatalysis of tungsten disulfide  
**Nguyen Thi Thanh Bich, Nguyen Duc Nhan, Huynh Huu Dien, Nguyen Tong Yen Nhu, Pham Thi Yen Nhi, Nguyen Van Phuc, Truong Duy Huong, Vo Vien**..... 96